

**POLITECNICO DI TORINO**

**SCUOLA DI DOTTORATO**

Dottorato in Scienza e Tecnologia dei Materiali  
XXV Ciclo

**Ph.D Thesis**

**Preparation, microstructure, mechanical and  
thermophysical properties of short carbon fibre/SiC  
multilayer composites by tape casting and  
pressureless sintering**



**Wenshu Yang**

**Advisor**

Prof. Claudio Francesco Badini

**Coordinator**

Prof. Claudio Francesco Badini

**Co-advisor**

Prof. Sara Biamino

# **Dedication**

To my parents

# Acknowledgments

I would like to express my sincere gratitude to my advisor, Prof. Claudio Francesco Badini, for his guidance, support and encouragement throughout the period of my graduate study at Politecnico di Torino. Without his wisdom, patience and persistence, it would be impossible to achieve the goals of this study. I learned not only the knowledge of research but also the wisdom of life from him. I count myself fortunate to have such an excellent advisor.

I would also like to extend my special appreciation to my co-advisor, Prof. Sara Biamino, for her invaluable support and advice during the experiments and dissertation. She has always been there to help me whenever I encounter an obstacle or require an advice, and it is really a pleasure working with her.

I would like to thank all members of HTMAT group for helping me in achieving my goal and for creating a friendly environment during these years: Prof. Paolo Fino, Prof. Matteo Pavese, Dr. Simona Ceresa Mio, Dr. Andrea Antonini, Dr. Claudia Vega Bolivar, Dr. Dreidy Vasquez Sandoval, Dr. Emiliano Derinaldis, Elisa Padovano, Silvia Marchisio, Eleonora Doglio, Xiang Chen, Muhammad Ramzan Abdul Karim, Veronica Malerba, Mathieu Ternier, Giuseppe D'Amico, Paolo Epicoco and Andrea Marchino. Their friendship, enlightening discussions and helps in experiments have made my stay at Politecnico di Torino pleasant and enjoyable.

The financial supports from European Project “SMARTEES” (G.A. n. 262749) and Chinese Scholarship Council (2009612050) are highly acknowledged. I would like to acknowledge Tecnogrande S.P.A and Dr. Laura Fuso for sintering the materials.

Last but most importantly, I would also like to extend my deepest gratitude to my family, especially to my parents Chuguang Yang and Dongjiao Zhang, who have always been a very important part of my life, for their love, support and encouragement.

# Abstract

Silicon carbide multilayer composites containing short carbon fibres ( $C_{sf}/SiC$ ) were prepared by tape casting and pressureless sintering. The short C fibres were firstly dispersed in solvents with the aid of dispersant and then mixed with SiC slurry to limit fibre breakage. The relative densities, mechanical properties, oxidation behavior of  $C_{sf}/SiC$  multilayer composites were evaluated. Thermal expansion, diffusivity and conductivity behavior in three directions were tested. The effect of addition of short C fibres on shrinkage, mechanical and thermophysical behavior was discussed.

Triton X100 was found to be the best one for Toho Tenax HTC124 (with water soluble coating) among BYK-163, BYK-410, BYK-2150, BYK-9076, BYK-9077 and Triton X100 dispersants. Although the average fibre length (0.5 to 0.6 mm) after mixing was only one-sixth or -fifth of original length (3 mm), it is still much longer than in other  $C_{sf}/SiC$  composites using ball-milling, indicating that mixing the SiC slurry with the fibre-predispersed solution is an effective method for adding fibres with limited breakage.

Fibres were homogeneously distributed in the tapes and tended to align fairly well along the tape casting direction. The relative density of the composite containing short C fibres decreased with the fibre amount. The  $C_{sf}/SiC$  multilayer composites demonstrated significant anisotropic shrinkage behavior in different directions, while the addition of short C fibres hindered the shrinkage in the plane containing the fibres (X and Y directions) during sintering. Elastic modulus, bending strength and fracture toughness decreased with increased porosity, which implies that bending properties are affected significantly by residual porosity. However, due to residual thermal stress, the fracture toughness of  $SiC/(C_{sf}/SiC)$  multilayer composites was higher than that of SiC multilayer, which indicates that the fracture toughness of SiC-based thermal protection system could be improved through

designing its architecture.

The weight loss during oxidation tests was larger for  $C_{sf}/SiC$  multilayer composites than for SiC multilayer and increased with the porosity and the fibre amount. Passive oxidation of SiC was still occurred after addition of short fibres. Specific heat of  $C_{sf}/SiC$  multilayer composites slightly increased with fibre amount. No significant different in thermal expansion behavior of SiC, 5 and 10 vol.%  $C_{sf}/SiC$  multilayer composites in different directions was found.

In X direction before oxidation treatment, the thermal conductivity firstly slightly increased after addition of 5 vol.% short C fibre, and then decreased with further fibre addition. However, in Y and Z directions, the thermal conductivities decreased with the increase of fibre amount before oxidation treatment. After oxidation treatment, the thermal conductivities decreased with the increase of fibre amount regardless of test directions. Since fibre aligned along tape casting direction,  $C_{sf}/SiC$  multilayer composites demonstrated highest thermal conductivity in X direction regardless of fibre amount. Moreover, due to the presence of the interface between adjacent layers, Z direction showed lowest thermal conductivity. Because of the oxidation of C fibre (in  $C_{sf}/SiC$  multilayer composites) and formation of silica (both in SiC multilayer and  $C_{sf}/SiC$  multilayer composites), thermal conductivities of SiC multilayer and  $C_{sf}/SiC$  multilayer composites decreased after oxidation treatment.

**Keywords:** Multilayer composite; Short C fibre; SiC; Tape casting; Mechanical properties; Thermophysical properties; Thermal conductivity.

# Content

Acknowledgments .....	I
Abstract .....	II
Content .....	IV
List of Figures .....	VII
List of Tables .....	XI
Chapter 1. Introduction.....	1
1.1 High temperature thermal protection materials .....	1
1.1.1 Monolithic ceramics.....	1
1.1.2 Ceramic foams .....	3
1.2 Ceramic matrix composites .....	3
1.2.1 Matrix .....	4
1.2.2 Reinforcement.....	4
1.2.2.1 Particulates .....	4
1.2.2.2 Whiskers.....	9
1.2.2.3 Nano-phases .....	11
1.3 Modified C/C composites .....	14
1.3.1.1 Processing of C/C composites.....	14
1.3.1.2 Oxidation resistance of C/C composites.....	15
1.4 Continuous fibre reinforced SiC matrix composites .....	16
1.4.1 SiC/SiC composites.....	16
1.4.1.1 SiC fibres.....	16
1.4.1.2 Processing of SiC/SiC composite.....	19
1.4.1.3 Interfaces .....	20
1.4.2 C/SiC composites .....	23
1.4.2.1 Carbon fibres .....	23
1.4.2.2 Processing and interface of C/SiC composites .....	23
1.4.2.3 Improvement of oxidation resistance .....	24
1.5 Short fibre reinforced SiC composites .....	26
1.5.1 SiC <sub>sf</sub> /SiC composites.....	27
1.5.2 C <sub>sf</sub> /SiC composites .....	28
1.6 Ceramic multilayers.....	31

1.6.1	Ceramic multilayers .....	31
1.6.2	Processing of ceramic multilayers .....	33
1.6.2.1	Slip casting .....	34
1.6.2.2	Gel casting.....	34
1.6.2.3	Freeze casting .....	36
1.6.2.4	Centrifugal casting.....	38
1.6.2.5	Electrophoretic Deposition .....	38
1.6.2.6	Tape casting.....	40
1.7	Ceramic multilayer composites.....	41
1.8	Scope of current research .....	45
Chapter 2.	Experimental .....	46
2.1	Materials and processing .....	46
2.1.1	Slurry preparation .....	46
2.1.2	Tape casting .....	48
2.1.3	Green samples preparation .....	48
2.1.4	Debinding process .....	52
2.1.5	Pressureless sintering .....	53
2.2	Experiment methods .....	54
2.2.1	Density measurement .....	54
2.2.2	Mechanical properties test.....	54
2.2.3	Oxidation properties test .....	55
2.2.4	Specific heat capacity measurement .....	55
2.2.5	Thermal expansion behavior test .....	55
2.2.6	Thermal diffusivity test.....	56
2.2.7	XRD analysis .....	57
2.2.8	Microstructure observation.....	57
Chapter 3.	Microstructure of C <sub>sf</sub> /SiC multilayer composites.....	58
3.1	Dispersion of short carbon fibres in solvent.....	58
3.2	Dispersion of short carbon fibres in SiC slurry .....	61
3.3	Microstructure of C <sub>sf</sub> /SiC multilayer composites .....	63
3.3.1	Green tapes .....	63
3.3.2	Debinded samples .....	64
3.3.3	Sintered C <sub>sf</sub> /SiC multilayer composites .....	65
Chapter 4.	Mechanical properties of C <sub>sf</sub> /SiC multilayer composite.....	68
4.1	Shrinkage behavior .....	68

4.2	Mechanical properties of C <sub>sf</sub> /SiC multilayer composite .....	70
4.2.1	Stress/displacement curves .....	70
4.2.2	Mechanical properties .....	72
4.2.3	Fracture toughness .....	73
4.2.4	Fracture surface.....	74
Chapter 5.	Thermophysical properties of C <sub>sf</sub> /SiC multilayer composite .....	76
5.1	Oxidation properties .....	76
5.2	Specific heat capacity .....	79
5.3	Thermal expansion behavior .....	80
5.4	Thermal diffusivity properties .....	83
5.5	Thermal conductivity properties .....	84
5.5.1	SiC multilayer .....	86
5.5.2	C <sub>sf</sub> /SiC multilayer composites .....	89
Conclusions	.....	94
Publications/ Conference proceedings	.....	96
Reference	.....	98

# List of Figures

Fig. 1.1 Schematic diagram showing how a hexagonal sheet of graphene is rolled to form a CNT with different chiralities. ....	11
Fig. 1.2 Typical creep curves for SiC fibres tested at 1400 °C in air under a constant stress of 270 MPa. ....	17
Fig. 1.3 Typical microstructure of multilayered matrix in (a) SiC/SiC and (b) C/SiC composites. ....	26
Fig. 1.4 Main toughening mechanisms in ceramic composites. (a) Crack deflection, (b) Pull-out and bridging of elongated grain, Pull-out of (c) nanotubes, (d) whiskers and (e) fibres. ....	30
Fig. 1.5 Typical microstructure of nacre. (a) Aragonite layers and (b) Fracture surface of aragonite layers in the nacre of a blue mussel. ....	32
Fig. 1.6 The load/deflection behavior of monolithic and laminated SiC. ....	33
Fig. 1.7 Laminates preparation method by gel casting reported by Baskin et al.. ..	36
Fig. 1.8 Laminates preparation method by gel casting reported by Hovis et al.. ..	36
Fig. 1.9 Typical microstructure and fracture behavior of Al <sub>2</sub> O <sub>3</sub> /PMMA composites prepared by Munch et al.. (a) Microstructure of lamellar architecture, (b) Microstructure of brick-and- mortar architecture, (c) Fracture behavior of lamellar architecture and (d) Fracture behavior of brick-and-mortar architecture. ....	37
Fig. 1.10 Schematic illustration of (a) cathodic and (b) anodic electrophoretic deposition process. ....	39
Fig. 1.11 Schematic diagram of the tape casting process. ....	40
Fig. 1.12 Dense and flexible SiC green tape prepared in our lab. ....	41
Fig. 2.1 Preparation process of C <sub>sf</sub> /SiC multilayer composite by tape casting and pressureless sintering. ....	46
Fig. 2.2 Stacking process of green multilayer samples. (a) Paint gluing solution and (b) Removal air inclusion. ....	48
Fig. 2.3 Roughness profiles of lower-side (in contact with Mylar film) and upper-side (in contact with air) of SiC green tape. ....	49
Fig. 2.4 Preparation process for green specimens for bending test. ....	49
Fig. 2.5 Three-dimensional Cartesian coordinate system used to describe test directions of thermal properties. X direction is parallel to the tape casting direction; Y direction is perpendicular to tape casting and thickness direction; Z direction is the through thickness direction. ....	50

Fig. 2.6 Preparation process of green samples for thermal properties test in Z direction. ....	50
Fig. 2.7 Preparation process of green samples for thermal properties test in Y direction. ....	51
Fig. 2.8 Preparation process of green samples for thermal properties test in X direction. ....	52
Fig. 2.9 Decomposition curves of binder, plasticizer and fibre dispersant. ....	52
Fig. 2.10 Schematic diagram of (a) debinding and (b) pressureless sintering process. ....	53
Fig. 2.11 The schematic diagram of cut samples for thermal diffusivity test in X, Y and Z directions. ....	57
Fig. 3.1 Effect of dispersant (1 wt.%) on fibre dispersion (0.075 vol.%) in mixture of ethanol and butanol. (a) without dispersant, (b) BYK-163, (c) BYK-410, (d) BYK-2150, (e) BYK-9077, (f)BYK-9076, (g) Triton X-100. ....	59
Fig. 3.2 Chemical structure of Triton X-100. ....	60
Fig. 3.3 Microstructure of (a) original commercial fibres, (b) dried fibres dispersed in solvent without any dispersant, (c) dried fibres dispersed in solvent with Triton X100. ....	61
Fig. 3.4 Typical fibre length distribution and statistical results after mechanical mixing of SiC slurry and fibre-predispersed solution. (a), (c) and (e) are the typical length distribution in the slurry whose fibre amount in final sintered samples were 5, 10 and 15 vol.% respectively. (b), (d) and (f) are the corresponding statistical results of (a), (c) and (e), respectively. ....	62
Fig. 3.5 Comparison of (a) fibre aggregation and (b) good fibre dispersion in $C_{sf}/SiC$ green tapes. ....	63
Fig. 3.6 Roughness profiles of upper-side (in contact with air) of SiC and $C_{sf}/SiC$ green tapes (a) SiC, (b) 5 vol.%, (c) 10 vol.%, (d) 15 vol.% $C_{sf}/SiC$ green tapes. ....	64
Fig. 3.7 Cross section surface of stacked green tapes of 10 vol.% $C_{sf}/SiC$ . (a) lower magnification and (b) higher magnification. ....	64
Fig. 3.8 Fracture surface of $C_{sf}/SiC$ multilayers with different fibre amount after debinding. (a) 5 vol.%, (b) 10 vol.% and (c) 15 vol.%. ....	65
Fig. 3.9 Representative morphologies of sintered SiC multilayer and $C_{sf}/SiC$ multilayer composites. (a) SiC multilayer, (b) 5 vol.%, (c) 10 vol.% and (d) 15 vol.% $C_{sf}/SiC$ multilayer composites. ....	66
Fig. 3.10 XRD patterns of SiC multilayer and $C_{sf}/SiC$ multilayer composites. ....	66

Fig. 4.1 Representative bending curve of SiC multilayer and C <sub>sf</sub> /SiC multilayer composites. ....	71
Fig. 4.2 Ladder-like bending curve in 5vol% C <sub>sf</sub> /SiC multilayer composite. ....	71
Fig. 4.3 Crack deflection in 5vol.% C <sub>sf</sub> /SiC multilayer composite. ....	72
Fig. 4.4 Relationships among fibre content, relative density and elastic modulus or bending strength of SiC multilayer and C <sub>sf</sub> /SiC multilayer composites. ..	73
Fig. 4.5 Relationships among fibre amount, relative density and fracture toughness ( <i>K<sub>IC</sub></i> ) of SiC multilayer and C <sub>sf</sub> /SiC multilayer composites .....	74
Fig. 4.6 Fracture toughness of multilayer composites composed by alternative layers of SiC and C <sub>sf</sub> /SiC layer. ....	74
Fig. 4.7 Fracture surface of SiC multilayer and C <sub>sf</sub> /SiC multilayer composites. (a) SiC multilayer, (b) 5, (c) 10 and (d) 15 vol.% C <sub>sf</sub> /SiC multilayer composites. ....	75
Fig. 5.1 Oxidation curves of SiC multilayer and C <sub>sf</sub> /SiC multilayer composites. ..	76
Fig. 5.2 Temperature dependence of specific heat capacity of SiC multilayer and C <sub>sf</sub> /SiC multilayer composites. The red line is the fitting curve in Munro's work, the olive line is the fitting result in present work, and purple line is the specific heat of graphite. ....	79
Fig. 5.3 The relative length changes of (a) SiC, (b) 5 and (c) 10 vol.% C <sub>sf</sub> /SiC multilayer composites in different directions from room temperature to 1500 °C. ....	81
Fig. 5.4 The relative length changes of SiC and C <sub>sf</sub> /SiC multilayer composites in X direction. ....	81
Fig. 5.5 Temperature dependence of CTE of SiC multilayer in X, Y and Z directions. ....	82
Fig. 5.6 Thermal diffusivities-temperature relationship of (a) (b) SiC multilayer, (c) (d) 5 and (e) (f) 10vol% C <sub>sf</sub> /SiC multilayer composites in three directions. (a) (c) (e) are before oxidation treatment and (b) (d) (f) are after oxidation treatment, respectively. ....	83
Fig. 5.7 Thermal diffusivities of SiC multilayer and C <sub>sf</sub> /SiC multilayer composites in Z direction from 30 to 1500 °C (a) before and (b) after oxidation treatment. ....	84
Fig. 5.8 Thermal conductivities-temperature relationship of (a) (b) SiC multilayer, (c) (d) 5 and (e) (f) 10vol% C <sub>sf</sub> /SiC multilayer composites in three directions. (a) (c) (e) are before oxidation treatment and (b) (d) (f) are after oxidation treatment, respectively. ....	85

Fig. 5.9 Thermal conductivities of SiC multilayer and C <sub>sf</sub> /SiC multilayer composites in Z direction from 30 to 1500 °C (a) before and (b) after oxidation treatment. ....	86
Fig. 5.10 Thermal conductivities comparison of SiC multilayer in X, Y and Z directions at room temperature before and after oxidation. ....	86
Fig. 5.11 Microstructure of SiC multilayer in (a) X-Y plane, (b) X-Z plane and (c) Y-Z plane. ....	87
Fig. 5.12 Fracture surface of sintered SiC multilayer buckle. ....	88
Fig. 5.13 Thermal conductivities of SiC multilayer and C <sub>sf</sub> /SiC multilayer composites before and after oxidation in (a) X, (b) Y and (c) Z directions. ....	90
Fig. 5.14 Thermal conductivities comparison of (a) 5 and (b) 10 vol.% C <sub>sf</sub> /SiC multilayer composites in X, Y and Z directions at room temperature before and after oxidation. ....	90
Fig. 5.15 Anisotropic factor $\Phi$ of SiC multilayer and C <sub>sf</sub> /SiC multilayer composites at different temperature. ....	92
Fig. 5.16 Prospective application of C <sub>sf</sub> /SiC multilayer for thermal protection system. ....	93

# List of Tables

Table 1.1 Some basic properties of several ceramics showing potential as thermal protection materials .....	2
Table 1.2 Basic properties of Hi-Nicalon, Tyranno-SA, Sylramic and SCS fibres ·	18
Table 1.3 Basic properties of some commercial carbon fibres .....	24
Table 1.4 Effect of different solvents, dispersants and dispersion method on the dispersion behavior of short carbon fibres (the dispersant amount is 5 wt.% with respect to the solvent) .....	44
Table 2.1 Composition of SiC slurry.....	47
Table 4.1 Density and shrinkage of the SiC multilayer and C <sub>sf</sub> /SiC composites ...	68
Table 4.2 Calculated $\Psi_{XZ}$ and $\Psi_{YZ}$ of SiC multilayer and C <sub>sf</sub> /SiC multilayer composites .....	69
Table 5.1 Comparison of weight loss during oxidation and carbon amount in materials.....	77

# Chapter 1. Introduction

Re-entry vehicles with higher flight speed (order of 8 km/s in plan) have to endure extreme environment during space mission. In order to be maneuverable at hypersonic velocities, controlled surface with sharp leading edges are required. However, the low-radius components would be subject to much greater aerothermal heating than blunt ones. For leading edges and nose cap, the maximum temperature may be more than 2000 °C [1]. Moreover, the other external components of these hypersonic vehicles would also experience high temperature over 1300 °C [2]. Thus, thermal protection systems (TPS) represent a key issue for the successful re-entry of future spacecrafts [3]. The TPS materials must be light-weight and be able to withstand high temperature, high heat flux and mechanical strength associated with vibrations at launch and re-entry into Earth's atmosphere [4]. Current available thermal protection materials will not survive such extreme condition. Therefore, new materials should be developed for advance TPS.

## 1.1 High temperature thermal protection materials

High temperature thermal protection materials include refractory metals, monolithic ceramics, ceramic foams, ceramic multilayer and ceramic matrix composites (CMCs).

Refractory metals include alloys of molybdenum, tantalum, tungsten and niobium. Although refractory metals were used in the first generation of solid propellant rockets, they are hard to be used as TPS materials of future reusable spacecraft due to their high density, high cost and low oxidation resistance [5].

### 1.1.1 Monolithic ceramics

Generally, monolithic ceramics are hard, strong in compression, chemical inert and can withstand very high temperature [6]. Considering the high temperature and corrosive environment, oxides, borides and silicides are preferred for this application. The passive oxidation of borides and silicides would generate glassy  $B_2O_3$  and  $SiO_2$  layers, respectively. These thin glass layers are very effective in limiting the inward diffusion of oxygen into the inner bulk and thus enhance the resistance to oxidation. Some basic properties of several ceramic materials, which are regarded as potential thermal protection materials, are listed in Table 1.1.

**Table 1.1** Some basic properties of several ceramics showing potential as thermal protection materials

Materials	Density (g/cm <sup>3</sup> )	Elastic modulus (GPa)	Thermal conductivity (W/(m•K))	Melting point (°C)	Reference
HfB <sub>2</sub>	~11.1	~480	~100	~3250	[22], [7]
MoSi <sub>2</sub>	~6.26	~441	~54	~2280	[8]
ZrC	~6.73	~407	21	~3530	[9], [10]
ZrO <sub>2</sub>	5.95	~242	0.6–2.3	~2710	[11], [12]
ZrB <sub>2</sub>	~6.09	~520	65–135	~3040	[13], [14]
Al <sub>2</sub> O <sub>3</sub>	3.9	400	18–40	~2070	[15], [16], [17]
Si <sub>3</sub> N <sub>4</sub>	~3.44	~310	~80	~1900	[18], [19]
SiC	~3.21	~450	120–270	~2800	[15], [20], [21]

HfB<sub>2</sub> present rather high density, which is unfavorable for future TPS materials [22]. MoSi<sub>2</sub> suffers from pest oxidation in the temperature range between 400 to 600 °C [23]. Oxidation of ZrC to ZrO<sub>2</sub> and CO<sub>2</sub> or CO could not generate the protection layer [24]. It should be noted that thermal conductivity is another essential parameter for advance thermal protection materials. Materials with low thermal conductivity would inhibit the conduction of heat to the interior of the vehicle, while the component with high thermal conductivity would help spread heat, avoid hot spots, and survive high heat flux environments [25]. Moreover, high thermal conductivity is also favorable for thermal shock resistance [26]. Therefore, ZrB<sub>2</sub> is very promising for thermal protection materials over 2000 °C. It is worth noting that the densities of Al<sub>2</sub>O<sub>3</sub>, Si<sub>3</sub>N<sub>4</sub> and SiC are much lower than that of ZrB<sub>2</sub>. Therefore, they are all good candidates for using below 1600 °C. Compared with Al<sub>2</sub>O<sub>3</sub> and Si<sub>3</sub>N<sub>4</sub>, SiC features lower density, higher elastic modulus and thermal conductivity. Therefore, SiC has long been

recognized as the ideal material for using below 1600 °C [27].

However, monolithic ceramics show a catastrophic fracture behavior under applied stress because only very small energy is absorbed during fracture [28]. Their low fracture toughness remains the major concern for widely application in severe environment.

### **1.1.2 Ceramic foams**

The porous structure of ceramic foams results in many attractive properties, such as low density, high chemical stability and high temperature resistance [29]. Thus, ceramic foams are very suitable for various applications including thermal insulating materials for furnace [30], fire protection materials [31], catalyst supports [32, 33] and gas combustion burners [33]. However, their compressive strength is very low (only a few MPa), which make them impossible to serve as multifunctional thermal protection materials since high mechanical properties and low thermal conductivity are essential.

As stated in “1.1.1 Monolithic ceramics”, the main drawback for monolithic ceramics ( $ZrB_2$  and SiC) is their low fracture toughness. Therefore, a great quantity of research has been carried out and many methods have been adopted to improve fracture toughness. These methods fall into two categories: (i). Introduction of second phases to prepare ceramic matrix composite, (ii). Processing ceramics with a multilayer structure. The key factor for improving toughness is the presence of weak interfaces/interlayers or residual stress, which allow energy dissipation before fracture through mechanisms of crack deflection, pull-out and bridging of fibre or whisker [34], and interface delamination [35]. Detailed literature survey of ceramic matrix composites and multilayers will be given in “1.2 Ceramic matrix composites” and “1.6 Ceramic multilayers”, respectively.

## **1.2 Ceramic matrix composites**

Composite is made from two or more constituents (matrixes and reinforcements) with significantly different physical or chemical properties [36]. The matrices in CMSs are ceramic materials while the reinforcements (usually other dispersed ceramic phases) are designed to improve toughness of conventional ceramics, the main disadvantage of which is brittleness.

## 1.2.1 Matrix

ZrB<sub>2</sub> and SiC have been regarded as most promising materials for TPS of future spacecraft, as discussed in “1.1.1 Monolithic ceramics”. Furthermore, density of SiC (3.21 g/cm<sup>3</sup>) is much lower than that of ZrB<sub>2</sub> (6.09 g/cm<sup>3</sup>), which makes SiC very attractive for application below 1600 °C. In the past decades, SiC-matrix composites have been widely investigated and its fracture toughness has been improved greatly. The different reinforcements and processing methods are general described in “1.2.2 Reinforcement”.

## 1.2.2 Reinforcement

The reinforcements and processing methods, which are currently used in other ceramic matrix composites, have also been adopted in SiC-matrix composite. Thus, in present dissertation, only developments in SiC-matrix composites are discussed. Generally, according to their aspect ratio (length/diameter ratio), the reinforcements in ceramic matrix composite could be classified into particulates, whiskers, nano-phases, short and continuous fibre [37]. These reinforcements could be added before CMCs preparation or in-situ formed during processing.

### 1.2.2.1 Particulates

Particulates generally mean the equiaxed ceramic reinforcements with an aspect ratio less than about 5. They are cheaper and more easy to obtain than other reinforcements. Moreover, the composites reinforced with ceramic particles could be fabricated by conventional ceramic processing methods. TiC and TiB<sub>2</sub> particles with higher coefficient of thermal expansion (CTE) than that of SiC matrix are widely used as reinforcements. The larger shrinkage of second phases, which is caused by higher CTE during cooling from the fabrication temperature, is expected to create residual compressive stress in surrounding SiC matrix. This compressive stress could partial counteract the tensile stress at the crack tip and improve fracture toughness of the composites.

Wei et al. [38] have studied the effect of TiC amount (up to 24.6 vol.%) on mechanical properties of SiC sintered by hot-pressing at 2000 °C with 1 wt.% Al and 1 wt.% C as sintering aids. Fracture toughness (maximum to about 6 MPa·m<sup>1/2</sup>) and four point flexure strength increased with TiC volume fraction. Fracture path

observation revealed that crack deflection by the TiC particles improved the toughness and strength. Endo et al. [39] further investigated the effect of TiC amount (0 to 100 wt.%) on elastic modulus, hardness, flexural strength and fracture toughness of SiC-TiC composites prepared by hot-pressing at while B<sub>4</sub>C and C were used as sintering aids. The maximum fracture toughness was about 6 MPa•m<sup>1/2</sup> with addition of 50 wt.% TiC (equal to volume percent of 40 vol.%). The toughening mechanism should be attributed to cracks deflection around the second phase. Endo et al. [40] also studied the effect of various processing parameters on density and mechanical properties of SiC-TiC composites obtained by hot-pressing. The additives (0.5 wt.% B and 1 wt.% C) helped to decrease sintering temperature from 2105 to 2000 °C. Significant densification in SiC -50 wt.% TiC (equal to 40 vol.% TiC) was observed above 2000 °C. Chae et al. [41] examined the effect of Cr<sub>3</sub>C<sub>2</sub> as additive on the densification and mechanical behavior of SiC-30 vol.% TiC composites. β→α transformation of SiC was observed in SiC-30 vol.% TiC-10 wt.% Cr<sub>3</sub>C<sub>2</sub> specimen during hot-pressing. The in situ growth of elongated α-SiC grains improved fracture toughness. Cho et al. [42, 43] prepared Si C-30 wt.% TiC composites by hot pressing with the liquid forming additives of Al<sub>2</sub>O<sub>3</sub> and Y<sub>2</sub>O<sub>3</sub>. The in situ growth of elongated α-SiC grains during annealing treatment improved the fracture toughness (4.4 MPa•m<sup>1/2</sup> of as-hot-pressed composites) to 6.9 MPa•m<sup>1/2</sup>. An et al. [44] further found that the initial α-SiC phase has a great effect on microstructure and mechanical properties of hot-pressed SiC-30 wt.% TiC composites. The β→α phase transformation during annealing led to the in-situ growth of elongated α-SiC grains. Moreover, a strong relationship between fracture toughness and aspect ratio of α-SiC was observed, which implies the improvement of fracture toughness could be mainly attributed to crack deflection around TiC phases and bridging of elongated SiC grains. At the same time, some researchers also explored other processing method to prepare SiC-TiC composites. Lin et al. [45] prepared SiC-TiC in-situ composites by low pressure chemical vapour deposition on graphite in SiCl<sub>4</sub>- TiCl<sub>4</sub>-C<sub>3</sub>H<sub>8</sub>-H<sub>2</sub> reaction gases. A dense SiC-TiC deposit without porosity was obtained. The maximum fracture toughness determined by the indentation method was 5.9 MPa•m<sup>1/2</sup>. Kim et al [46] sintered SiC-TiC composites (up to 45 wt.% TiC amount) by pressureless sintering with help of Al<sub>2</sub>O<sub>3</sub> and Y<sub>2</sub>O<sub>3</sub>. As a result of crack deflection and bridging by elongated SiC grains, fracture toughness as high as 7.8 MPa•m<sup>1/2</sup> was obtained in SiC-30 wt.% TiC composites. Luo et al. [47] fabricated SiC-TiC composites (up to 45 wt.% TiC amount) by spark plasma sintering (SPS) in vacuum without additive. The

bending strength and fracture toughness showed a strong trend with relative density, and the maximum fracture toughness was  $6.2 \text{ MPa}\cdot\text{m}^{1/2}$ .

TiB<sub>2</sub> is another reinforcement which has been widely used in SiC matrix composites. Janney [48] prepared SiC-15 vol.% TiB<sub>2</sub> composites by hot-pressing with B and C as sintering aids. The addition of particles increased the strength and fracture toughness by 28% and 45%, respectively, over that of monolithic SiC. Furthermore, addition of TiB<sub>2</sub> also improved the oxidation between 1000 and 1200 °C. Cho et al. [49] investigated the effect of additives (Al<sub>2</sub>O<sub>3</sub> and Y<sub>2</sub>O<sub>3</sub>) amount on the microstructure and mechanical properties of SiC-TiB<sub>2</sub> composites. The β→α phase transformation of SiC grains during annealing could be accelerated by the addition of Al<sub>2</sub>O<sub>3</sub> and Y<sub>2</sub>O<sub>3</sub>. Since these in-situ elongated α-SiC grains were beneficial to fracture toughness, fracture toughness increased with additives amount and reached  $7.1 \text{ MPa}\cdot\text{m}^{1/2}$  at addition of 14 wt.% Al<sub>2</sub>O<sub>3</sub> and 6 wt.% Y<sub>2</sub>O<sub>3</sub>. Cho et al. [50] further investigated the effect of TiB<sub>2</sub> amount on properties of SiC-TiB<sub>2</sub> composites by hot-pressing at 1850 °C with Al<sub>2</sub>O<sub>3</sub> and Y<sub>2</sub>O<sub>3</sub> as additives. Coarsening of TiB<sub>2</sub> and in situ growth of elongated α-SiC grains occurred during annealing treatment. A maximum fracture toughness of  $7.3 \text{ MPa}\cdot\text{m}^{1/2}$  was obtained in SiC-50 wt.% TiB<sub>2</sub> composites. Kim et al. [51, 52] tested the solid-particle erosion properties of hot-pressed SiC-14 vol.% TiB<sub>2</sub> composites with 5 vol. % Al<sub>2</sub>O<sub>3</sub> and Y<sub>2</sub>O<sub>3</sub> as sintering aids. The materials exhibited maximum erosion at 60°, and their erosion rates did not increase monotonically with increasing particle size. The plastic deformation is observed for both materials and more prominent for monolithic SiC, and the presence of plastic deformation may be reflected in the anomalous angular dependence of the steady state erosion rate. Kuo et al. [53] evaluated relationship between microstructure and toughness characteristics of α-SiC/TiB<sub>2</sub> and β-SiC/TiB<sub>2</sub> composites by indentation tests. Crack bridging and sliding and pullout of TiB<sub>2</sub> particulates were observed in β-SiC/TiB<sub>2</sub> composites while only crack bridging of TiB<sub>2</sub> particulates was found in α-SiC/TiB<sub>2</sub> composites. They contributed the enhanced long-crack toughness to the weak interface created by the TiB<sub>2</sub> and sintering additives. However, commercially available TiB<sub>2</sub> powders are in large particle size and are highly reactive with water which makes them not favorable as a starting powder. Therefore, SiC matrix composites with in situ TiB<sub>2</sub> have been researched extensively. Miyamoto et al. [54] firstly fabricated TiB<sub>2</sub>-TiC and TiB<sub>2</sub>-SiC composites by a high pressure (3 GPa) combustion sintering process without sintering aids. TiB<sub>2</sub> particles were formed by an in situ reaction between Ti and B (Ti+2B→TiB<sub>2</sub>). However, the explosive reaction would cause defects and ceramic

parts with complicated shapes are difficult to prepare. Tani et al. [55] used TiN and amorphous B as reactants to form in situ TiB<sub>2</sub> ( $2\text{TiN}+4\text{B}\rightarrow 2\text{TiB}_2+\text{N}_2$ ) in the hot-pressing process. The composites containing 20 vol.% TiB<sub>2</sub> presented 80% higher fracture toughness than hot-pressed monolithic SiC ceramic. Ohya et al. [56, 57] prepared TiB<sub>2</sub> particles by in situ reaction between TiC and B ( $\text{TiC}+2\text{B}\rightarrow \text{TiB}_2+\text{C}$ ). A dense (> 98% of theoretical) of TiB<sub>2</sub>-SiC composites was obtained by pressureless sintering and the fracture toughness increased 30% with respect to the monolithic SiC ceramic. Zhang et al. [58, 59] developed another process to form in situ TiB<sub>2</sub> by reaction between TiH<sub>2</sub>, Si and B<sub>4</sub>C ( $\text{Si}+2\text{TiH}_2+\text{B}_4\text{C}\rightarrow \text{SiC}+2\text{TiB}_2+2\text{H}_2$ ). The composite containing 30 vol.% TiB<sub>2</sub> exhibited a fracture toughness of 6.21 MPa•m<sup>1/2</sup> and the main toughening mechanism were stress-induced microcracking, crack bridging by TiB<sub>2</sub> particles and crack deflection around TiB<sub>2</sub> particles. In-situ reaction between TiO<sub>2</sub>, B<sub>4</sub>C and C ( $2\text{TiO}_2+\text{B}_4\text{C}+2\text{C}\rightarrow 2\text{TiB}_2+4\text{CO}$ ) was also reported to prepare SiC-TiB<sub>2</sub> composites [60, 61]. The presence of TiB<sub>2</sub> particles suppressed the grain growth of SiC and facilitated different toughening mechanisms to operate which increased fracture toughness of the composite.

As discussed above, in-situ elongated  $\alpha$ -SiC grains formed by  $\beta\rightarrow\alpha$  phase transformation are beneficial to fracture toughness via elongated grains bridging. Therefore, great efforts have been paid to develop SiC-based materials reinforced with elongated SiC grain (named as self-reinforced SiC). The self-reinforced microstructure can be obtained by (i) selection of the starting SiC powders and (ii) post-sintering treatment at temperature between 1800 to 2000 °C to promote formation of large elongated or platelet-like grains. Kim et al. [62] investigated effect of initial  $\alpha$ -phase amount on the microstructure and mechanical properties of liquid-phase-sintered and subsequently annealed SiC materials. The average size of grain decreased with increasing initial  $\alpha$ -SiC amount and the aspect ratio reached the maximum at 10%  $\alpha$ -SiC and then decreased with increasing  $\alpha$ -SiC amount. The strength increased while the fracture toughness decreased with increasing initial  $\alpha$ -SiC amount. Cho et al. [63] added 1 wt.% of  $\alpha$ -SiC particles as a seed in fine  $\beta$ -SiC powders. The introduction of  $\alpha$ -SiC seeds accelerated the grain growth of elongated large grains during annealing, which led to a coarser microstructure. Zhan et al. [64] added 2.7 wt.%  $\alpha$ -SiC particles into ultra-fine  $\beta$ -SiC (~90 nm) to control the final microstructure. The samples without  $\alpha$ -SiC seed showed fine, uniform, and equiaxed grains after hot-pressing and subsequent annealing treatment. However, materials with  $\alpha$ -SiC seed presented anisotropic microstructure consisting of elongated grains, owing

to the overgrowth of  $\beta$ -phase on  $\alpha$ -seeds. Mechanical test results indicated that a small amount of grain growth in the fine grained region ( $<1 \mu\text{m}$ ) was beneficial for mechanical properties. Kim et al. [65] compared R-curves of two liquid-phase sintered  $\alpha$ -SiC. The SiC with fine and equiaxed microstructure was obtained by hot-pressing and subsequently annealing without seed. Another SiC with coarse and bimodal grain size distribution was prepared using  $\alpha$ -SiC with large  $\alpha$ -SiC as seed. It was found that the coarse microstructure was beneficial to toughening and damage tolerance while a fine microstructure was beneficial to strengthening. Padture [66] firstly developed a SiC-based materials with uniformly distributed elongate-shaped  $\alpha$ -SiC grains and high amounts (20 vol.%) of second-phase yttrium aluminum garnet (YAG). The fracture pattern of the in situ-toughened SiC was intergranular. Crack-wake bridgings, which were enhanced by elongated  $\alpha$ -SiC grains and high thermal-residual stresses in the microstructure, were observed copiously. A measured twofold increase in the indentation toughness was obtained in the in situ-toughened SiC relative to a commercial SiC. Padture et al. [67] further evaluated the crack growth resistance curve (R-curve) of the in situ toughened SiC. The R-curve is a plot of the total energy dissipation rate as a function of the crack size and can be used to examine the processes of slow stable crack growth and unstable fracture. Their evaluation revealed an enhanced toughness in the long-crack region and degraded toughness in the short-crack region. The enhanced long-crack toughness was the result of crack-interface bridging, while the degraded short-crack toughness was due to weakened grain or interface boundaries and to internal residual stresses from thermal expansion mismatch. Kim et al. [68] hot-pressed  $\alpha$ -SiC particles containing 7.2 wt.%  $\text{Y}_3\text{Al}_5\text{O}_{12}$  and 4.8 wt.%  $\text{SiO}_2$  as sintering aids. The microstructure changed from equiaxed to elongated grains during subsequent annealing treatment. This self-reinforced microstructure improved the fracture toughness from 3.2-3.8 (as hot-pressed) to 5.2–6.4  $\text{MPa}\cdot\text{m}^{1/2}$  (annealed 8 h). Kim et al. [69] prepared a fine-grained SiC materials from  $\beta$ -SiC by hot-pressing. Although unobvious  $\beta \rightarrow \alpha$  phase transformation was observed during subsequent annealing treatment, the grain growth of  $\beta$ -SiC improved the fracture toughness of fine-grained SiC from 1.9  $\text{MPa}\cdot\text{m}^{1/2}$  to 6.1  $\text{MPa}\cdot\text{m}^{1/2}$ . Lee et al. [70] tested two SiC materials with equiaxed grain structure and plate-like grains due to grain growth related to  $\beta \rightarrow \alpha$  phase transformation during sintering, respectively. It was found that the more sharply rising R-curve behavior and the better flaw tolerance of SiC materials with phase transformation were attributed mainly to grain bridging of crack faces by plate-like

grains. Lee et al. [71] investigated the effect of sintering-additive composition on fracture toughness of SiC ceramics. The fracture toughness as high as  $8.4 \text{ MPa}\cdot\text{m}^{1/2}$  was obtained while 5.7 wt.%  $\text{Al}_2\text{O}_3$ -3.3 wt.%  $\text{Y}_2\text{O}_3$ -1 wt.% CaO was used as sintering aids. Kim et al. [72] studied the effect of seed shape on the microstructural development in liquid-phase sintered SiC. The samples with large  $\beta$ -SiC particles as seeds showed a bimodal microstructure with large equiaxed grains dispersed in small grain matrix. However, the materials with  $\beta$ -SiC whiskers as seeds presented bimodal microstructure of small matrix grains and large elongated (rod-like) grains. Sciti et al. [73] discussed in detail the effect on annealing on the microstructure and mechanical properties of liquid-phase-sintered silicon carbide. After annealing, grain coarsening, formation of elongated grains and gradual elimination of equiaxed grain would be occurred. Furthermore, through movement toward surface and subsequent volatilization, reduction of secondary phases would also be found. Moreover, due to the movement of liquid phases toward sample surface, an inhomogeneous microstructure would be observed. They also concluded that the best condition of annealing to modify microstructure without creation of pores and other defects should be at  $1900 \text{ }^\circ\text{C}$  and holding more than 2 h.

### 1.2.2.2 Whiskers

Whiskers are dislocation-free filamentary single crystals whose aspect ratios are greater than 10. They are remarkable for their high strength which could approach the theoretical strength of the material [74]. Therefore, ceramic whiskers are very attractive materials for reinforcement in ceramic matrix composites to enhance the mechanical and thermal properties for high temperature and stress applications.

The main toughening mechanism in whisker-reinforced ceramic matrix composites are formation of microcracks, elastic strain energy absorbing, bridging and pull-out of whiskers and crack deflection around whiskers [75]. SiC whiskers, which present typical tensile strength about 8.4 GPa [76], are commonly used in SiC system. She et al. [77] firstly reported the preparation of the SiC whisker reinforced SiC ( $\text{SiC}_w/\text{SiC}$ ) composites (up to 10 vol.%). Although the addition of SiC whiskers inhibited the densification process, the fracture toughness increased with whisker amount from 4.65(monolithic SiC) to  $6.9 \text{ MPa}\cdot\text{m}^{1/2}$  (with 10 vol.% whiskers). Kim et al. [78] studied the effect of different  $\beta$ -SiC whiskers amount (0 to 20 wt.%) on the microstructure and mechanical properties of  $\text{SiC}_w/\text{SiC}$  composite. SiC whiskers grew abnormally, consuming neighboring fine grains and resulted a bimodal microstructure

consisted of large, rod-like  $\beta$ -SiC grains and fine, equiaxed  $\beta$ -SiC grains when 1-10 wt.% whiskers were added. Further addition of whiskers (20 wt.%) or annealing at higher temperatures led to a unimodal microstructure due to impingement of whiskers growth. The fracture toughness of bimodal microstructure increased with increasing whisker's amount from 2.8 (monolithic SiC) to 6.7  $\text{MPa}\cdot\text{m}^{1/2}$  (with 10 wt.% whiskers). Zhang et al. [79] dispersed 5 wt.% SiC into SiC powder by ball-milling and obtained  $\text{SiC}_w/\text{SiC}$  composites after subsequent pressureless sintering. The addition of SiC whiskers was beneficial to the densification process. The fracture toughness was slightly improved from 5.96 to 6.5  $\text{MPa}\cdot\text{m}^{1/2}$  while the bending strength was enhanced greatly from 416 to 1122 MPa (2.5 wt.%  $\text{SiC}_w$ +2.5wt.% TiN/SiC composites). However, the whiskers would be damaged during ball milling, which weakens their toughening effect. Moreover, continuous intergranular glassy phase from sintering aids, which will be softened and volatilized at elevated temperature, has a negative effect on high temperature properties of composites. Therefore, CVI method was adopted to fabricate  $\text{SiC}_w/\text{SiC}$  composites to avoid damage of whiskers and to eliminate sintering aids. Hua et al. [80] prepared 25 vol.%  $\text{SiC}_w/\text{SiC}$  composites without sintering aids by CVI method. The density, flexural strength and fracture toughness of obtained  $\text{SiC}_w/\text{SiC}$  composites were 88.72%, 305 MPa and 7.21  $\text{MPa}\cdot\text{m}^{1/2}$ , respectively. The improved fracture toughness was attributed to crack deflection, the bridging and pullout of whiskers. The low flexural strength was attributed to the random orientation of whiskers and weak bonding strength between whiskers and SiC matrix. Hua et al. [81] compared the mechanical properties of 37.2 vol.%  $\text{SiC}_p/\text{SiC}$  and 25.0 vol.%  $\text{SiC}_w/\text{SiC}$  composites prepared by CVI. The flexural strength and fracture toughness of  $\text{SiC}_p/\text{SiC}$  and  $\text{SiC}_w/\text{SiC}$  composites were 373 and 425 MPa, and 6.18 and 8.34  $\text{MPa}\cdot\text{m}^{1/2}$ , respectively. Hua et al. [82] further tested the high temperature properties of 25.0 vol.%  $\text{SiC}_w/\text{SiC}$  composites fabricated by CVI.  $\text{SiC}_w/\text{SiC}$  composites presented a constant strength of  $475 \pm 32$  MPa below 1000 °C, and then gradually declined to  $208 \pm 15$  MPa in range of 1000 to 1500 °C due to the decreased whisker-matrix interfacial bonding strength. Their fracture mode changed from the toughened to the brittle fracture above 1000 °C. Therefore, it could be concluded that the high temperature mechanical properties of  $\text{SiC}_w/\text{SiC}$  composites depends on the whiskers-matrix interfacial bonding strength. Wu et al. [83] firstly used rice husks to pyrolyze SiC whiskers, particles and amorphous carbon, which was mixed with  $\text{B}_4\text{C}$  as well as Mo powders to prepare a porous preform. Then molten Si was infiltrated into the preform to react with amorphous carbon,  $\text{B}_4\text{C}$  as well as Mo

and formed SiC,  $B_{12}(C,Si,B)_3$  as well as  $MoSi_2$ . The SiC whiskers acted as strong framework and improved the hardness of the composites.

### 1.2.2.3 Nano-phases

Carbon nanotubes (CNTs) are one dimensional carbon materials with length-diameter ratio greater than 1000. They can be envisioned as cylinders composed of rolled-up graphite planes with diameters in nanometer scale. The cylindrical nanotube usually has at least one end capped with a hemisphere of the buckyball structure. CNTs exist as either single-walled or multi-walled structures, and multi-walled carbon nanotubes (MWCNTs) are simply composed of concentric single-walled carbon nanotubes (SWCNTs). Generally, according to the rolling angle, the whole family of CNTs is classified as armchair, zigzag and chiral tubes of different diameters, as shown in Fig. 1.1 [84].

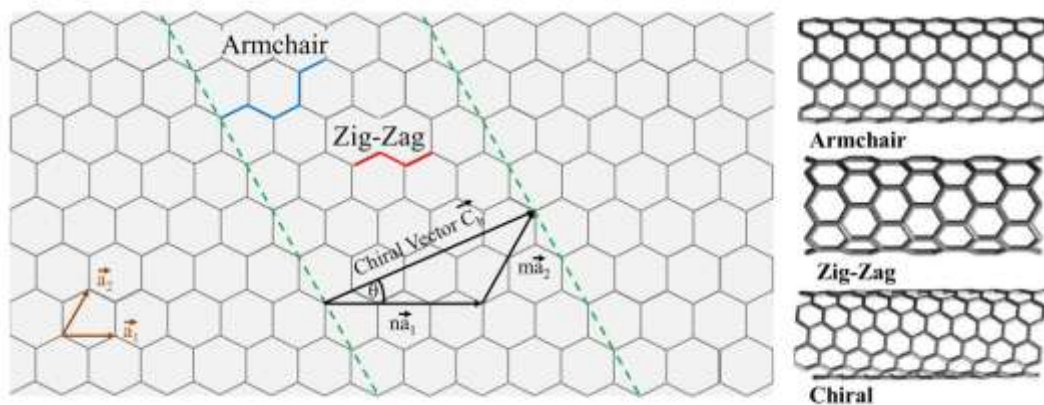


Fig. 1.1 Schematic diagram showing how a hexagonal sheet of graphene is rolled to form a CNT with different chiralities [84].

CNTs present very low density (typically lower than  $1.5 \text{ g/cm}^3$ ), extremely high elastic modulus (higher than 1 TPa) and strength (above 13 GPa). Furthermore, the high length-diameter ratio (greater than 1000), which is relevant to load transfer with the matrix, also make them very attractive as reinforcement. Moreover, they undergo plastic deformation under tensile strength and have an expected elongation to failure of 20–30% [85]. Therefore, the usage of CNTs to improve fracture toughness of brittle ceramic has been widely investigated in the past decades [86]. One of the biggest challenges in processing composites containing nanotubes is to achieve a good dispersion [87]. It is very important that the individual nanotubes are distributed uniformly throughout the matrix and well-separated from each other. The presence of

agglomerates is extremely detrimental to properties, especially in ceramic matrices, since they can act as defects leading to stress-concentration and premature failure. Moreover, with a good dispersion, strengthening and toughness effect of each nanotube could be fully developed. Another crucial factor for composites containing nanotubes is the interfacial bonding between the CNTs and the inorganic matrix [88], whose effect has been well proved in other composites system. Based on the experience of fibre-reinforced composite, their interfaces should be of intermediate strength to maximize the energy involved in debonding the CNTs from the matrix at the same time as maintaining effective interfacial load transfer. In the case of poor or strong interfacial bonding, CNTs may even act as a source of microcracks and lead to failure. Besides the common toughening mechanism (cracks deflection at the CNT/matrix interface, crack bridging by CNTs and CNT pullout), instead of crack formation, a new mechanism of nanotube collapse in “shear bands” was observed in some samples with certain geometries [89].

Ma et al. [90] firstly reported the preparation and mechanical properties of CNTs/ SiC composites. They dispersed nano-SiC powders and carbon nanotubes (10 wt.%) in butylalcohol using an ultrasonic shaker, and then hot-pressed the mixed powders. Sintering aids ( $B_4C$  in their work) was necessary for densification of CNTs/SiC composites. The addition of carbon nanotube slightly improved the bending strength and fracture toughness. Zhan et al. [91] fabricated fully dense nanocomposites of single-wall carbon nanotubes with nanocrystalline alumina matrix by spark-plasma sintering, and fracture toughness of  $9.7 \text{ MPa}\cdot\text{m}^{1/2}$ , which was nearly three times that of pure nanocrystalline alumina, have been achieved. These results demonstrated that the potential of CNTs as reinforcement in Ma’s research [90] had not been fully exploited. Hereafter, Kamalakaran et al. [92] synthesized CNTs/SiC composite flakes by spray pyrolysis, and observed their microstructure. Thostenson et al. [93] prepared CNTs/SiC composites by a reaction bonding technique. The addition of a small amount of CNTs decreased electrical resistivity of the ceramic composites significantly. Wang et al. [94] reported a rapid, low temperature microwave-induced reaction to create a novel nanoscale CNTs/SiC composite. The reaction, which was completed within 10 min, involved the decomposition of chloro-trimethylsilane and the simultaneous nucleation of nanoscale SiC spheres on the CNTs. The bulk composite was a branched tree-like structure comprised of three-dimensionally arrayed CNTs/SiC composite. Li et al [95] firstly modified the SWNTs by (iodomethyl)trimethylsilane via a radical reaction, and then SWNT/Si-C-N ceramics

with nanotube contents of up to 1 wt. % were obtained through pyrolysis of cross-linked SWNT/polymer composites at 1000 °C. The high viscosity of the SWNT/polysilazane mixtures was found to be the most important prerequisite for attaining good nanotube dispersion in the Si-C-N matrix. Wang et al. [96] fabricated MWNT-C<sub>f</sub>/SiC composite by polymer infiltration and pyrolysis process. After chemical treatment, MWNTs were dispersed in the antimony-substituted polymethylsilane (A-PMS). Then A-PMS containing MWNTs was infiltrated into 3D carbon fibre preforms and then the samples were pyrolyzed. The addition of 1.5 wt.% of MWNTs to the C<sub>f</sub>/SiC composite improved the flexural strength and fracture toughness 29.7% and 27.9%, respectively. Jiang et al. [97] prepared MWCNTs/SiC composites by tape casting, lamination and hot-pressing. It was found that the MWCNTs were retained after sintering. An improvement in toughness was observed in composite with 0.25 wt.% MWCNTs.

Carbon nanofibres (CNFs) are cylindrical nanostructures with graphene layers arranged as stacked cones, cups or plates. They have similar dimensions to MWNTs, and also present excellent mechanical properties (tensile strength: ~2.20 GPa and modulus: 100–300 GPa for 0.15 µm diameter nanofibres) [98]. In the composite application areas, CNFs are considered as relatively thick and long nanotubes without compromising on composite properties in comparison with CNTs. Therefore, CNFs have attracted remarkable attention as reinforcements of materials recently. Hirota et al. [99] dispersed CNFs into β-SiC powder and synthesized CNF/SiC composites (up to 15 vol.%) by pulsed electric-current pressure sintering. The 10 vol.% CNF/SiC composite exhibited a bending strength of ~720 MPa and a fracture toughness of ~5.5 MPa·m<sup>1/2</sup>. Moreover, CNF/SiC composite also presented higher mechanical properties at higher temperature (890 MPa at 1200 °C). Shimoda et al. [100] investigated the effect of CNFs (between 1 and 10 wt.%) on the thermal and mechanical properties of CNFs/SiC composites prepared by hot-pressing. CNFs dispersed well in CNFs/SiC composite with low CNFs contents (below 5 wt.%), and CNFs agglomerates and many pores located inside the agglomerates were observed in composite with 10 wt.% CNFs. The CNFs/SiC composite with 5 wt.% well dispersed CNFs exhibited enhanced thermal conductivity (80 W/m·K) and fracture toughness (5.7 MPa·m<sup>1/2</sup>). Kita et al. [101] fabricated CNFs/SiC composite by hot-pressing. The introduction of un-treated CNFs improved the fracture toughness from 3.8 (monolithic SiC) to 5.2 MPa·m<sup>1/2</sup> (with 6 wt.% CNTs). Moreover, the addition of acid-treated CNFs enhanced the relative density and fracture toughness to 99.0% and

5.7 MPa•m<sup>1/2</sup>, respectively. Taguchi et al. [102] discussed the effect of CNFs on the mechanical and thermal properties of SiC/SiC composites fabricated by the polymer impregnation and pyrolysis process. The addition of CNFs slightly decreased the bending strength and elastic modulus while improved the thermal conductivity of SiC/SiC composites. Borrell et al. [103] investigated the effect of CNFs (0–100 vol.%) on tribological behaviour of CNFs/SiC composites prepared by spark plasma sintering. Since CNTs acted as a sort of lubricating media in the interface, the wear rate CNFs/SiC composites decreased with increasing CNFs content.

Yang et al. [104–107] directly formed SiC nanowires on the surface of Tyranno-SA fibres, and then the SiC fibre preforms containing SiC nanowires were infiltrated by SiC matrix by CVI method. The formation of SiC nanowires significantly improved the bending strength and fracture toughness. Zheng et al. [108] reported the preparation of large-scale composite powders containing SiC particles and Si<sub>3</sub>N<sub>4</sub> nanowires by combustion synthesis. The obtained Si<sub>3</sub>N<sub>4</sub> nanowires were straight with uniform diameters of 20–350 nm and lengths of tens of microns. The growth directions of the nanowires were characterized to be [101] and [100].

As a promising thermal protection material, carbon fibre reinforced carbon (C/C) composite is different to other ceramic matrix composites (such as ZrB<sub>2</sub>- or SiC-based composite) since its matrix is graphite. The detailed literature survey of C/C composite will be discussed in “1.3 Modified C/C composites” individually. The research in fibre (mainly SiC and C fibre) reinforced SiC matrix composite is very extensive, detailed literature survey of fibre (continuous and chopped) reinforced SiC matrix composites will be given in “1.4 Continuous fibre reinforced SiC matrix composites” and “1.5 Short fibre reinforced SiC composite”, respectively.

## 1.3 Modified C/C composites

### 1.3.1.1 Processing of C/C composites

C/C composites are the material consisting of carbon fibres as the reinforcement in the matrix of graphite. They were developed for the nose cones of intercontinental ballistic missiles [109], and have been most widely known as the material for the nose cone and wing leading edges of the Space Shuttle [110].

The conventional preparation route of C/C composites could be divided into three stages [111]: (i). Carbon fibres are weaved to prepare preform of the desired structure

and shape. (ii). Densification of the composite, (iii). Transformation of amorphous carbon to crystalline graphite (graphitization heat treatment). The temperature of the graphitization treatment may vary within the range 1500–3000 °C. Typical graphitization temperature is 2500 °C. Graphitization of carbon-carbon composites results in increase of elastic modulus and strength of the composite [112].

The densification (second step) is the most essential process for preparation of C/C composite. This process could be achieved by liquid phase infiltration (LPI) [113,114] or chemical vapor infiltration (CVI) method [115,116]. The LPI route starts with the impregnated carbon fibre preform which consists of carbon fibres and a polymeric liquid carbon precursor (such as resin or pitch). The followed pyrolysis process at high temperature transforms the polymer to a carbon matrix [117]. The CVI process involves the infiltration of a carbonaceous gas (such as methane) into the carbon fibre preform at elevated temperatures. The gas decomposes and creates pyrolytic carbon matrix starting from fibre surface under proper processing condition [118]. The C/C composite fabricated by CVI presents higher mechanical properties than that by LPI method [119,120].

It should be noted high porosity accompanied by low strength is generally observed after once densification process, which due to mass loss of volatile materials and volume shrinkage of precursors during pyrolysis [121]. Therefore, three or more densification cycles are required to obtain desired density for C/C composite regardless of methods. Since the decomposition or pyrolysis processes are indispensable and very slow, it generally requires several weeks and several processing steps to make a single part [122]. Thus, the preparation process of C/C composites is very time- and cost-consuming, which greatly limits their applications.

### **1.3.1.2 Oxidation resistance of C/C composites**

C/C composites are very attractive for TPS application because of their low density, high specific stiffness, high specific strength, small thermal expansion coefficient, good corrosion and heat shock resistance ability [123]. Despite such many advantages, C/C composites without efficacious anti-oxidation coating could not be used above 500 °C due to severe oxidation [124]. Therefore, research work on C/C composites is mainly focused on promotion of oxidation resistance.

To present, there are two methods to improve oxidation properties of C/C composites, i. e. enhancing their own oxidation resistance and using anti-oxidation coatings. In the

first research field, B<sub>2</sub>O<sub>3</sub> [125], B<sub>4</sub>C [126], Si [127, 128], SiC [128, 129], MoSi<sub>2</sub> [130], ZrB<sub>2</sub> [126, 131], HfC [132], TaC [133] and ZrC [134] have been introduced into the graphite matrix as oxidation inhibitors. However, the improvement of this method is limited since the oxidation of carbon fibre could not be fully inhibited.

Making a thin oxidation-resistant coating (such as borides and silicides) on C/C composites has been proved to effectively improve the performance [135,136]. The coatings could be prepared by chemical vapor deposition (CVD) [137, 138], plasma activated chemical vapor deposition (PACVD) [139], sol-gel [140] and liquid-phase methods [141]. However, large thermal stress would be generated at the interface between coatings and C/C composites due to large thermo-physical difference. It will lead to the initiation and propagation of cracks and finally failure of coatings [142]. Therefore, optimization coating structure to avoid the thermo-physical mismatch of coatings and C/C composites plays an important role in developing future coatings. Recently, multi-component [143,144], multilayer [145,146] and composite graded coatings [147,148] have been widely investigated. However, to the present, there is still no C/C composite which could be used in oxidizing atmosphere above 2000 °C for long time.

## **1.4 Continuous fibre reinforced SiC matrix composites**

SiC and C are most commonly used fibre to improve the fracture toughness of ceramic matrix composites, and very exciting results have been obtained. The research in SiC and C fibre reinforced SiC matrix composites will be discussed in “1.4.1 SiC/SiC composites” and “1.4.2 C/SiC composites”, respectively.

### **1.4.1 SiC/SiC composites**

#### **1.4.1.1 SiC fibres**

Silicon carbide fibre reinforced silicon carbide matrix (SiC/SiC) composites have been suggested for high-temperature engineering applications due to their excellent specific mechanical properties at elevated temperature [149], and their good microstructural stability under high-energy neutron irradiation makes them attractive to be used as blanket components in fusion or structural material in fission reactors [150]. Properties of SiC fibres have a great influence on the final SiC/SiC composites. Hi-Nicalon, Tyranno-SA, Sylramic and SCS fibres, whose basic properties are listed

in Table 1.2 [151], are commercially available SiC fibres and have been widely investigated as reinforcement.

The performance of SiC fibres could be greatly affected by their composition and microstructure. Tensile strength and creep resistance of Nicalon fibre, which containing 11.7 wt.% oxygen, would be degraded due to carbothermal reduction reactions above 1200 °C [152]. Fig. 1.2 shows typical creep strain versus time curves for typical SiC fibres as measured at 1400 °C in air under a constant stress of 270 MPa [153].

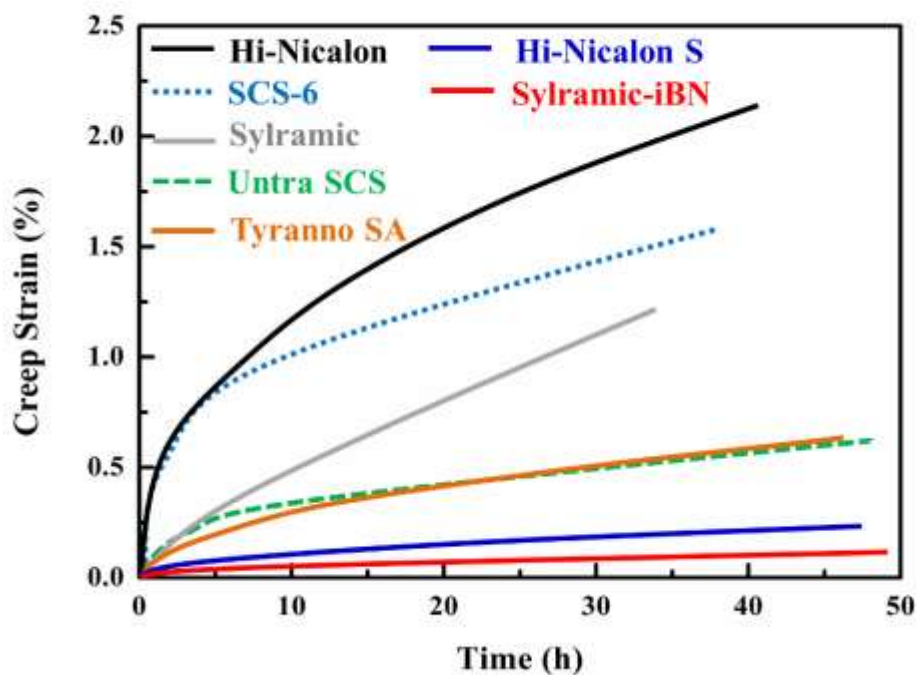


Fig. 1.2 Typical creep curves for SiC fibres tested at 1400 °C in air under a constant stress of 270 MPa [153].

Generally, the creep properties could be deteriorated by small grain size and by the high diffusion of impurity second phases at the grain boundaries. Growth of fine grain and decomposition of oxy-carbide second phases lead to a concurrent reduction in creep rate of Hi-Nicalon. SCS-6 and Sylramic fibres, which coarser grain (~100 nm) and high impurity, also show a high creep behavior. After elimination or minimization of second phases from grain boundaries, the fibres with coarser grain (~100 nm) demonstrate excellent creep resistance.

Table 1.2 Basic properties of Hi-Nicalon, Tyranno-SA, Sylramic and SCS fibres [151]

Trade Name	Manufacturer	Composition (wt.%)	Density (g/cm <sup>3</sup> )	Grain size (nm)	Average diameter ( $\mu$ m)	Room temperature properties		Cost (US\$/Kg)
						Tensile strength (GPa)	Tensile modulus (GPa)	
Hi-Nicalon	Nippon Carbon	62Si+37C+0.5O	2.74	5	14	2.8	270	8000
Hi-Nicalon Type S	Nippon Carbon	69Si+31C+0.2O	3.05	100	12	2.5	400	13000
Tyranno SA 1–3	UBE Industries	68Si+32C+0.6Al	3.02	200	7.5–10	2.8	375	5000
Sylramic	COI Ceramics	67Si+29C+0.8O +2.3B+0.4N+2.1Ti	3.05	100	10	3.2	400	10000
Sylramic-iBN	COI Ceramics	SiC+BN	3.05	>100	10	3.2	400	>10000
SCS-6-9/Ultra SCS	Specialty Materials	70Si+30C+traceSi+C	3	10–100	70–140	3.5–6	350–390	9000

Although ultra SCS display very high strength and creep properties, the diameter of these fibres is too larger (140  $\mu\text{m}$ ), which is not conducive to fibre shaping into complex architectural preforms and limits their applications. Therefore, Hi-Nicalon (the firstly developed second generation fibre), Hi-Nicalon Type S, Tyranno SA and Sylramic fibres are the most common SiC fibre used in SiC matrix composite.

#### **1.4.1.2 Processing of SiC/SiC composite**

After winding the SiC fibre into preform, common methods used to create the SiC matrix include chemical vapor infiltration (CVI) [154], polymer impregnation and pyrolysis (PIP) [155] and direct conversion processes (such as liquid silicon infiltration (LSI) [156]). CVI is very attractive because the damage of SiC fibre during processing is minimized. However, since the matrix densification would stop when surface pores are closed, CVI-SiC/SiC composites usually contain 10–20 vol.% porosity [157], which is very detrimental to their mechanical and thermal conductivity properties. PIP process offers the advantages of low processing temperature, high impregnation efficiency, controllable microstructure, availability of large-scale component with complicated shape and near-net shape technologies. However, significant volume shrinkage (larger than 60%) will occur due to extraordinary high volume shrinkage and pronounced density increase in the polymer-ceramic conversion. Therefore, several repetitions have to be performed to obtain a high densification level, which makes the process both time and cost-consuming [158]. Moreover, the insufficient crystallization of polymer-derived matrix also limits application of PIP process [159]. LSI process is well known to produce dense SiC with an applied pressure. It possesses the advantages of high density, good leak-tightness, good thermal conductivity and reasonable production cost. However, its application is still limited by several drawbacks. The presence of residual silicon phases from the infiltration of molten silicon will make the microstructure instable. Moreover, these residual silicon phases would also be detrimental to creep resistance and radiation behavior of SiC/SiC composites [160]. Meanwhile, significant fibre damages would occur in the reactive environment at elevated temperatures, which is also unfavorable for mechanical and thermal properties of SiC/SiC composites [161]. Since each method has its limitation, hybridization of two or three techniques seems to be an effective way to obtain a high-strength and homogeneous matrix. Hybrid CVI-PIP [162, 163], PIP-LSI [164, 165] techniques have been reported to prepare SiC/SiC composites. Improved SiC/SiC composites with high density and high

strength were successfully fabricated. In order to further improve the properties, CVI/Slurry infiltration/PIP has also been developed [166]. For compensation the polymer shrinkage during pyrolysis, CVI/ reaction bonding/PIP has been adopted [167]. Al powders, whose carburization and nitridation resulted in volume expansion, were added in the first infiltration process.

Recently, nano-infiltrated transient eutectoid (NITE) process [168–172] and electrophoretic deposition (EPD) [173–175] have been exploited to prepare SiC/SiC composite with high performance. Liquid phase sintering, which has long been considered inapplicable to SiC<sub>f</sub>/SiC processing due to too harsh sintering conditions for SiC-based fibres, is adopted in NITE process. The successful development of NITE attributes to optimization of sintering condition, appropriate protection of fibre, and emergence of the advanced SiC fibres. The matrix of NITE SiC/SiC consists of polycrystalline SiC and small amount of isolated oxide grains. However, there are some critical issues, such as stabilization of second phases at high temperatures and improvement of creep and oxidation resistance, that need to be overcome. Recently, in order to improve the thermo-mechanical performances of SiC/SiC composite, a process combined NITE and CVI was studied [176]. Although a nearly-full matrix densification was obtained, the prepared SiC/SiC composite presented a lower strength due to severe degradation of fibres and interphase. EPD is another technique adopted in fabrication of SiC/SiC composites recently. After hybridization with PIP method [175], SiC/SiC composites with relative high density and good thermal conductivity properties were obtained.

Despite their heterogeneous microstructure and their complex processing, hybrid processes demonstrate a very promising route to combine advantage of high material purity and process controllability of the CVI and cheaper process of LSI or PIP with less time-consuming. However, additional research and development have to be done in order to exploit the whole potential of combined processes.

#### **1.4.1.3 Interfaces**

The interface between reinforcement and matrix plays a very important role in the mechanical behavior of composites. It transfers load from matrix to fibres, prevents the early failure of the fibres and deflects the microcracks parallel to fibre axis. Therefore, great efforts have been made to optimize the interface in SiC/SiC composites. Coating SiC fibres with interphases layers is the simplest way to treat the

fibre surface. The best interphase materials for SiC/SiC composites have been postulated to be those with a layered structure paralleling to SiC fibre surface, while these layers are weakly bonded to each other but strongly adhere to fibres.

Pyrocarbon (PyC) and boron nitride (BN) have been well investigated as the single interphase. PyC has a structure similar to that of graphite in which graphene layers are stacked roughly parallel to each other. However, these elementary graphene layers are of limited size and stacked with rotational disorder [177]. The rough lamina-PyC, which is usually deposited by CVI, has a tendency to grow with grapheme layers parallel to fibre surface. To achieve a strong fibre/interphase (FI) bonding, Nicalon fibre should be pre-cleaned due to enrichment of oxygen and free carbon at the surface [178] while Hi-Nicalon fibres should be pre-treated to stabilize the microstructure [179]. The bonding between PyC and stoichiometric SiC fibres (Hi-Nicalon type S and Tyranno SA), which are more stable in microstructure and consist of free carbon on surface, is expected to be relative strong. Moreover, the thickness of PyC layer also has a great influence on the thermal residual stresses and fibre surface roughness, which finally affect the mechanical properties of SiC/PyC/SiC composites. Yang et al. [180] found that the tensile strength of SiC/PyC/SiC composites increased from 60 to near 300 MPa when the carbon layer thickness increases to 100 nm. Although PyC was thought to be the best interphase in SiC/SiC composite in terms of mechanical behavior, the oxidation of the PyC can occur even at low temperature (500 °C) and leads to interfacial degradation. Based on self-sealing mechanisms, boron (B) is doped into the single layer [181]. However, B<sub>2</sub>O<sub>3</sub> would volatilize at 600 °C in environments containing water, which significant reduce the lifetime of composite. Another method to improve PyC oxidation resistance is replace part of PyC by SiC or TiC to make a multilayer interphases, which will be discussed independently later. As an alternative, hexagonal BN, which has a layered structure similar to that of graphite, presents better oxidation behavior than PyC. The BN interphase could be deposited on SiC fibre by CVI from BF<sub>3</sub>-NH<sub>3</sub> [182], BCl<sub>3</sub>-NH<sub>3</sub>-H<sub>2</sub> [183] and B[N(CH<sub>3</sub>)<sub>2</sub>]<sub>3</sub> [184]. BN interphase could be formed by in situ reaction [185]. The occurrence of corrosion and chemical reactivity of BN with oxygen and moisture when prepared at low temperature still need to be solved.

As mentioned above, another method to improve the oxidation resistance of PyC or BN interphases is to prepare multilayer interphases. Multilayer interphases, which extend the concept of layered structure to the nanometer scales, are a stack of films of

different materials whose elementary sequence repeated several times. The oxidation resistance of SiC/SiC could be greatly improved after replacing oxidation-prone PyC or BN single-layer interphases (100–200 nm thick) by  $(\text{PyC-SiC})_n$  or  $(\text{BN-SiC})_n$  multilayer interphases in which the thickness of the PyC or BN is reduced to a few nanometers. This design is based on diffusion of oxygen element and formation of healing condensed oxides ( $\text{SiO}_2$  or/and  $\text{B}_2\text{O}_3$ ).  $(\text{PyC-SiC})_n$  are the most investigated multilayer interphases since the pioneering work of Droillard and his colleagues [186]. SiC sublayers are either microcrystallized (with rough SiC/PyC interfaces) [180] or nanocrystallized (with smooth SiC/PyC interfaces) [187]. Sublayer thickness is ranging from 3 to 100 nm for PyC and 10 to 500 nm for SiC while the number of PyC-SiC sequences is in the range of 3 to 10. PyC is usually deposited firstly on the fibre surface while SiC has also been deposited prior to increase fibre-interphases bonding [188]. Replacing the PyC single interphase by a  $(\text{PyC-SiC})_n$  multilayer interphase has little effect on the room-temperature tensile behavior of SiC/SiC composite with Hi-Nicalon fibres [189]. Similar conclusion has also been observed in SiC/SiC composite with Tyranno-SA fibres [190]. The lifetime of SiC/SiC composites with multilayer interphases at high temperature in air is improved over that with single PyC layer [189].

$(\text{BN-SiC})_n$  [191] and  $(\text{PyC-TiC})_n$  [192] have been studied also to improve the oxidation resistance. The advantage of  $(\text{BN-SiC})_n$  is that B atoms, which are beneficial for crack healing at intermediate temperatures, have already been in the interphases. Although the lifetime of Hi-Nicalon/SiC composites with  $(\text{BN-SiC})_n$  multilayer interphases demonstrated significant improvement over that with BN single interphase at 700 °C under load, the interfacial bonding between pretreated Hi-Nicalon fibre and BN was too weak, and then the crack deflection occurred at that interface and not within the multilayer interphases [191]. Although  $\text{TiO}_2$  is not commonly regarded as healing oxides,  $(\text{PyC-TiC})_n$  multilayer interphases could also improve the oxidation resistance of SiC/SiC composite. The lifetime of Hi-

Nicalon/SiC composites with  $(\text{PyC-TiC})_n$  multilayer interphases is much higher (>300 h) than that with PyC single-layer interphase (20 h) at 700 °C under load, which could be explained by the strong fibre-interphases bonding [192].

## 1.4.2 C/SiC composites

### 1.4.2.1 Carbon fibres

Although SiC/SiC composites have demonstrated very good mechanical and thermal properties, the high price of SiC fibres makes their adoption very difficult for wide application. Carbon fibre reinforced silicon carbide matrix (C/SiC) composites represent a relatively new class of structural materials for space and military applications.

Compared with SiC fibres, C fibres present lower density, high strength (for high strength fibre), high modulus (for high or ultra-high modulus fibre) and a very high thermal stability well above 2000 °C in inert atmosphere. Moreover, the price of continuous C fibre is much lower than that of SiC fibres (usually higher than 10000 US\$/Kg, as shown in [Table 1.2](#)). Intermediate-modulus carbon fibres can now be purchased for about 20 US\$/Kg, while high-modulus, highly conducting fibres can cost as much as 3000 US\$/Kg. The basic properties of some commercial carbon fibres are listed in [Table 1.3](#). The main drawback of C fibres is their low oxidation resistance which will lead to degradation in an oxidizing atmosphere beyond 450 °C [\[193\]](#).

Commercial carbon fibres are fabricated by using pitch or polyacrylonitrile (PAN) as the precursor. Producing C fibres from PAN involves polymerization of PAN, spinning of fibres, thermal stabilization, carbonization and graphitization. Production of pitch-based C fibres involves melt spinning of pitch precursor fibres, stabilization (oxidation), carbonization and graphitization. Pitch-based carbon fibres are theoretically capable of modulus equal to that of graphite single crystal (about 1000 GPa), which is significantly higher than the highest modulus obtained from PAN-based carbon fibres (650 GPa) [\[194\]](#). Pitch-based carbon fibres also demonstrate better electrical and thermal properties than PAN-based fibres.

### 1.4.2.2 Processing and interface of C/SiC composites

Generally, manufacturing techniques that have been used in processing SiC/SiC composite have all been adopted in fabrication of C/SiC composite. C/SiC composite have been prepared by CVI [\[195\]](#), PIP [\[196\]](#), liquid silicon infiltration (LSI) [\[197\]](#) and hybrid methods [\[198, 199\]](#). Since the advantage and disadvantage of these methods have been discussed in “[1.4.1.2 Processing of SiC/SiC composite](#)”, their application in C/SiC composite will not be further reviewed.

**Table 1.3** Basic properties of some commercial carbon fibres

Trade Name	Manufacturer	Density (g/cm <sup>3</sup> )	Room temperature tensile properties	
			Strength (GPa)	Modulus (GPa)
T300	Toray	1.76	3500	230
T700	Toray	1.80	4900	230
T1000	Toray	1.80	6400	300
M40	Toray	1.81	4400	380
HTA40	Toho	1.76	3950	238
IMS65	Toho	1.80	6000	290
UMS45	Toho	1.79	4500	430
SIGRAFIL C	SGL	1.80	3800	230
Panex35	Zoltek	1.81	4100	240
P-120S	Cytec Thornel	2.17	2400	820

Note: The data is from manufacturers' website.

To control the interfacial bonding between carbon fibre and SiC matrix, similar interphases (such as PyC [200, 201] and multilayer interphases [201, 202]) that developed for SiC/SiC composite have also been used in C/SiC composite. Thus, research in this field will not be dissertated.

#### **1.4.2.3 Improvement of oxidation resistance**

Due to thermal expansion mismatch between carbon fibre and SiC matrix, there are many pores and micro-cracks in the matrix. Therefore, combining with the low oxidation resistance of carbon fibre, C/SiC composites demonstrate very poor oxidation resistance, which cannot meet the requirement for long term application in

high temperature. Same to C/C composite, there are two methods to improve oxidation properties of C/SiC composites, i. e. enhancing their own oxidation resistance and using anti-oxidation coatings.

Boron-based particles, such as  $B_4C$  [203],  $ZrB_2$  [204] and  $SiB_4$  [205, 206], have been introduced into the SiC matrix to improve the oxidation resistance of C/SiC composite. Furthermore, Viricelle et al. [207, 208] designed multilayer self-sealing matrix to improve the oxidation resistance of SiC/SiC composites (by alternate chemical vapor infiltration of the boron-containing phases and SiC). The typical microstructure of multilayer matrix is shown in Fig. 1.3. SiC and boron-containing phases are expected to act as “mechanical fuse” (deflecting matrix cracks) and glass formers, respectively. At temperature range of 600 to 1200 °C,  $B_2O_3$ , which is formed due to oxidation of boron-containing phases, could fill the matrix cracks and improve oxidation properties. Moreover, microcracking and debonding between the different layers could occur in the multilayered matrix. The function is as same as that of multilayered interface between the fibre and the matrix, and could improve the fracture toughness. Furthermore, the deflection of microcracks in the matrix and debonding between layers will provide new energy-dissipating mechanisms, apart from matrix microcracking, fibre/matrix debonding and fibre pull-out. Therefore, it will be very interesting to investigate the mechanical behavior of this new multilayered matrix. Liu et al. [209] prepared this new kind matrix in C/SiC composite, and found that flexural strength of C/SiC- $BC_x$  composites decreased about 20% while fracture toughness increased about 19% due to weak-bonding interface between  $BC_x$ /SiC. However, Zhang et al. [210] observed that tensile strength and failure strain of the C/Si-B-C increase with temperatures up to 1000 °C, then decreased with temperature. The interlaminar shear strength (ILSS) and the in-plane shear strength (IPSS) demonstrated the similar tendency to the tensile strength. He attributed these behaviors to the thermal residual stress and crystallization of  $B_4C$  in the multilayered matrix. Therefore, the processing and composition have a great influence on the mechanical behavior of this new kind matrix, and more work should be done for fully understanding the properties of the matrix.

Anti-oxidation coatings based on SiC or other self-healing glass oxides for C/SiC composite have been well investigated in the past decades. CVD SiC is a fundamental coating material because the oxidation of SiC is passive up to 1700 °C and the formed  $SiO_2$  film has a low oxygen diffusion coefficient. Yttrium silicate, which has similar

thermal expansion coefficient with SiC, low evaporation rate and low permeability for oxygen, is another candidate for anti-oxidation coating materials [211]. However, the defect such as cracks in coating, which is unavoidable due the thermal expansion mismatch between composites and matrix, lead to oxygen diffusion inward and oxidation of interface and fibre [212]. Therefore, composite coatings (Si-MoSi<sub>2</sub> [213], 3Al<sub>2</sub>O<sub>3</sub>-2SiO<sub>2</sub> mullite [214], HfB<sub>2</sub>-SiC [215], SiOC-barium-strontium aluminosilicate [216] and SiCN-Sc<sub>2</sub>Si<sub>2</sub>O<sub>7</sub> [217]), multilayer coatings (SiC/B/SiC [218], SiC/C-B/SiC [219] and ZrC/SiC [220]) and composite multilayer coatings (Y<sub>2</sub>Si<sub>2</sub>O<sub>7</sub>/celsian-Y<sub>2</sub>SiO<sub>5</sub> [221] and ZrB<sub>2</sub>-SiC/SiC [222]) have been studied.

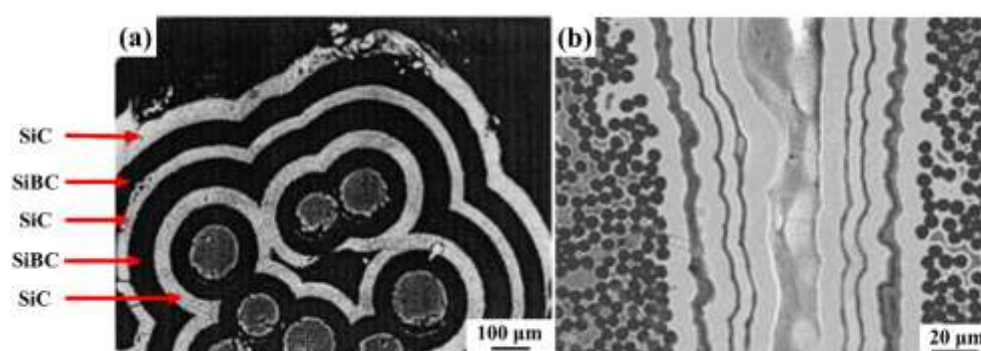


Fig. 1.3 Typical microstructure of multilayered matrix in (a) SiC/SiC [207] and (b) C/SiC composites [210].

However, due to the anisotropic thermal expansion behavior of C/SiC, the oxidation protection is more difficult than for non-reinforced carbon or graphite bulk materials. Therefore, cracks are apt to form due to the thermal expansion mismatch between coating and the C/SiC composite when temperature changes dramatically. As a result, sophisticated oxidation and corrosion coatings could only reduce the material degradation in a certain temperature interval under static conditions, but all available protection coatings are not able to prevent oxidation completely under dynamic conditions.

## 1.5 Short fibre reinforced SiC composites

Although SiC-based composites with long carbon fibres display greatly improved toughness, processing of these composites (CVI, PIP and LSI) is usually time-consuming and very expensive. Moreover, owing to their high matrix porosity, they easily undergo oxidation and then need tailored surface coatings for application

as TPS of space vehicles. Therefore, as an alternative, SiC composites reinforced with short SiC or C fibres have been widely studied recently, because of their easy adaptability to conventional manufacturing techniques and low fabrication cost [223]. Additionally, only the short fibres which directly get in touch with the oxidizing atmosphere suffer degradation, whereas the inner fibres would be protected by the SiC matrix [224]. The research in SiC matrix composite reinforced with short SiC and carbon fibre ( $\text{SiC}_{\text{sf}}/\text{SiC}$  and  $\text{C}_{\text{sf}}/\text{SiC}$ ) will be dissertated in “1.5.1  $\text{SiC}_{\text{sf}}/\text{SiC}$  composites” and “1.5.2  $\text{C}_{\text{sf}}/\text{SiC}$  composites”, respectively.

### 1.5.1 $\text{SiC}_{\text{sf}}/\text{SiC}$ composites

Itatani et al. [225] firstly prepared 10-50 wt.% (10.5–51.2 vol.%)  $\text{SiC}_{\text{sf}}/\text{SiC}$  composites by hot-pressing with sintering aid of  $\text{Al}_4\text{C}_3$ . The chopped SiC fibres were dispersed with SiC powders by ball-milling. The 5 mol.% of  $\text{Al}_4\text{C}_3$  was found to be the best amount for densification of SiC composite. The fracture toughnesses of SiC composites with 20-40 wt.% were between 3.2–3.4  $\text{MPa}\cdot\text{m}^{1/2}$ , which was about 1.5 times of that of hot-pressed SiC ceramic (2.4  $\text{MPa}\cdot\text{m}^{1/2}$ ). Furthermore, 40 wt.%  $\text{SiC}_{\text{sf}}/\text{SiC}$  composites with 5 mol.%  $\text{Al}_4\text{C}_3$  showed excellent heat-resistance at 1300 °C in air due to the formation of a  $\text{SiO}_2$  layer at and near exposed surfaces. Sato et al. [226] further investigated the effect of SiC fibre length on the mechanical properties of  $\text{SiC}_{\text{sf}}/\text{SiC}$ . The original mean fibre lengths were 214, 394 and 706  $\mu\text{m}$ , respectively. The short SiC fibres were mixed with SiC powder by ball-milling, and the  $\text{SiC}_{\text{sf}}/\text{SiC}$  composites containing 0–50 wt.% chopped SiC fibre were fabricated by hot-pressing. Flexural strength decreased with increasing of mean fibre length from 380 (214  $\mu\text{m}$ ) to 281 MPa (706  $\mu\text{m}$ ) for 30.wt.%  $\text{SiC}_{\text{sf}}/\text{SiC}$  composites. However, fracture toughness increased with mean fibre length from 3.4 (214  $\mu\text{m}$ ) to 4.7  $\text{MPa}\cdot\text{m}^{1/2}$  (706  $\mu\text{m}$ ) for 40.wt.%  $\text{SiC}_{\text{sf}}/\text{SiC}$  composites. Moreover, 100 nm carbon layer on 706  $\mu\text{m}$  SiC fibre further improved the fracture toughness to 6.0  $\text{MPa}\cdot\text{m}^{1/2}$ . They also investigated the effect of short SiC fibre on the thermal conductivity properties of  $\text{SiC}_{\text{sf}}/\text{SiC}$  composites [227]. Addition of chopped SiC fibres (more than 20 wt.%) increased the thermal conductivity, and the 100 nm carbon interface showed little effect on the thermal properties.

Lee et al. [228, 229] prepared the  $\text{SiC}_{\text{sf}}/\text{SiC}$  composites by tape casting and hot-pressing. Short SiC fibres (3 mm) were added into SiC slurry by ball-milling and  $\text{Al}_2\text{O}_3\text{-Y}_2\text{O}_3\text{-CaO}$  was used as sintering additive. Most of SiC short fibres were

oriented along the tape casting direction. The relative density increased with sintering temperature. They also observed that the bending strength and fracture toughness increased with sintering temperature, which indicates the mechanical properties have a very strong relationship with relative density from my point of view. They tested the high temperature mechanical properties of SiC<sub>sf</sub>/SiC composites up to 1400 °C. The maximum strength decreased with fibre amount and testing temperature, and all samples demonstrated almost same strength at 1400 °C. These results imply that the degradation of SiC fibre at high temperature affected strength, and weakening of matrix grain boundary phase dominates the strength at 1400 °C. Therefore, it could be concluded that the Al<sub>2</sub>O<sub>3</sub>-Y<sub>2</sub>O<sub>3</sub>-CaO system, which will be softened at high temperature, is not a favorable sintering aid for application at high temperature. Moreover, in order to modify the interfacial bonding between fibre and matrix, polycarbosilane (PCS) was coated on the short SiC carbon surface [230]. However, the PCS coating did not form a uniform, weak and reaction barrier layer in their work.

### 1.5.2 C<sub>sf</sub>/SiC composites

Ju et al. [231] firstly prepared 10 vol.% C<sub>sf</sub>/SiC composites by hot-pressing. The short carbon fibres and SiC powder with sintering aids were dispersed by ultrasonic in *n*-octyl alcohol. A mixture of 2 wt.% AlN and 0.5 wt.% graphite was found to be the most effective sintering aid for SiC and C<sub>sf</sub>/SiC composites among AlN, Al<sub>2</sub>O<sub>3</sub>, B<sub>4</sub>C, graphite, AlN+B<sub>4</sub>C, AlN+graphite, B<sub>4</sub>C+graphite and Al<sub>2</sub>O<sub>3</sub>+B<sub>4</sub>C. Addition of short carbon fibres decreased the density and strength of C<sub>sf</sub>/SiC composites due to the higher porosity level. However, introduction of short C fibre improved the wear properties because of the formation of a thin, smooth and adherent debris film.

Li et al. [232] fabricated C<sub>sf</sub>/SiC functionally graded composites by spark plasma sintering (SPS). The short carbon fibres and SiC powder with sintering aids (graphite together with Al<sub>2</sub>O<sub>3</sub>, AlN, and B<sub>4</sub>C in different ratios, respectively) were dispersed by ultrasonic in cyclohexanol. They concluded that B<sub>4</sub>C+graphite were not suitable for C<sub>sf</sub>/SiC composites. However, only microstructure of C<sub>sf</sub>/SiC composites with 10 to 40 vol.% short carbon fibre was shown in the literature and no follow-up research was reported.

Zhou et al. [233] obtained 0–20 vol.% C<sub>sf</sub>/SiC composites by hot-pressing. The chopped C fibres (3–5 mm) were dispersed in SiC powder with sintering aids (0.4 wt.% B<sub>4</sub>C+2 wt.% C) by ball-milling. The fibres were dispersed well in the obtained

the composite. However, relative density and bending strength decreased while fracture toughness increased with fibre amount. The added C fibre did not demonstrate any lubricating effect under low load condition while the friction coefficients of C<sub>sf</sub>/SiC composites were much lower than that of monolithic SiC.

Tang et al. [234] investigated the mechanical and tribological properties of C<sub>sf</sub>/SiC composites with fibre amount up to 53 vol.%. The short C fibres were firstly dispersed in ethanol with OP-10 as dispersing agents by magnetic stirrer for 2 h, and then mixed with SiC and 1 wt.% Si+Al+B additives by ball-milling. The composites were prepared by hot-pressing. The average friction coefficients decreased linearly with fibre amount. Fracture toughness increased with fibre amount to 7.1 MPa•m<sup>1/2</sup> (with 53 vol.% fibre). However, bending strength decreased with increasing fibre amount over 15 vol.%.

He et al. [235–237] prepared 20 vol.% C<sub>sf</sub>/SiC composites by hot-pressing. The short C fibres (4–6 mm) were dispersed in ethanol by ultrasonic for 30 min, and then the mixed SiC+polycarbosilane (PCS) was added to the suspension and this new suspension was further dispersed for 30 min. MgO+Al<sub>2</sub>O<sub>3</sub>+Y<sub>2</sub>O<sub>3</sub> was used as sintering aids. The relative density, bending strength and fracture toughness increased with amount of additives [235]. The amorphous interphase in the composites protected the fibres from direct contact with matrix and improved the fibre-matrix bonding [235, 236]. Actually, the relative density increased firstly with PCS amount (0–20 wt.%) and then decreased with more PCS (20–40 wt.%), and bending strength and fracture toughness showed the same trend [237]. Although they did not conclude in their work [237], it is obvious that the mechanical properties of C<sub>sf</sub>/SiC composites have a very strong relationship with relative density.

Zhang et al. fabricated 30 vol.% C<sub>sf</sub>/SiC composites by hot-pressing using Al<sub>2</sub>O<sub>3</sub>/Y<sub>2</sub>O<sub>3</sub> [238] or Al<sub>2</sub>O<sub>3</sub>/La<sub>2</sub>O<sub>3</sub> [239, 240] as sintering additives. They mixed the short carbon fibre with SiC powder by ball-milling. Reaction of Al<sub>2</sub>O<sub>3</sub>/Y<sub>2</sub>O<sub>3</sub> additives with SiO<sub>2</sub> on the surface of SiC or its oxidation products caused formation and distribution of an amorphous low-eutectic-point phase around the SiC grains and carbon fibres. Coupling with high sintering temperature, severe diffusion of yttrium ions into carbon fibre with the contribution of the amorphous film was observed. Excess sintering additives improved the room-temperature flexural strength but decreased the fracture toughness [238]. Al<sub>2</sub>O<sub>3</sub>/La<sub>2</sub>O<sub>3</sub> was found to be another effective additive in their work. It is very interesting to observe the formation of SiC nano-whisker structure during

annealing at 1750 °C for 1 h. Although the formation mechanism was not clear, this kind of whisker structure was beneficial for mechanical properties.

Ding et al. [241] prepared  $C_{sf}/SiC$  composites by spark plasma sintering (SPS). The short C fibres (3 mm) were ultrasonically dispersed into the mixed slurry with SiC and sintering aids to avoid the damage of the fibres. The mechanical properties of obtained  $C_{sf}/SiC$  composites were much lower than the monolithic SiC. However, the relative density, bending strength and modulus increased with sintering temperature. The poor mechanical properties of obtained  $C_{sf}/SiC$  composites should be attributed to the micro-cracks which are generated during process due to large thermal expansion mismatch between fibre and matrix.

Zhang et al. [242] fabricated  $C_{sf}/SiC$  composites by liquid silicon infiltration. Chopped C fibres (3 mm) were pretreated by ultrasonic and then mixed with SiC+C suspension by ball milling. SiC matrix was bonded by the reaction between liquid infiltrated Si and C. Relative density, bending strength and fracture toughness increased with fibre amount up to 30 vol.% and then decreased. However, due to the reaction with liquid silicon, C fibres have been completely converted into SiC. Moreover, the average C fibre length in the final composite was about 60  $\mu m$  due to high velocity impact during ball-milling.

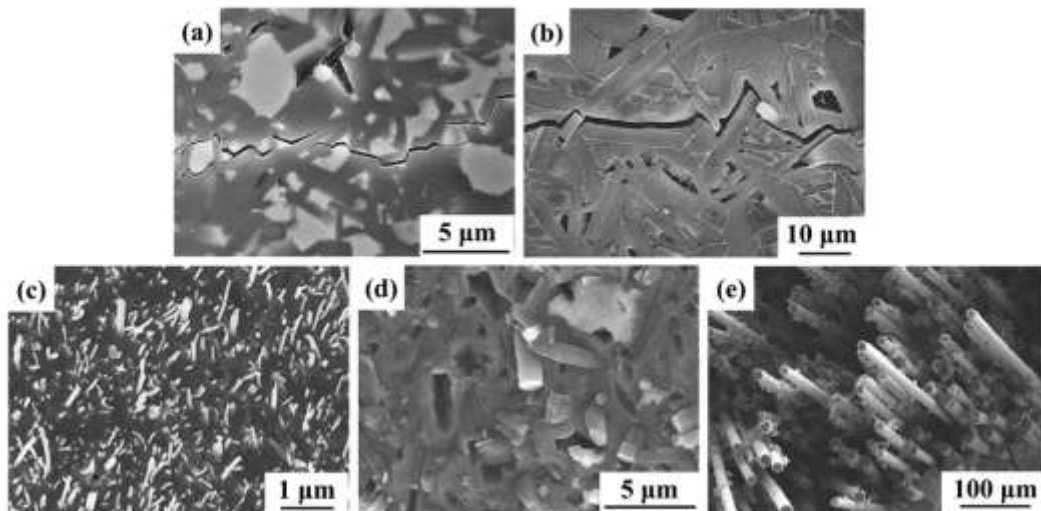


**Fig. 1.4** Main toughening mechanisms in ceramic composites. (a) Crack deflection [44], (b) Pull-out and bridging of elongated grain [63], Pull-out of (c) nanotubes [158], (d) whiskers [80] and (e) fibres [167].

Raether et al. [243] investigated the oxidation behavior of  $C_{sf}/SiC$  composites. The

short C fibres were not dispersed but in bundle. The oxidation occurred along the short C fibre bundles and their contact was the dominating mechanism while the effect of micro-cracks on the oxidation behavior could be neglected.

As a summary of above literature discussion about ceramic composites, the main toughening mechanisms in ceramic matrix composites are crack deflection by second phases, pull-out and bridging of reinforcement, as shown in Fig. 1.4.

## 1.6 Ceramic multilayers

### 1.6.1 Ceramic multilayers

Although a great progress in toughening ceramic has been achieved by introduction of secondary phases, the brittleness of ceramic has not been overcome in nature except of long fibre reinforced ceramic matrix composite. In research of natural biomaterials, such as turtleshell and nacre, it has been found that these natural biomaterials have well-constructed laminated structures, as shown in Fig. 1.5 [244, 245]. Nacre consists of more than 99 vol.% inorganic phase, aragonite wafers, and less than 1 vol.% organic phase, mortar of proteins. This particular configuration imparts over one order of magnitude higher bending strength and toughness than those of aragonite single crystals. The work of fracture of nacre is 3000 times higher than that of pure aragonite [246].

Clegg et al. [247] originally reported the preparation and mechanical properties of SiC/C multilayer in 1990. SiC powder with 0.4 wt.% B was firstly mixed, and the dough-like material was pressed into a 2-mm-thick-sheet and then rolled into flat sheets (about 200  $\mu\text{m}$  in thickness). After cutting, the thin SiC sheets were coated with graphite, stacked and pressed to form a plaque  $\sim 2$  mm thick. After debinding and sintering, a SiC/C multilayer with relative density of 98% was obtained. The load/deflection behavior of monolithic and laminated SiC is shown in Fig. 1.6. The monolithic SiC behaved in a linear elastic fashion until catastrophic failure. The laminated materials also deformed in a linear elastic fashion until the crack reached the same stress intensity as the monolithic SiC, and then the cracks deflected along the SiC-C interface. The apparent toughness increased from 3.6 to 15  $\text{MPa}\cdot\text{m}^{1/2}$ , and the work of fracture increased from 28 to 4625  $\text{J}/\text{m}^2$ . Furthermore, Clegg et al. built a numerical model (using Monte Carlo method) to simulate the fracture behavior of SiC-graphite lamillates [248–253]. The built model allowed accurate prediction of both

load/distancement curves and the absorption of energy within the specimens (by interfacial cracking).

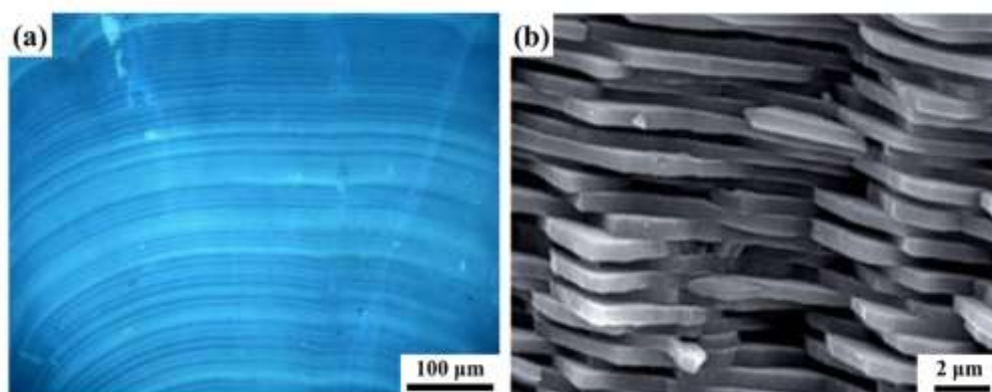


Fig. 1.5 Typical microstructure of nacre. (a) Aragonite layers [244] and (b) Fracture surface of aragonite layers in the nacre of a blue mussel [245].

However, due to difference in thermal expansion behavior between the SiC and interlayer (i.e. graphite), delamination was usually found during sintering. The interfacial materials must be chemically compatible with the laminate to be both co-fired and later used at an elevated temperature. Moreover, it must also reliably deflect cracks [254]. The requirement of chemical compatibility suggests that both lamina and interlayer should ideally be made from the same material, which implies that porous interlayers could be used. Group of Clegg firstly established that the levels of porosity to ensure crack deflection should be more than 37 vol.% [254], which is in accordance with their experimental results [255]. However, Reynaud et al. [256] found that even composites containing more than 40 vol.% porosity interlayers behaved in a brittle manner, and Tariolle et al. [257] found a significant deflection for a rather high value (46 vol.%) in  $B_4C$ . Actually, Leguillon and his coworkers calculated that the porosity required for crack deflection decreases with the porous layers thickness [258], which can explain the contradictions. Although increase of porosity in the porous interlayers could promote crack deflection and hence increase the fracture toughness, pore interaction effect in the porous interlayers cannot be neglected. There is a critical volume fraction (60 vol.% observed by Ma et al. [259] in  $Al_2O_3$  lamillates) above which the fracture energy of the system decreased with porosity.

Up to the present, many ceramic multilayer structures have been reported in the literature: SiC [260–264], SiC/C [247–253], SiC/porous SiC [255, 257], SiC/porous

Al<sub>2</sub>O<sub>3</sub> [265, 266], SiC/BN [267], Al<sub>2</sub>O<sub>3</sub>/porous Al<sub>2</sub>O<sub>3</sub> [259], Al<sub>2</sub>O<sub>3</sub>/SiC [268, 269], Al<sub>2</sub>O<sub>3</sub>/TiN [270], Al<sub>2</sub>O<sub>3</sub>/TiC [271], Al<sub>2</sub>O<sub>3</sub>/Ti<sub>3</sub>SiC<sub>2</sub> [272, 273], Al<sub>2</sub>O<sub>3</sub>/ZrO<sub>2</sub> [274, 275], Si<sub>3</sub>N<sub>4</sub> [276], Si<sub>3</sub>N<sub>4</sub>/SiC [277], Si<sub>3</sub>N<sub>4</sub>/BN [278, 279], Si<sub>3</sub>N<sub>4</sub>/Ti<sub>3</sub>SiC<sub>2</sub> [280], MoSi<sub>2</sub>/SiC [281].

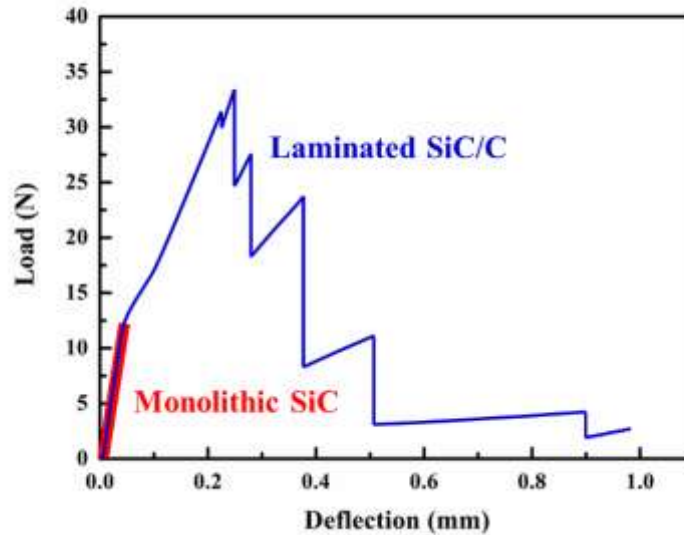


Fig. 1.6 The load/deflection behavior of monolithic and laminated SiC [247].

Theoretically, coupling the toughening mechanism in composites (microcracks, bridging and pull-out of secondary phases and crack deflection around reinforcements) and multilayer structures (residual thermal stress, crack deflection at weak interface, crack bifurcation in compressive layers [275, 282] and tunnel cracks in tensile layers [283]) could further improve the toughness. Therefore, many efforts have been devoted to preparation of multilayer with toughening single composite layer. Detail literature survey of ceramic multilayer composites will be given in “1.7 Ceramic multilayer composites”.

### 1.6.2 Processing of ceramic multilayers

Mechanical rolling was used in the first work of ceramic multilayer structure. Clegg et al. [247, 248] mixed the powder with aqueous solution and then pressed samples into 2-mm-thick sheets, which was finally rolled into 200- $\mu$ m-thick flat sheets. Sputtering [281], extrusion-molding [269] and powder injection molding [284] have also been reported to prepare ceramic multilayers. In the past decades, many methods, such as slip casting, gel casting, freeze casting, centrifugal casting, electrophoretic deposition

and tape casting, have been adopted for preparation of ceramic multilayers. Recently, deposition methods have also been adopted to fabricate multilayers.

### 1.6.2.1 Slip casting

Slip casting of ceramics is a technique that has long been used for manufacturing traditional ceramics. Slurry, also known as slip, is firstly prepared by ball-milling ceramic powders along with binders, plasticizers, deflocculants, etc., in a solvent or water. Subsequently, the slip is poured into a porous mold (usually plaster of Paris), where the liquid parts of slip will be absorbed by capillary action, and then a ceramic layer with desired thickness could be formed against the plaster. After sequential slip casting of different powder- suspension and sintering, the multilayer composites could be obtained.

Requena et al. [285] fabricated  $\text{Al}_2\text{O}_3/\text{Al}_2\text{O}_3+4 \text{ vol.}\% \text{ZrO}_2$  multilayer composites by slip casting. The layer thickness of  $\text{Al}_2\text{O}_3$  and  $\text{Al}_2\text{O}_3+4 \text{ vol.}\% \text{ZrO}_2$  was about 170  $\mu\text{m}$ . Zhang et al. [286] prepared SiC/C multilayers by slip casting. The thicknesses of graphite layers and SiC layers were varied from 3 to 20 and 100 to 600  $\mu\text{m}$ , respectively. Apparent fracture toughness increased from 4 to 14  $\text{MPa}\cdot\text{m}^{1/2}$ , and a strong effect of SiC and graphite layer thickness on apparent fracture toughness and bending strength was observed. Yu et al. [287] obtained SiC/C multilayers by slip casting. The SiC/C multilayers demonstrated a non-linear load-displacement behavior and exhibited gradual, non-catastrophic failure. Yu et al. [277] further prepared SiC/ $\text{Si}_3\text{N}_4$  multilayer composites by slip casting. The work of fracture as high as 406  $\text{kJ}/\text{m}^3$ , fracture toughness as high as 21  $\text{MPa}\cdot\text{m}^{1/2}$  and a strength of 380 MPa have been achieved.

### 1.6.2.2 Gel casting

Gel casting is a forming process similar to slip casting for making complex-shaped parts. It was first developed for ceramic forming by Prof. Omatete and his coworkers [288]. In the process, ceramic powders are dispersed into a water-based monomer solution. After a catalyst and initiator are added, the slurry solidifies to form a strong, crosslinked solvent-polymer gel filled with the ceramic powder. This forming process has two outstanding advantages: (I) Capability of producing ceramic components with complicated shape; (II) Green body could be machined due to its high strength [289]. However, in the initial period after its invention, the process did not appear very attractive from industry due to usage of toxic organic additives. Then, Janney et al.

[290] reported that methacrylamide (MAM) with methylene bisacrylamide (MBAM) as monomer and cross-linker were suitable for aqueous gelcasting, and they were much lower in toxicity as compared to the previously used acrylamides [288].

Montgomery et al. [291] prepared the  $\text{Al}_2\text{O}_3$ /porous  $\text{Al}_2\text{O}_3$  bilayers by gel casting. They first casted a lower density slurry, and a higher density slurry was then immediately casted beneath the first layer, and then both layers were gelled simultaneously. This method induced a small gradation between the two layers. They found that the volume change of each layer can be matched by tailoring the  $\text{Al}_2\text{O}_3$  particle size and Al volume fraction, which resulted in a density step and no macroscopic cracking. Montgomery et al. [292] reported another method to produce a sharp interface between two layers. They partially filled a steel mold with initiated slurry, which was then frozen immediately by dry ice. A glass slide was placed in contact with the slurry to close the system and create a flat surface. After removal of the glass slide, the second initiated slurry containing pore-forming fugitive filler was cast on the solid surface of the frozen layer. Finally, the entire filled mold system was heated to simultaneously gel both layers. It was observed that the failure initiated at the interface between the layers due to stress redistribution by modulus mismatch. Baskin et al [293] fabricated single-phase laminates with alternating layers of aligned and randomly oriented  $\text{FeTiO}_5$  by gel casting. A mold with removable dividers was used in their work, and the preparation process of laminates is shown in Fig. 1.7. Hovis et al. [294] using a stackable mold system, Neoprene gaskets and Escalt film-covered glass slides to produce  $\text{BaFe}_{12}\text{O}_{19}$  laminates by gel casting, as shown in Fig. 1.8.

Based on the similar laminate processing method of Hovis et al [294], Montgomery et al. [295, 296] used thermoreversible gelcasting (TRG) to produce  $\text{Al}_2\text{O}_3$  laminates. TRG involves a rapid, reversible, cross-linking process to form a polymer network rather than a monomer reaction as in traditional gelcasting. The reversible polymer gel is a triblock copolymer, whose midblock is selectively solvated by an alcohol. Below  $T_{\text{gel}}$  (60 °C in their work), the triblock copolymer end blocks aggregate into nanometer size spherical domains, which are randomly dispersed in a matrix of solvent and solvated midblocks. The aggregates provide the sites for physical crosslinking. Above  $T_{\text{gel}}$  (60 °C in their work), the end blocks dissociate and create a freely flowing liquid. The thermoreversible gel can maintain its thermoreversibility even being filled with high amount ceramic powder. Since the solid can be reheated to form a liquid and

then be re-casted, the waste of ceramic powders and polymers could be minimized [295, 296].

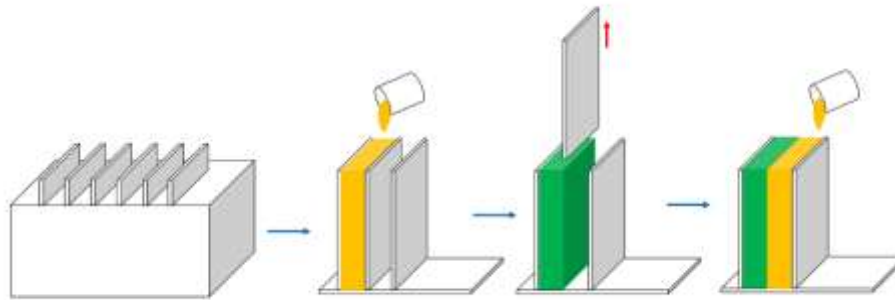


Fig. 1.7 Laminates preparation method by gel casting reported by Baskin et al. [293].

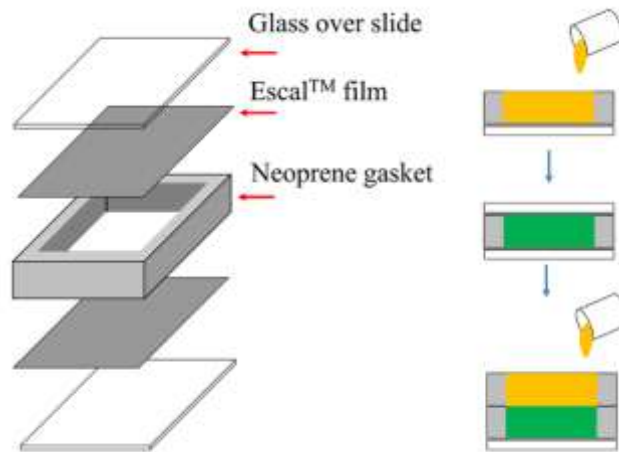


Fig. 1.8 Laminates preparation method by gel casting reported by Hovis et al. [294].

### 1.6.2.3 Freeze casting

Freeze casting technique is a novel environmentally friendly forming method, which has attracted much attention due to its simplicity and the absence of organic substances [297]. In the forming process, the ceramic suspension (water is used as solvent) is poured into a mold, then frozen and subjected to sublimative drying of the solvent (water) under vacuum. Frozen water (ice) temporarily acts as a binder to hold the parts together for unmolding. The sublimation of the solvent (water) is made to eliminate the drying stress, and to avoid shrinkage, cracks and warpage of the green body that generally existing in the normal drying [298].

Munch et al. [299] formed large porous  $\text{Al}_2\text{O}_3$  scaffolds with architectures by freeze

casting. The layered  $\text{Al}_2\text{O}_3$  scaffolds were subsequently infiltrated with the polymeric second phase. They also fabricate nacre-like “brick-and-mortar” structures, with very high ceramic content, by subsequently pressing the scaffolds in the direction perpendicular to the lamellae in order to collapse them, followed by a second sintering step to promote densification and the formation of ceramic bridges between the “bricks”. The lamellar composites and brick-and-mortar architectures are shown in Fig. 1.9a and b, respectively. The final composites demonstrated bending strength over 200 MPa and fracture toughness as high as  $30 \text{ MPa}\cdot\text{m}^{1/2}$ . Their fracture behavior is similar to that of nature nacre, as shown in Fig. 1.9c and d.

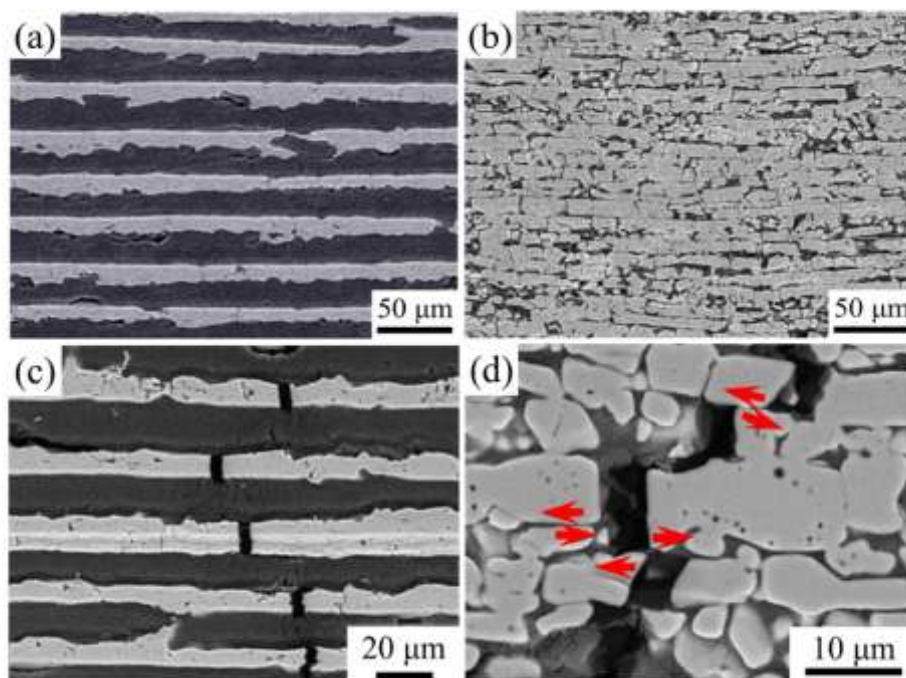


Fig. 1.9 Typical microstructure and fracture behavior of  $\text{Al}_2\text{O}_3/\text{PMMA}$  composites prepared by Munch et al. [299]. (a) Microstructure of lamellar architecture, (b) Microstructure of brick-and-mortar architecture, (c) Fracture behavior of lamellar architecture and (d) Fracture behavior of brick-and-mortar architecture.

Freeze casting technique is mainly used for the preparation of porous ceramics with widely controllable porosity. Aligned pore channels and a porous gradient can be achieved via controlling the freezing direction and temperature gradient [300]. Koh et al. [301] prepared in-situ dense/porous bi-layered yttria-stabilized zirconia (YSZ) composites by freeze casting technique. The thickness of dense and porous layers were  $125 \mu\text{m}$  and  $1.7 \text{ mm}$ , respectively. Zhang et al. [302] fabricated dense/porous

bilayered  $\text{Al}_2\text{O}_3$  by introducing an electric field into the freeze-casting process, and they found that the thickness of dense layers could be controlled by electric field intensity. However, a major problem of freeze casting is the low strength of green body, when the frozen suspension is volatilized, the green body becomes very brittle and difficult to handle, and further efforts are underway to improve the strength of green body. Up to present, dense ceramic multilayer materials prepared by freeze casting technique have not been reported yet.

#### **1.6.2.4 Centrifugal casting**

Centrifugal casting, which could prepare thin layers (down to about 10  $\mu\text{m}$ ), has been adopted to produce ceramic multilayers. Chang et al. [303] found that the addition of high concentration electrolyte could modify the interaction potential while the short-range attractive forces were diminished. This is beneficial because the resulting weakly attractive network of particles resists mass segregation during centrifuging, yet the short-range repulsive forces are sufficiently strong to have a lubricating influence, thus promoting high packing densities. In this manner, Marshall et al. [304] fabricated Ce-ZrO<sub>2</sub>/Al<sub>2</sub>O<sub>3</sub> multilayer. Strong interaction between these layers and martensitic transformation zones surrounding cracks and indentation were observed. The transformation zones spread along the region adjacent to the layer, which increased the fracture toughness. Lucchini et al. [305] also successively obtained Al<sub>2</sub>O<sub>3</sub>/ZrO<sub>2</sub> multilayer by centrifugal casting.

#### **1.6.2.5 Electrophoretic Deposition**

Electrophoretic deposition (EPD) is another wide-used method to prepare multilayer materials. EPD is usually carried out in a two electrode cell, and its mechanism involves two steps. In the first step an electric field is applied between two electrodes and charged particles suspended in a suitable liquid move toward the oppositely charged electrode (electrophoresis). In the second step the particles accumulate at the deposition electrode and create a relatively compact and homogeneous film (deposition) [306]. There can be two types of electrophoretic deposition depending on which electrode the deposition occurs, as shown in Fig. 1.10. When the particles are positively charged, the deposition happens on the cathode and the process is called cathodic electrophoretic deposition (Fig. 1.10a). The deposition of negatively charged particles on positive electrode (anode) is termed as anodic electrophoretic deposition (Fig. 1.10b). It is essential to produce a stable charged-particles-suspension for

applying EPD technique to process materials.

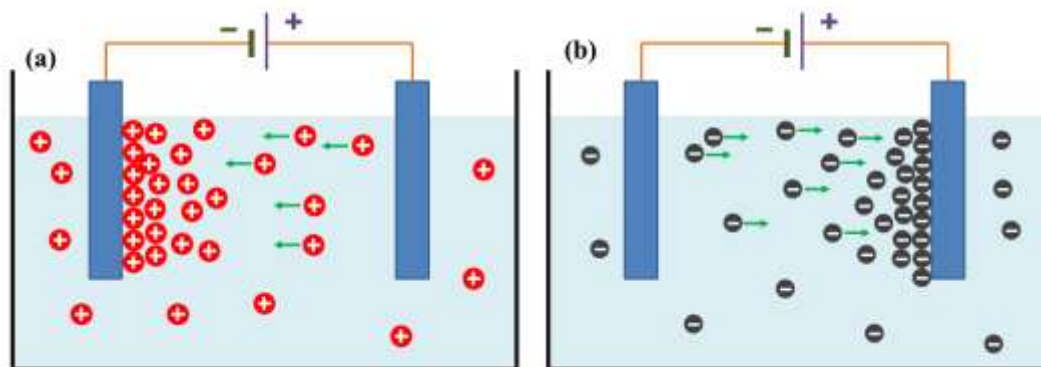


Fig. 1.10 Schematic illustration of (a) cathodic and (b) anodic electrophoretic deposition process.

The application of EPD to layered ceramics has been pioneered by Sarkar and his co-workers [307, 308] ( $\text{ZrO}_2/\text{Al}_2\text{O}_3$  in their work) in ethanol. When the desired thickness of the first layer is reached, the deposition electrode could be moved to a second suspension for deposition of a layer with different composition. By changing back and forth, a green multilayer material is obtained. The deposited samples demonstrated a high green density (about 60% of theoretical) [307, 308]. Hatton et al. [309] prepared  $\text{ZrO}_2/\text{Al}_2\text{O}_3$  multilayer by EPD in ethanol suspension. They found that the fracture behavior of obtained  $\text{ZrO}_2/\text{Al}_2\text{O}_3$  multilayer was related to the compressive residual stress ( $\sigma_r$ ) and layer thickness ( $t$ ), while  $\sigma_r$  is a function of  $t$ . With decreasing  $\sigma_r^2 t$ , the fracture followed a sequence from spontaneous delamination, multistage fracture with extensive crack deflection, to catastrophic failure with, and finally without, deflection steps [309]. The work of Ferrari et al. [310] and Fischer et al. [311] focused on optimized  $\text{ZrO}_2$  and  $\text{Al}_2\text{O}_3$  aqueous suspensions, which are always more preferable than organic solvents due to environmental and economic considerations. Furthermore, Hvizdoš et al. [312] produced symmetrical planar functionally graded material of  $(\text{Al}_2\text{O}_3+10\% \text{ZrO}_2)/(\text{Al}_2\text{O}_3+30\% \text{ZrO}_2)/(\text{Al}_2\text{O}_3+10\% \text{ZrO}_2)$  by EPD and pressureless sintering. The obtained materials exhibited excellent hardness in the exterior layers (comparable to that of pure alumina) and highly enhanced resistance against transversal propagation of surface cracks during thermal shock tests [312].

$\text{SiC}/\text{graphite}$  [313, 314] and  $\text{SiC}/\text{TiC}$  [315, 316] have also been fabricated by EPD method. Vandeperre et al. [314] prepared  $\text{SiC}/\text{graphite}$  multilayer tube and concluded that it is possible to manufacture tough complex-shaped  $\text{SiC}/\text{graphite}$  multilayer by

EPD. You et al. [315, 316] prepared SiC/TiC multilayer by EPD from acetone-based suspensions. The growth rate of the SiC was almost twice that of the TiC at the same deposition voltage and solids loading. They found that the SiC/TiC multilayer without sintering aids could not be densified by pressureless sintering, even at 2000 °C [315, 316]. However, SiC/TiC multilayer could be densified by spark plasma sintering (SPS) at 1800°C and 35 MPa, while the relative density was 98.9% [316].

#### 1.6.2.6 Tape casting

Tape casting, which is also known as “doctor blading” or “knife coating”, is a well-established technique for large-scale fabrication of products with large areas and small thicknesses (ranging from 5 to 500  $\mu\text{m}$ ), such as multilayered capacitors, multilayered ceramic packages, piezoelectrics, ceramic fuel cells, and lithium ion batteries [317]. The chief advantage of the tape casting process is that it is the best way to form large-area, thin, flat ceramic or metallic parts, which are impossible to prepare by other techniques such as pressing or extrusion. In the ceramic industries, tape casting process is considered comparable to traditional slip casting since it also uses a fluid suspension of ceramic particles as the starting point for processing. In tape casting technique, ceramic particles, dispersants, solvents (aqueous or organic), plasticizers and binders are firstly well mixed (usually by ball-milling or ultrasonic method) to prepare a stable slurry with required viscosity. Then, the slurry is poured into a reservoir, and it is made to flow under a blade and onto a plastic substrate, as shown in Fig. 1.11 [318].

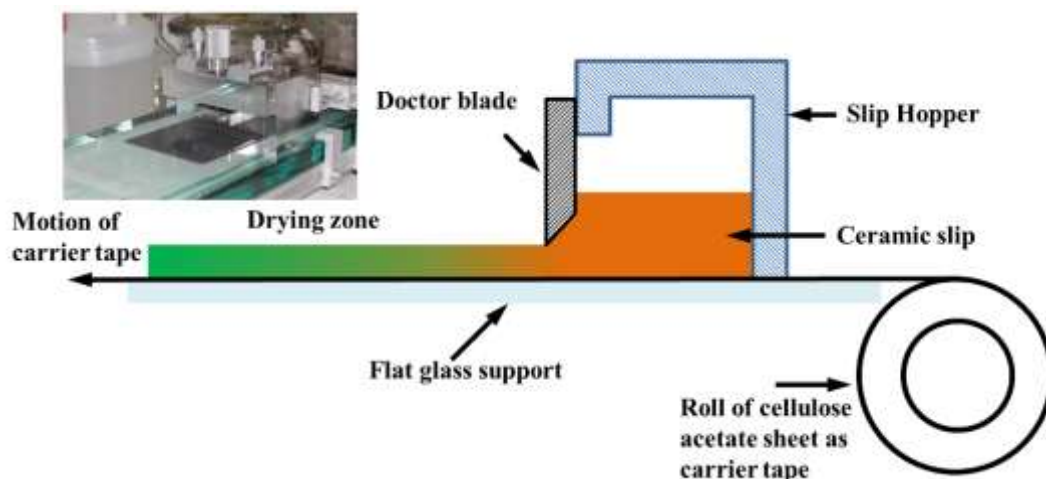


Fig. 1.11 Schematic diagram of the tape casting process [318].

Then dense and flexible ceramic green tape (Fig. 1.12) could be obtained after fully

evaporation of solvent. Thick ceramic green multilayers can be obtained simply by stacking and pressing together a large number of green tapes with desired sequence. After debinding and subsequent sintering, ceramic multilayer could be prepared.

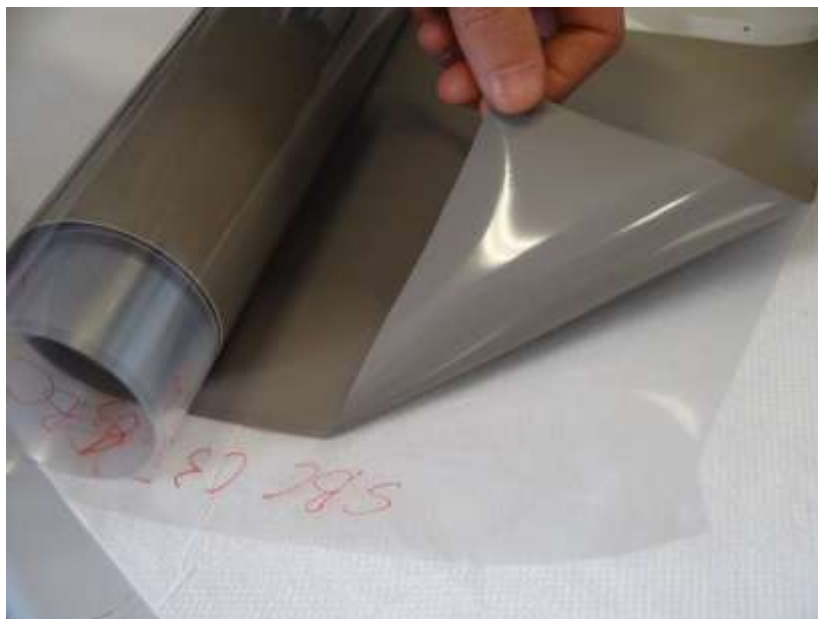


Fig. 1.12 Dense and flexible SiC green tape prepared in our lab.

Moreover, pore forming agents (usually starch) could be added into the slurry during milling. During debinding, these pore forming agents could be decomposed and form uniformly dispersed pores. The size of the pores could be controlled by changing the size of pore forming agents [261]. Therefore, dense, porous or dense/porous multilayer could be easily produced by tape casting method. To present, tape casting process is the most widely used method to prepare ceramic multilayer, and following ceramic systems have been successively fabricated by this process: SiC [260–264], SiC/C [319], SiC/porous SiC [254, 256, 258], SiC/BN [267], Al<sub>2</sub>O<sub>3</sub>/porous Al<sub>2</sub>O<sub>3</sub> [259], Al<sub>2</sub>O<sub>3</sub>/SiC [268], Al<sub>2</sub>O<sub>3</sub>/TiN [270], Al<sub>2</sub>O<sub>3</sub>/TiC [271], Al<sub>2</sub>O<sub>3</sub>/ZrO<sub>2</sub> [274], Si<sub>3</sub>N<sub>4</sub> [276], MoSi<sub>2</sub> [320] and B<sub>4</sub>C/BN [321].

## 1.7 Ceramic multilayer composites

As stated in above literature review, processing ceramic matrix composites and ceramic multilayers are the most investigated method to improve the fracture toughness. The key factor for improving toughness is the presence of weak interfaces/interlayers or residual stress, which allow energy dissipation before fracture through mechanisms of crack deflection, pull-out and bridging of fibre or whisker

[34], and interface delamination [35]. Theoretically, coupling the above methods (multilayer with toughened single composite layer) may further improve the toughness. In this case there are toughening phenomena both inside the single layer and between the layers.

Boch et al. [274] prepared  $\text{Al}_2\text{O}_3/\text{ZrO}_2$  multilayer composite by tape casting. They found that fracture toughness of pure  $\text{Al}_2\text{O}_3/\text{Al}_2\text{O}_3$  multilayer ( $4.8 \text{ MPa}\cdot\text{m}^{1/2}$ ) was higher than that of conventional  $\text{Al}_2\text{O}_3$  ( $3.7 \text{ MPa}\cdot\text{m}^{1/2}$ ), and  $\text{Al}_2\text{O}_3+5\text{vol.}\%\text{ZrO}_2/\text{Al}_2\text{O}_3+10\text{vol.}\%\text{ZrO}_2$  multilayer composite demonstrated highest fracture toughness ( $5.65 \text{ MPa}\cdot\text{m}^{1/2}$ ). Bueno et al. [322] prepared  $\text{Al}_2\text{O}_3/\text{Al}_2\text{TiO}_5$  multilayer composite by slip casting and the apparent toughness value as high as  $12 \text{ MPa}\cdot\text{m}^{1/2}$  was achieved. Tomaszewski et al. [323] fabricated  $\text{Al}_2\text{O}_3/\text{LaPO}_4$  multilayer composite by tape casting and the greatest work of fracture was  $1100 \text{ J/m}^2$ . Zhou et al. [324] stacked  $\text{ZrB}_2$ -SiC layers with different SiC amount to prepare  $\text{ZrB}_2$ -SiC multilayer composites. The flexural strength and fracture toughness of the  $\text{ZrB}_2+20\text{vo.}\%\text{SiC}/\text{ZrB}_2+30\text{vo.}\%\text{SiC}$  multilayer composites were  $960\pm 84 \text{ MPa}$  and  $8.8\pm 0.3 \text{ MPa}\cdot\text{m}^{1/2}$  respectively, which were much higher values than those of monolithic  $\text{ZrB}_2$ -SiC composites. They attributed the significant improvement in mechanical properties to the presence of residual compressive stresses arising from the thermal expansion mismatch between the adjacent layers [324]. Zhang et al. [325] found that the apparent fracture toughness of  $\text{ZrB}_2$ -SiC multilayer composites was strongly dependent on the position of the notch tip, which was accordance with theoretical calculation. The  $\text{ZrB}_2$ -SiC multilayer composites showed a higher fracture load when the notch tip located in the compressive layer, whereas a lower fracture load as the notch tip within the tensile layer. Therefore, the toughening effect of residual compressive stresses was verified by the appearance of crack deflection and pop-in event. However, their calculation indicated that the highest residual compressive stress did not correspond to the highest apparent fracture toughness [325]. Wang et al. [326] fabricated SiC/ $\text{ZrB}_2$  multilayer composites by roll-compaction and spark plasma sintering, and a maximum fracture toughness of  $12.3\pm 0.3 \text{ MPa}\cdot\text{m}^{1/2}$  was measured. The significant improvement in fracture toughness could be attributed to the crack deflection along the interfacial layer and the presence of residual stresses in the sample [326].

Wu et al. [327] fabricated SiC<sub>w</sub>/mullite multilayer composites by tape casting and hot pressing. The SiC whiskers were added during ball-milling process. High degrees of SiC whisker orientation was determined by visually and by X-ray diffraction. Lim et

al. [328] prepared SiC<sub>w</sub>/Al<sub>2</sub>O<sub>3</sub> multilayer composites by tape casting and hot pressing. The SiC whiskers were added during ball-milling process. The wear rate was highest in the direction parallel to the tape casting direction and lowest in the direction normal to lamination direction, respectively. They suggested that the matrix grain size and roughness due to whisker orientation were responsible for wear behavior. Lim et al. [329] further investigated the effect of temperature on the tribological behavior of SiC<sub>w</sub>/Al<sub>2</sub>O<sub>3</sub> multilayer composites. It was found that the effect of whisker orientation on friction and wear characteristics was not dependent on test temperatures. The highest wear rate was always obtained with a SiC whisker oriented parallel to the tape casting direction at all tested temperatures. As reviewed in “1.5.1 SiC<sub>sf</sub>/SiC composites”, Lee et al. [228–230] prepared the SiC<sub>sf</sub>/SiC composites by tape casting and hot pressing. Short SiC fibres were added into SiC slurry by ball-milling. Most of SiC short fibres were oriented along the tape casting direction. The relative density, bending strength and fracture toughness increased with sintering temperature.

After successfully prepared SiC multilayers [260–263], our group has been exploring the possibility to prepare, by tape casting, sheets of C<sub>sf</sub>/SiC composites, which can be stacked into a multilayer structure, and finally strengthened by pressureless sintering. This processing path could provide an alternative method for C<sub>sf</sub>/SiC composite preparation; such a kind of C<sub>sf</sub>/SiC composite layers could be also integrated into a SiC-based multilayer TPS, with the aim to optimize its thermal conductivity behavior. The uniform distribution of short C fibres within the SiC matrix entails the greatest importance in the processing of these composite tapes. Generally, as mentioned in above paragraphs, short fibres, as well as other reinforcements, could be introduced easily by conventional powder processing techniques, such as ball-milling. Fuso et al. [330] firstly tested the effect of dispersants and dispersion method on the dispersion of Toho Tenax HTA40 fibres (with epoxy coating). The results are listed in Table 1.4. After the powders were well-dispersed by ball-milling, carbon fibres, solvent and TEA were added into the slurry for 12 h ball-milling. Finally, 5, 12, 17 and 23 vol.% C<sub>sf</sub>/SiC multilayer composites were obtained after tape casting, debinding and pressureless sintering. However, due to high velocity impact during ball-milling, short carbon fibres would be greatly shortened during ball-milling process, which would hinder the strengthening and toughening effect of fibres. After 2 h- ball milling, Zhang et al. [242] found that the average carbon fibre length in the final C<sub>sf</sub>/SiC composite was about 60 μm, which was much shorter than that of original length (3 mm). Additionally, the breakage of C fibres would also produce large amount of residual C.

Although C and B were used as sintering aids in SiC system, redundant C would be detrimental to the densification of the SiC-based composite [331]. Therefore, mixing the SiC slurry with a fibre-predispersed solution seems to be an effective method for adding fibres without breakage.

**Table 1.4** Effect of different solvents, dispersants and dispersion method on the dispersion behavior of short carbon fibres (the dispersant amount is 5 wt.% with respect to the solvent) [330]

Sovent	Dispersant	Dispersion method	Efficacy
Water	No	Ultrasonic	Very low
Ethanol	No	Ultrasonic	Very low
Butanol	No	Ultrasonic	Very low
Mixture	No	Ultrasonic	Low
Water	PVA	Ultrasonic	Very low
Water	TEA	Ultrasonic	Very low
Mixture	BYK	Ultrasonic	Low
Mixture	TEA	Ultrasonic	Low to medium
Mixture	TEA	Mechanical	Good
Mixture	BYK	Mechanical	Medium to good

Note: The “Mixture” means the mixture of ethanol and butanol.

Vega Bolivar et al. [332] firstly dispersed short carbon fibres in the mixture of ethanol and butanol by ultrasonic method, and then the fibre-predispersed solution was added into SiC slurry by mechanical stirring. Toho Tenax fibres (with epoxy coating) and Alfa Aesar (uncoated) were tested, and the C<sub>f</sub>/SiC composite green tapes with 5 vol.% short C fibres were obtained. However, the short C fibres were not well dispersed and bundles of fibres were observed in the composites. Particularly, the bundles of

fibres and increased porosity in the neighbor matrix [332]. Therefore, more efficacious fibre dispersion should be achieved to develop the effect of short C fibres.

## **1.8 Scope of current research**

Since the dispersion of C fibres with epoxy coating in water or organic solvent was difficult [330, 332], The C fibres with water-soluble coating, which is more compatibility with water or organic solvent (based on alcohols), are expected to demonstrate better dispersion result. In present work, the effect of seven dispersants on the dispersion behavior of Toho Tenax HTC124 fibres (with water-soluble coating) was tested. Then the C<sub>sf</sub>/SiC multilayer composites with different fibre amount were prepared by tape casting and pressureless sintering. The relative density, mechanical properties, oxidation behavior and thermophysical properties were evaluated, and the effect of addition of short C fibres on these properties was discussed.

# Chapter 2. Experimental

## 2.1 Materials and processing

SiC multilayer and C<sub>sf</sub>/SiC multilayer composite specimens were fabricated by tape casting technique and pressureless sintering. The preparation of SiC multilayer involves SiC slurry preparation, tape casting, green samples preparation, debinding and pressureless sintering. However, the processing method for C<sub>sf</sub>/SiC multilayer composite involves (Fig. 2.1): SiC slurry preparation, fibre dispersion in solvents, addition of the fibre-predispersed solution into the SiC slurry, tape casting, debinding and pressureless sintering.

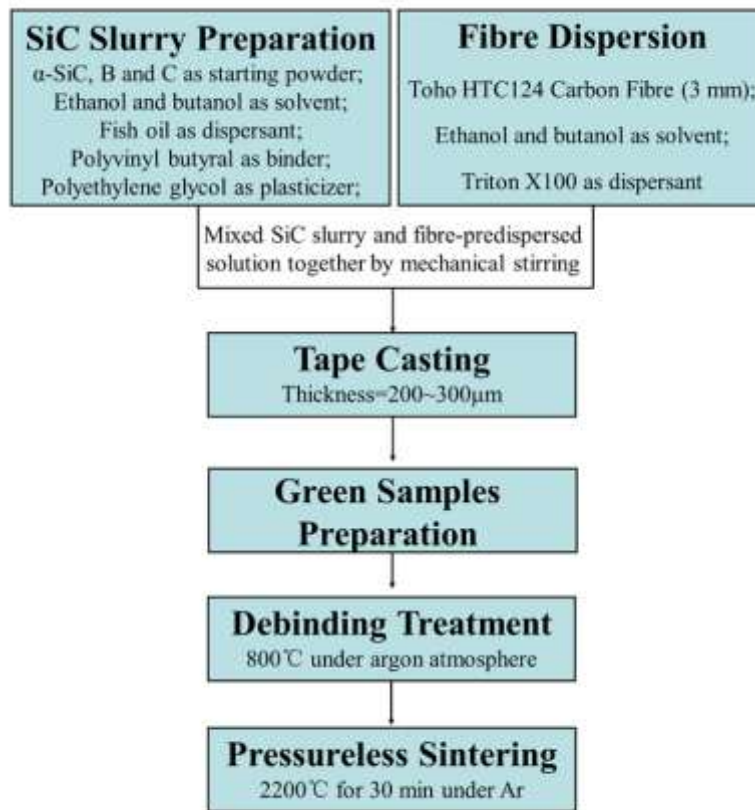


Fig. 2.1 Preparation process of C<sub>sf</sub>/SiC multilayer composite by tape casting and pressureless sintering.

### 2.1.1 Slurry preparation

The composition of SiC slurry is shown in Table 2.1. α-SiC powders (H.C. Starck UF-15, 15 m<sup>2</sup>/g, with a mean particle size of 0.7 µm), ethanol (≥ 99.8%,

Sigma-Aldrich, Germany), butanol ( $\geq 99.4\%$ , Sigma-Aldrich, Germany), fish oil (Afom medical, Italy), carbon (Alfa Aesar flake 7–10  $\mu\text{m}$ ) and boron (H.C. Starck amorphous grade I 1–2  $\mu\text{m}$ ) were firstly mixed for 24 h in an alumina jar with alumina milling balls. Fish oil was added as dispersant for SiC particles. Carbon and boron were used as sintering additives. Afterward, plasticizer (polyethyleneglycole, Bisoflex 102 Cognis) and binder (polyvinilbutyral, Butvar B76 Solutia) were added into the above slurry and then mixed for 48 h.

**Table 2.1** Composition of SiC slurry

Components		Composition (wt.%)
Solvents	Ethanol	19.87
	Butanol	30.50
Dispersant	Fish oil	0.10
Ceramic powder	SiC	33.58
	B	0.34
Sintering Aids	C	1.01
	Binder	Polyvinylbutyral (PVB)
Plasticizer	Polyethyleneglycol (PEG)	9.61

In preliminary study, Toho Tenax HTA40 fibre with epoxy coating was used as reinforcement [330, 332]. However, the epoxy coating made it very difficult to disperse HTA40 fibre in a mixture of ethanol and butanol, hence a bad dispersion of fibre in SiC slurry was occurred. Therefore, Toho Tenax HTC124 (fibre length of 3 or 6 mm) with water soluble coating was used as reinforcement. With the help of dispersant, the short fibres were firstly dispersed in the solvent by ultrasonic (750 W Ultrasonic Processor, Sonics). The solvent was chosen as mixture of 40 wt.% ethanol and 60 wt.% butanol, same as to the SiC slurry in which it has been successfully used for tape casting. The dispersion effect of BYK-163, BYK-410, BYK-2150, BYK-9076, BYK-9077 (BYK Additives & Instruments) and Triton X100 (Sigma-Aldrich) were tested. Nonionic surfactant Triton X100 (7 wt.%) showed the best dispersion result, which will be discussed in in detail. It should be noted that the

dispersion of fibre does not mean to disperse C fibre as uniform slurry. It means separate fibre from bundles to single fibre, which results in a good dispersion of single fibre in SiC slurry after mixing. The time for dispersion of 5, 10 and 15 vol.% fibre content were 20, 40 and 60 min, respectively. Then fibre-predispersed solution was obtained.

The SiC slurry and the fibre-predispersed solution were mixed together by mechanical stirring at 200 rpm in Stirrer Tyler PW (Velp Scientifica s.r.l, Italy) at room temperature, and then the slurry with homogeneous fibre dispersion was obtained. The higher the fibre amount, the longer the mixing time (2, 4 and 6 h for 5, 10 and 15 vol.%, respectively).

### 2.1.2 Tape casting

After degas, the slurry was casted on a moving Mylar support, with the layer thickness controlled by the height of the blade (1 mm) and by the advancement speed of the Mylar support (100 mm/min). The organic solvents were then slowly removed by controlled evaporation in air at ambient temperature. The width and thickness of green layer were 100 mm and 200 - 250  $\mu\text{m}$ , respectively.

### 2.1.3 Green samples preparation

The green tapes of SiC and  $C_{sf}/\text{SiC}$  were cut into proper shape and then carefully detached from the plastic support. The multilayer specimens were obtained by painting a gluing solution before stacking next layer, as shown in [Fig. 2.2a](#).

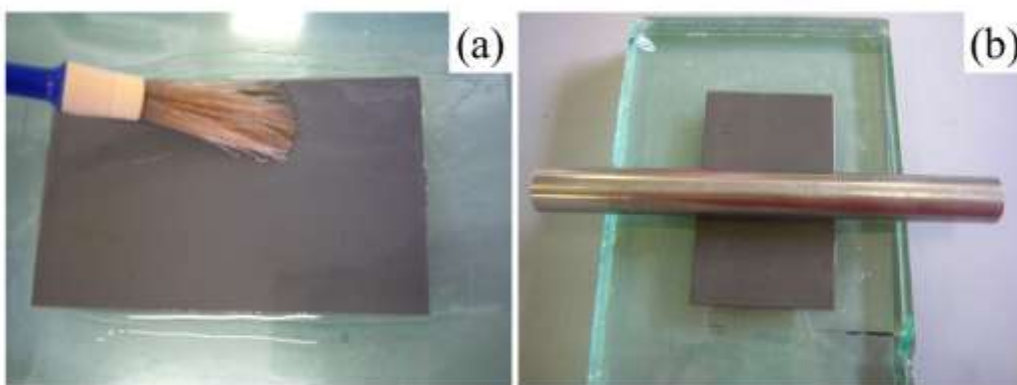


[Fig. 2.2](#) Stacking process of green multilayer samples. (a) Paint gluing solution and (b) Removal air inclusion.

The gluing solution was made of water, ethanol and polyvinyl alcohol (PVA) in the weight proportion of 10:10:1. A mandrel was passed on the samples to make successive layer adhere without the formation of air inclusion, as shown in Fig. 2.2b.

It should be noted that the roughness of lower-side (in contact with Mylar film) and upper-side (in contact with air) is different due to the presence of the Mylar film, as shown in Fig. 2.3. The rougher upper-side was always pasted with the smoother lower-side of another tape during stacking.

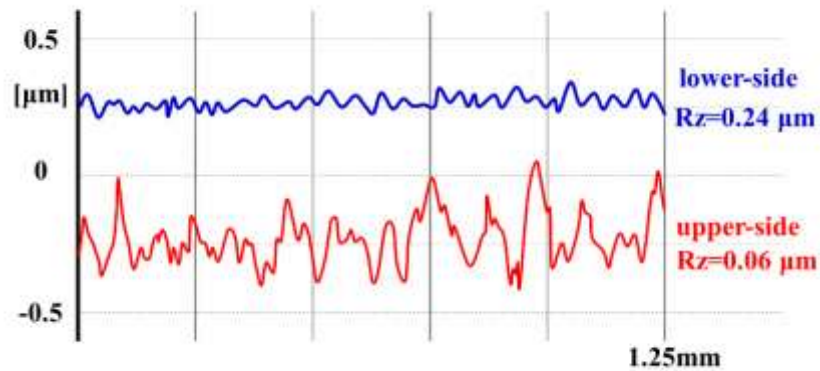


Fig. 2.3 Roughness profiles of lower-side (in contact with Mylar film) and upper-side (in contact with air) of SiC green tape.

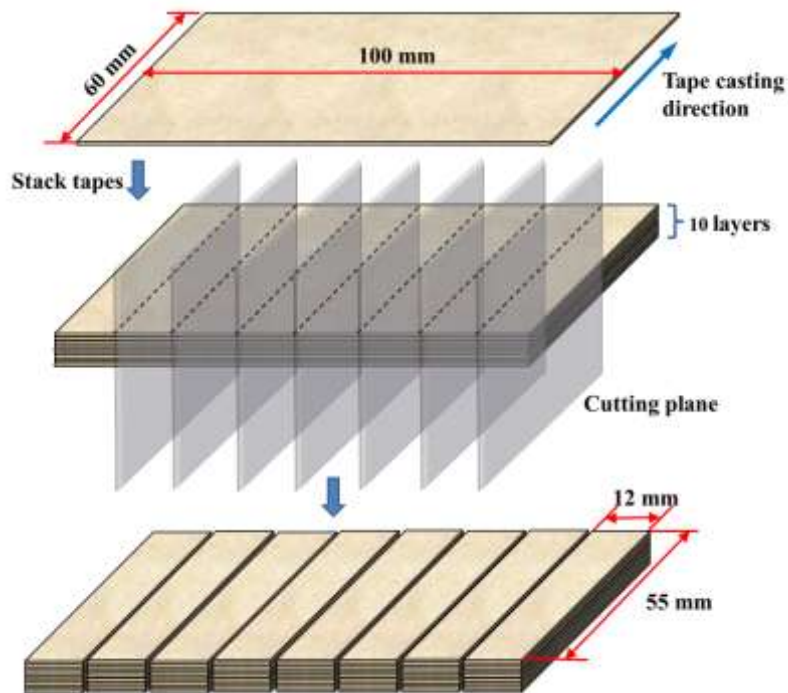


Fig. 2.4 Preparation process for green specimens for bending test.

The preparation process for green specimens for three point bending test is shown in Fig. 2.4. Ten tapes with dimension of  $100 \times 60$  mm were stacked. The length direction of cut tapes was perpendicular to the tape casting direction. After removed of the edging, eight specimens with dimension of about  $60 \times 12 \times 2.5$  mm were obtained.

In order to meet the thickness requirement for fracture toughness test, twenty layers were stacked and 9 samples with dimension of about  $50 \times 8 \times 5$  mm were cut. For preparing SiC/(C<sub>sf</sub>/SiC) multilayer composites, two SiC layers and one C<sub>sf</sub>/SiC layer (total 18 layers) were stacked alternatively, and then another two SiC layers (thus total 20 layers) were stacked on the upper surface of C<sub>sf</sub>/SiC layer to make sure both side of the composites were SiC layer.

The preparation process of samples for thermal diffusivity test is more complex. Thermal conductivity properties in X (parallel to tape casting direction), Y (perpendicular to tape casting and thickness direction) and Z (through thickness direction) directions were tested, as shown in Fig. 2.5.

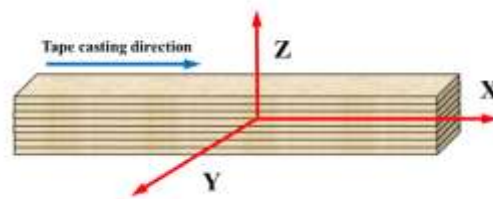


Fig. 2.5 Three-dimensional Cartesian coordinate system used to describe test directions of thermal properties. X direction is parallel to the tape casting direction; Y direction is perpendicular to tape casting and thickness direction; Z direction is the through thickness direction.

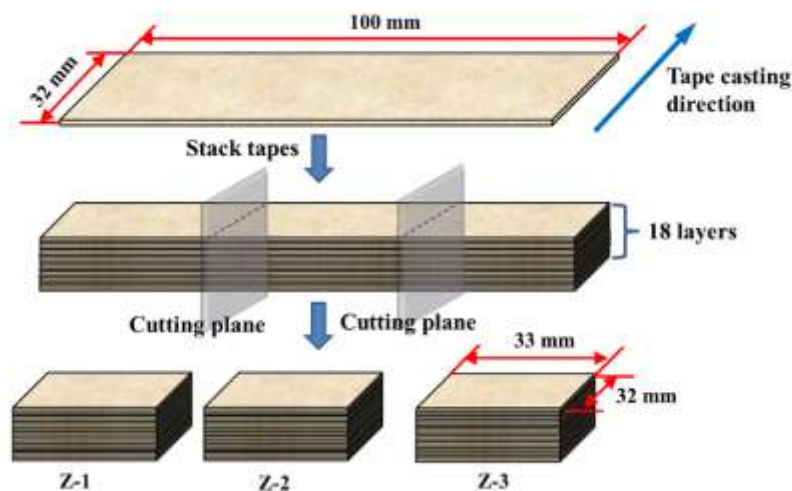


Fig. 2.6 Preparation process of green samples for thermal properties test in Z direction.

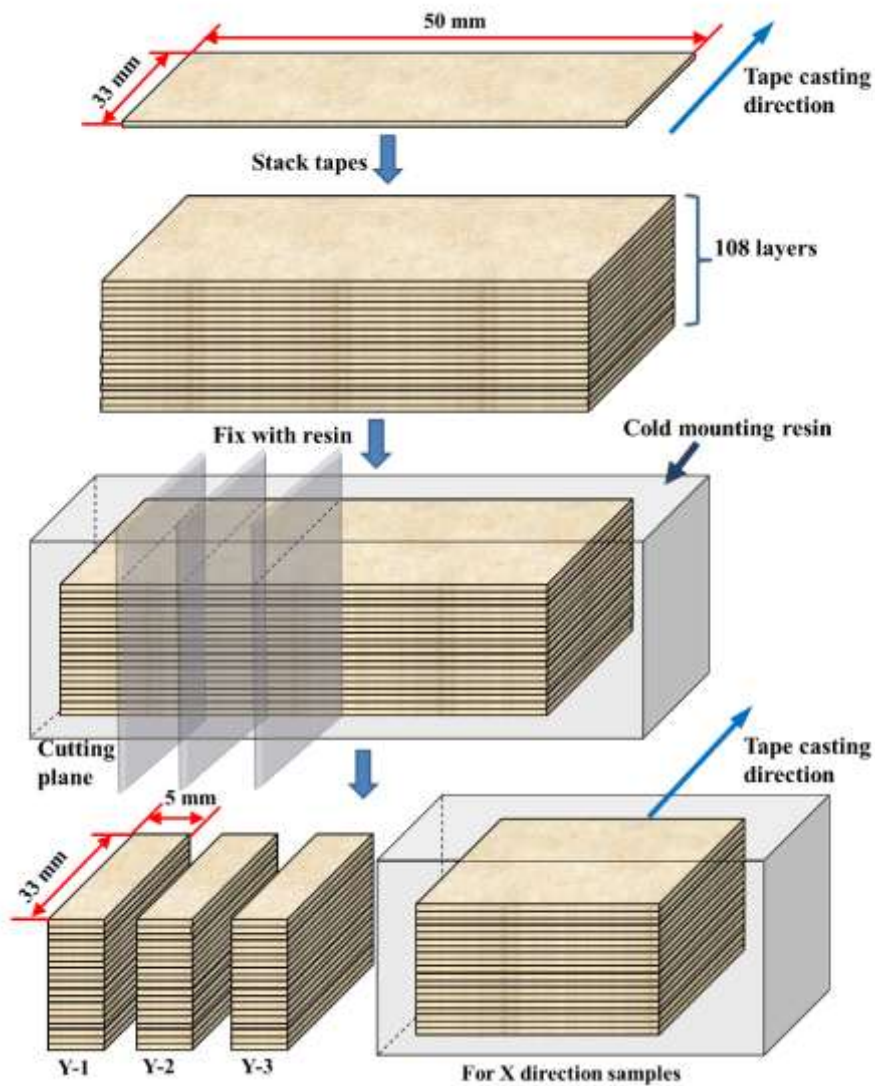


Fig. 2.7 Preparation process of green samples for thermal properties test in Y direction.

One hundred and eight layers of green tape with dimension of 50×33 mm were cut and stacked. The length direction of cut tapes was perpendicular to the tape casting direction. Then the stacked samples were fixed by cold mounting resin (Presi S.A, France). After removed of the edging by cutting machine (Isomet 4000, Buehler, Lake Bluff, IL, USA), three samples for thermal conductivity test in Y direction were cut firstly, as shown in Fig. 2.7. Finally, three samples for thermal conductivity test in X direction were cut, as shown in Fig. 2.8. The thickness of green samples for thermal conductivity test in X and Y directions were 5 mm. The slowest speed of the cutting machine (1.2 mm/min) was used to avoid delamination of green tapes during cutting.

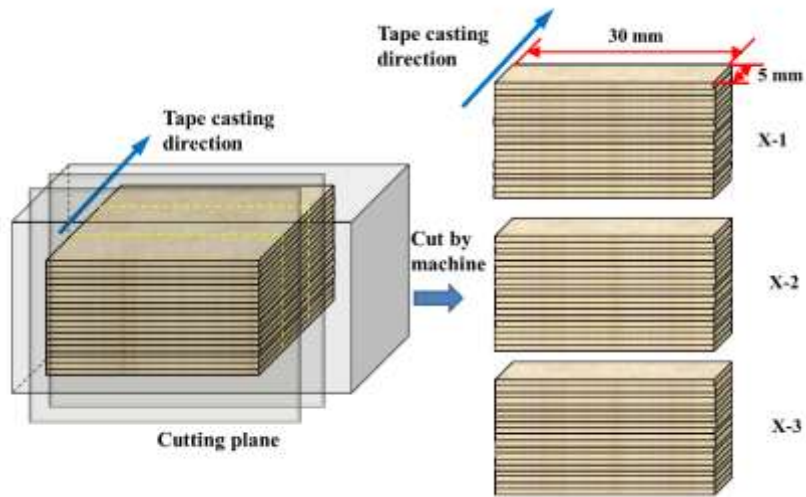


Fig. 2.8 Preparation process of green samples for thermal properties test in X direction.

### 2.1.4 Debinding process

In order to remove the binder and the other organic components, a debinding treatment should be performed before sintering.

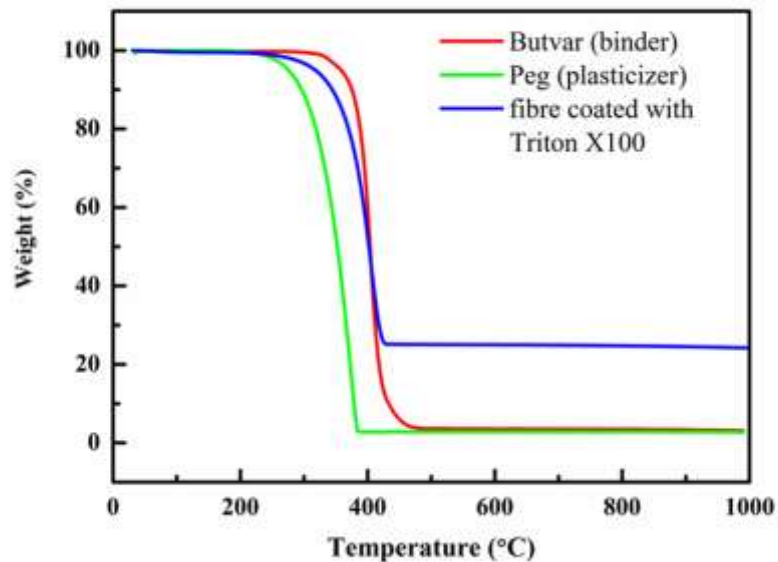


Fig. 2.9 Decomposition curves of binder, plasticizer and fibre dispersant.

The main organic components in SiC green samples are binder and plasticizer. However, in  $C_{sf}/SiC$  green samples, there is also the presence of fibre dispersant (Triton X100) in addition to binder and plasticizer. The decomposition behavior of

binder, plasticizer and dispersant was tested by TGA from room temperature to 1000 °C at a constant rate of 20 °C/min in flowing chromatographic air (50 ml/min). Fibre coated with Triton X100 was used to evaluate the decomposition behavior of Triton X100. The result is shown in Fig. 2.9.

Most of the organic components would be decomposed before 400 °C (Fig. 2.9). Moreover, the organic materials will decompose faster and completely at comparatively lower temperature under slower heating rate (3 °C/h) [333]. Therefore, the process, as shown in Fig. 2.10a, was used for debinding treatment. The debinding treatment was performed up to 800 °C in argon atmosphere in Elite thermal systems limited (Tersid s.r.l, Italy).

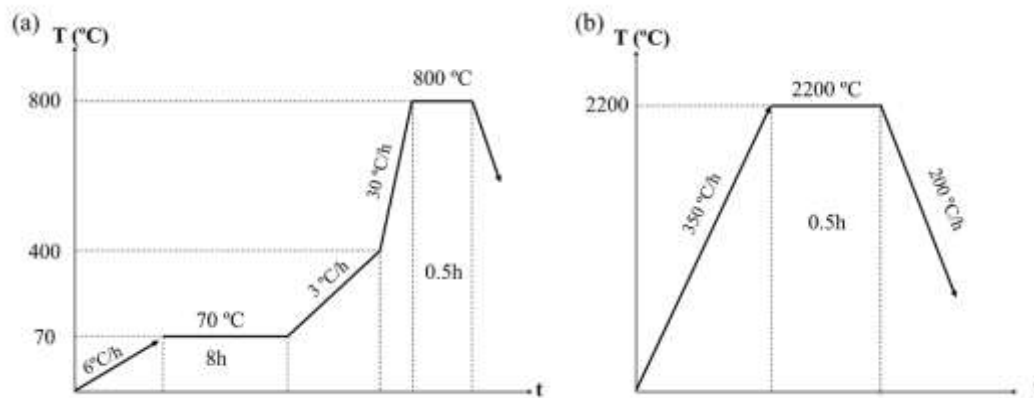


Fig. 2.10 Schematic diagram of (a) debinding and (b) pressureless sintering process.

### 2.1.5 Pressureless sintering

Usually, pressure requiring techniques are widely applied in fabrication of ceramic composites and multilayers. However, due to shape and size limitations and high equipment cost, these methods are difficult to extend towards large industrial applications. Thus, pressureless sintering was adopted in present work. The samples were submitted to pressureless sintering treatment in argon (partial pressure of 55 Pa) at 2200 °C for 30 min in a furnace operating under controlled pressure and atmosphere (TAV. S.p.A, Italy). The sintering temperature and time were based on the preliminary experiment [262, 330]. The sintering process is shown in Fig. 2.10b. During debinding and sintering process, the samples were placed on a graphite support and a graphite weight was put over them to avoid sample deviation from planarity.

## 2.2 Experiment methods

### 2.2.1 Density measurement

Geometric density and Archimedes' density were measured in present work. The geometric density measurements were performed by measuring weight and dimensions of geometrically regular samples. The Archimedes' densities of the samples at room temperature were measured with deionized water as immersion medium according to Archimedes' principle. Theoretical density was calculated by the rule of mixtures.

### 2.2.2 Mechanical properties test

Elastic modulus was evaluated by an impulse excitation technique involving the analysis of the transient composite natural vibration on GrindoSonic MK5 instrument and RFDA MF basic instrument (IMCE n.v. Belgium). The flexural strength was determined on sintered specimens without surface polishing with a span of 40 mm and a cross-head speed of 0.1 mm/min. All tests have been performed on at least seven samples, in order to improve statistical significance of the results.

Fracture toughness tests were measured at room temperature using the single edge V notch beam (SEVNB) method. The samples preparation and testing process were in accordance with CEN/TS 14425-5 standard. A starter notch of depth and width approximately 0.5 mm was prepared by a thin diamond saw blade in Erbicol S.A, Switzerland. Afterward, diamond paste (1  $\mu\text{m}$ ) was applied to the starter notch, and then the V-notch was prepared by reciprocating a razor blade in the sawn notch for 2 min. The depth of the V-notch was measured by calibrated optical microscope (Reichert Microscope, Austria). Depths of the V-notch at both sides were read as  $a_1$  and  $a_2$ , and the average depth ( $a$ ) of and average relative depth ( $\eta$ ) of the V-notch ( $a$ ) was calculated by Eq.2.1 and 2.2, respectively. Fracture toughness tests were performed on sintered specimens with a span of 20 mm and a cross-head speed of 0.1 mm/min. The fracture toughness  $K_{IC}$  was calculated by Eq.2.3 and 2.4.

$$a = \frac{a_1 + a_2}{2} \quad (2.1)$$

$$\eta = \frac{a}{W} \quad (2.2)$$

$$K_{IC} = \frac{F}{B \cdot \sqrt{W}} \times \frac{S}{W} \times \frac{3\sqrt{\eta}}{2(1-\eta)^{1.5}} \times Y \quad (2.3)$$

where:

$$Y = 1.9472 - 5.0247\eta + 11.8954\eta^2 - 18.0635\eta^3 + 14.5986\eta^4 - 4.6896\eta^5 \quad (2.4)$$

where  $F$  is the fracture load,  $B$  is the test piece width,  $W$  is the specimens' depth,  $S$  is the support span (20 mm in the present work), respectively.

### 2.2.3 Oxidation properties test

Bulk samples (dimension of about 4×4×2 mm, and 100–200 mg in weight) were cut from sintered materials for oxidation test. Thermogravimetric analysis (TGA) was carried out on a Mettler-Toledo TGA/SDTA851e system up to 1600 °C at a constant rate of 10 °C/min in flowing chromatographic air (50 ml/min).

### 2.2.4 Specific heat capacity measurement

Specific heat capacity ( $C_p$ ) of SiC multilayer was measured by a calibrated differential scanning calorimeter (Pyris 1 DSC, Perkin–Elmer Instrument Co., USA) from 30 to 600 °C with a heating rate of 10 °C/min. Details of the principle and procedure of the experiment can be found elsewhere [334] and will not be elaborated here. Samples (dimension of about 3×3×1.5 mm, and about 50 mg in weight) were cut from sintered materials for specific heat test. Three measurements of  $C_p$  were performed to improve statistical significance of the results.

### 2.2.5 Thermal expansion behavior test

The thermal expansion behavior of SiC multilayer and  $C_{sf}/SiC$  multilayer composites in X, Y and Z directions were examined on thermo-mechanical analyzer (TMA) (Setaram Instrumentation, France) from 25 to 1500 °C with a heating rate of 10 °C/min. The cuboid samples with dimension of 8×4×4 mm were used for thermal expansion behavior test, while the height (8 mm) direction was the testing direction.

The argon atmosphere was maintained at a flow rate of 20 ml/min to ensure the equilibrium of temperature and prevent oxidation of samples. The coefficient of thermal expansion (CTE) in X, Y and Z directions were calculated from the thermal expansion curves. In order to improve statistical significance of the results, thermal diffusivity and expansion tests have been performed on three samples on each direction.

An average linear CTE was obtained according to Eq.2.5:

$$\alpha_{T,T_0} = \frac{dl}{l_0 \cdot dT} = \frac{l_T - l_0}{l_0 \cdot (T - T_0)} \quad (2.5)$$

where  $l_0$  and  $l_T$  are referred to the length at  $T_0$  (room temperature in present work) and temperature  $T$ , respectively.

## 2.2.6 Thermal diffusivity test

Drills coated with diamond were used to prepare the samples for thermal conductivity test. The internal and outer diameters of the drills were 13 and 15 mm, respectively. The schematic diagram of cut samples for thermal diffusivity test in X, Y and Z directions is shown in Fig. 2.11.

The sides of the disk samples were polished with SiC waterproof sandpaper. In order to investigate the effect of oxidation, the thermal diffusivity properties in three directions before and after oxidation were measured. The oxidation treatment was performed at 1500 °C for 2 h in Nabertherm HT64/17 furnace (Nabertherm GmbH, Germany) in air. The remaining SiC materials after drilled were cut to prepare samples for thermal expansion test in different directions. The thermal diffusivity ( $D$ ) tests were performed on a thermal properties analyzer (Flashline 4010, Anter Corporation, USA) from room temperature to 1500 °C with a heating rate of 5 °C/min in argon atmosphere. The diameters of the samples were about 12.7 mm.

The thermal conductivities ( $\kappa$ ) of SiC multilayer in three directions were calculated by Eq.2.6:

$$\kappa = \rho \cdot C_p \cdot D \quad (2.6)$$

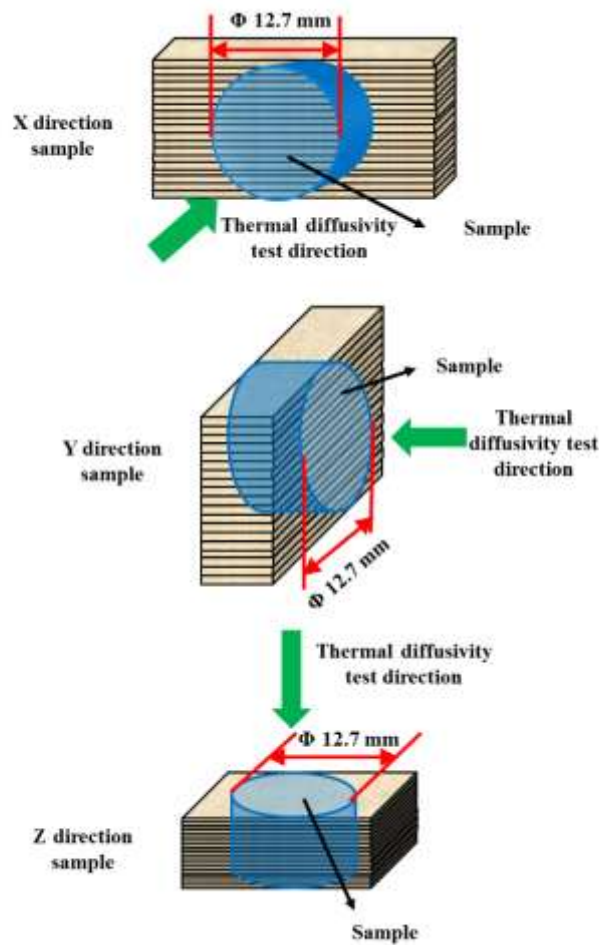


**Fig. 2.11** The schematic diagram of cut samples for thermal diffusivity test in X, Y and Z directions.

### 2.2.7 XRD analysis

X-ray diffraction (XRD) analysis was performed on Rigaku D/MAX diffractometer between  $20$  and  $80^\circ$  ( $2\theta$ ) with  $\text{Cu K}\alpha$  radiation ( $\lambda=0.1504$  nm) at a generator voltage of  $30$  kV and generator current of  $20$  mA. The scanning speed and the step size were  $0.08^\circ/\text{min}$  and  $0.02^\circ$ , respectively.

### 2.2.8 Microstructure observation

The polished surface was observed by optical microscope (Reichert Microscope, Austria) and Zeiss Supra 25 Field Emission Scanning Electron Microscope (SEM). The fracture surface was observed on Zeiss Supra 25 Field Emission SEM.

# Chapter 3. Microstructure of C<sub>sf</sub>/SiC multilayer composites

As mentioned in “1.7 Ceramic multilayer composites”, the uniform distribution of short C fibres within the SiC matrix entails the greatest importance in the processing of these composite tapes. Generally, short fibres could be introduced easily by conventional powder processing techniques, such as ball-milling [233, 234, 238].

However, carbon fibre would be cut shorter during ball milling, which would hinder the strengthening and toughening effect of fibres [241]. Additionally, the breakage of C fibres could also produce large amount of residual C. Although C and B were used as sintering aids, redundant C would be detrimental to the densification of the SiC-based composite [331]. Therefore, mixing the SiC slurry with a solution containing fibres, dispersed in solvents previously, seems to be an effective method for adding fibres without severe breakage.

Vega Bolivar et al. [332] tried to disperse Toho Tenax HTA40 fibres with epoxy coating (sizing), and C<sub>f</sub>/SiC composite green tape with 5 vol.% short C fibres was obtained. However, the short C fibres were not well dispersed and bundles of fibres were observed in the composites [332]. The fibre without sizing or without solvent-soluble sizing seems to be more suitable for dispersion. Therefore, Toho Tenax HTC124 fibres with water-soluble coating were tested in present work.

## 3.1 Dispersion of short carbon fibres in solvent

BYK-163 [335], BYK-410 [336], BYK-2150 [337], BYK-9076 [337, 338], BYK-9077 [337] and Triton X100 [339] are widely used for dispersion carbon black and nanotubes. Therefore, these six dispersants were used in present work to disperse short carbon fibres. It should be noted that it is beneficial for the processing and properties of C<sub>sf</sub>/SiC multilayer composites to use small amount dispersant. The dispersion effect of the six dispersants is shown in Fig. 3.1.

It is obvious that the nonionic surfactant Triton X100 demonstrated the best dispersion effect among the six dispersants. In order to disperse carbon fibre in the solvent, surfactant molecules orient themselves in such a way that hydrophobic tail groups face toward the fibre surface while hydrophilic head groups face toward the aqueous phase, producing a lowering of the fibre/solvent interfacial tension [340]. The

chemical structure of nonionic surfactant, Triton X-100, is given in Fig. 3.2. The hydrophobic octyl group of Triton X100 (polyethylene glycol) can interact with carbon fibre through adsorption and cover the carbon fibre over its axial length, while the hydrophilic segment can interact with the solvent through hydrogen bonding.

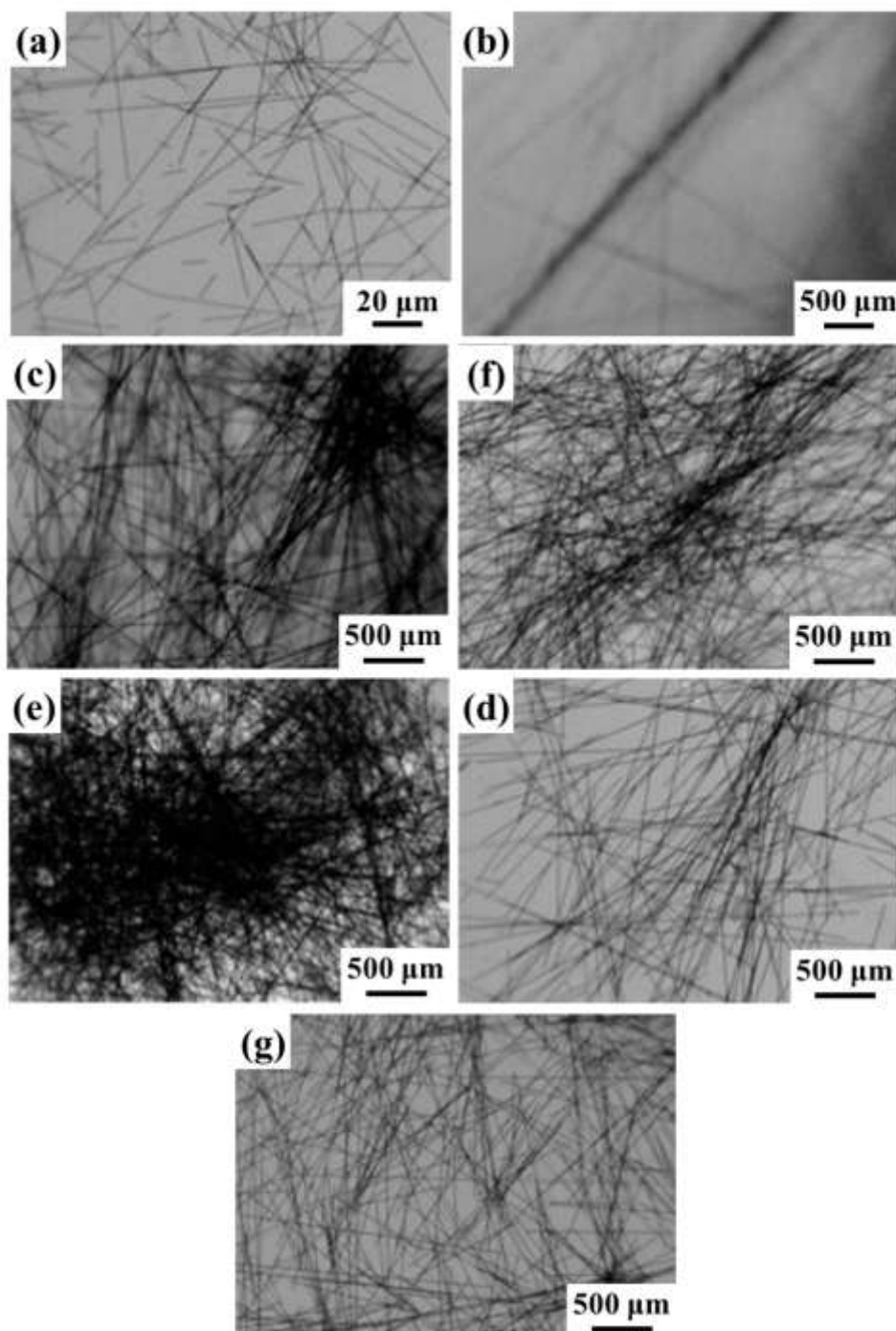


**Fig. 3.1** Effect of dispersant (1 wt.%) on fibre dispersion (0.075 vol.%) in mixture of ethanol and butanol. (a) without dispersant, (b) BYK-163, (c) BYK-410, (d) BYK-2150, (e) BYK-9077, (f)BYK-9076, (g) Triton X-100.

The dispersing power of the surfactant depends on how firmly it adsorbs onto the fibre surface and produces by this adsorption energy barriers of sufficient height to hinder aggregation. Generally, hydrophobic tail groups tend to lie flat on the graphitic surface because graphitic unit cells match well with the methylene units of hydrocarbon chains [341]. Longer tails means high spatial volume and more steric hindrance, thus providing greater repulsive forces between individual carbon fibres. Thus, efficiency of adsorption and consequently dispersing power of surfactants are greatly affected by the tail length of the surfactant, i.e. tail length factor. Triton X100 has an effective chain length of nine atoms only. It means Triton X-100 should exhibit weak dispersing power theoretically, which is contrary to the experimental observations. It is assumed that the benzene ring in the tail group of Triton X-100 (benzene ring factor) contributes more to dispersion effect [342]. Actually, molecules having the benzene ring structure adsorb more strongly to the graphitic surface due to  $\pi$ - $\pi$  stacking type interaction [341, 343]. Whenever “tail length factor” and “benzene ring factor” compete, the latter contributes more to dispersion effect [342].

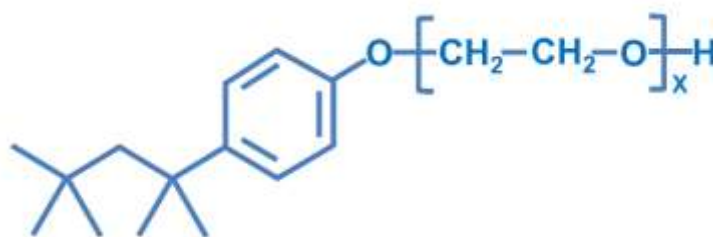
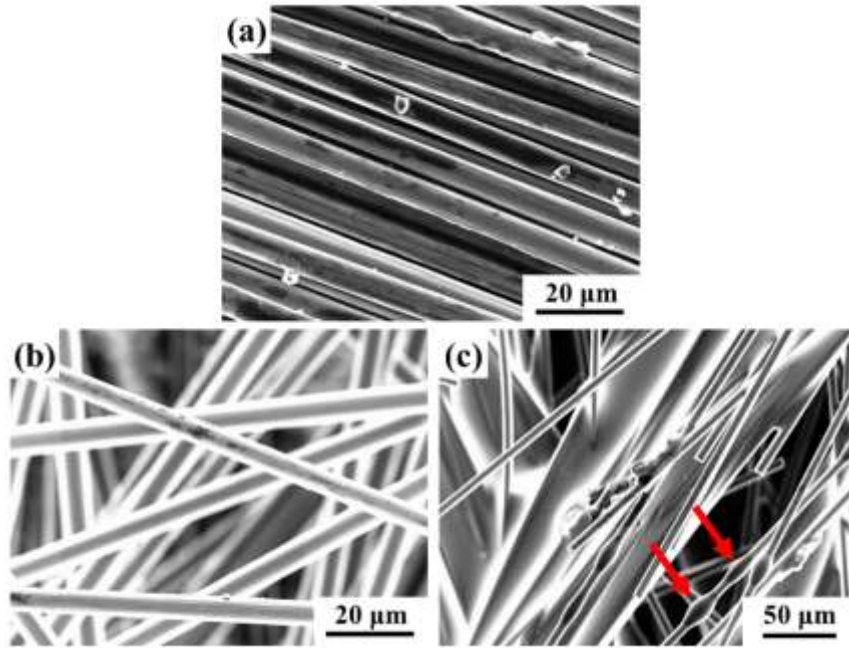


Fig. 3.2 Chemical structure of Triton X-100.

In order to observe the presence of Triton X100 on the surface of carbon fibre, the microstructure of dried fibres dispersed in solvent with Triton X100 were observed, as shown in Fig. 3.3c. The original commercial fibres (Fig. 3.3a) and dried fibres dispersed in solvent without any dispersant (Fig. 3.3b) were used for comparison. There is no significant difference between original fibres and fibres after dispersion without any dispersant. However, on the surface of dried fibres after dispersion with dispersant, the presence of Triton X100 was very clear, and even drop-like Triton X100, as pointed out by red arrows in Fig. 3.3c, was observed.

However, it should be noted that the good dispersion of fibre in present work does not mean to disperse C fibre as uniform slurry. It means to separate fibre from bundles to single fibre, which results in a good dispersion of single fibre in SiC slurry after mixing.



**Fig. 3.3** Microstructure of (a) original commercial fibres, (b) dried fibres dispersed in solvent without any dispersant, (c) dried fibres dispersed in solvent with Triton X100.

### 3.2 Dispersion of short carbon fibres in SiC slurry

After a good dispersion of fibres was obtained, the fibre-predispersed solution was then mixed with SiC slurry by mechanical stirring. It should be noted that the carbon fibre would also be shortened in present work due to the mechanical stirring. The fibre length distribution after mixing was observed. Parts of mixed slurry containing different C fibre amount (corresponding to 5, 10 and 15 vol.% in the final sintered samples) was dissolved in a large amount of ethanol. Afterward, the diluted slurry was taken out by dropper and then dropped on Mylar film. After the solvent was evaporated completely, the fibre length distribution was observed by optical microscope. Forty-two different areas were observed to improve statistical significance of the results.

Typical fibre length distribution and the statistical results in the mixed slurry are shown in Fig. 3.4. The original fibre length was about 3 mm. As shown in Fig. 3.4b, d and f, the average fibre length in the slurry, whose fibre amount in final sintered samples were 5, 10 and 15 vol.%, were about 0.6, 0.55 and 0.5 mm, respectively. The mixing time for preparation of slurry with 5, 10 and 15 vol.% fibre amount was 2, 4 and 6 h, respectively. Therefore, prolongation of mechanical mixing time slightly

decreased the average fibre length. However, it should also be noted that the amount of very short fibre (less than 0.1 mm) or fibre fragment increased very sharply with mixing time. Meanwhile, the amount of longer fibre (longer than 1 mm) also decreased with mixing time.

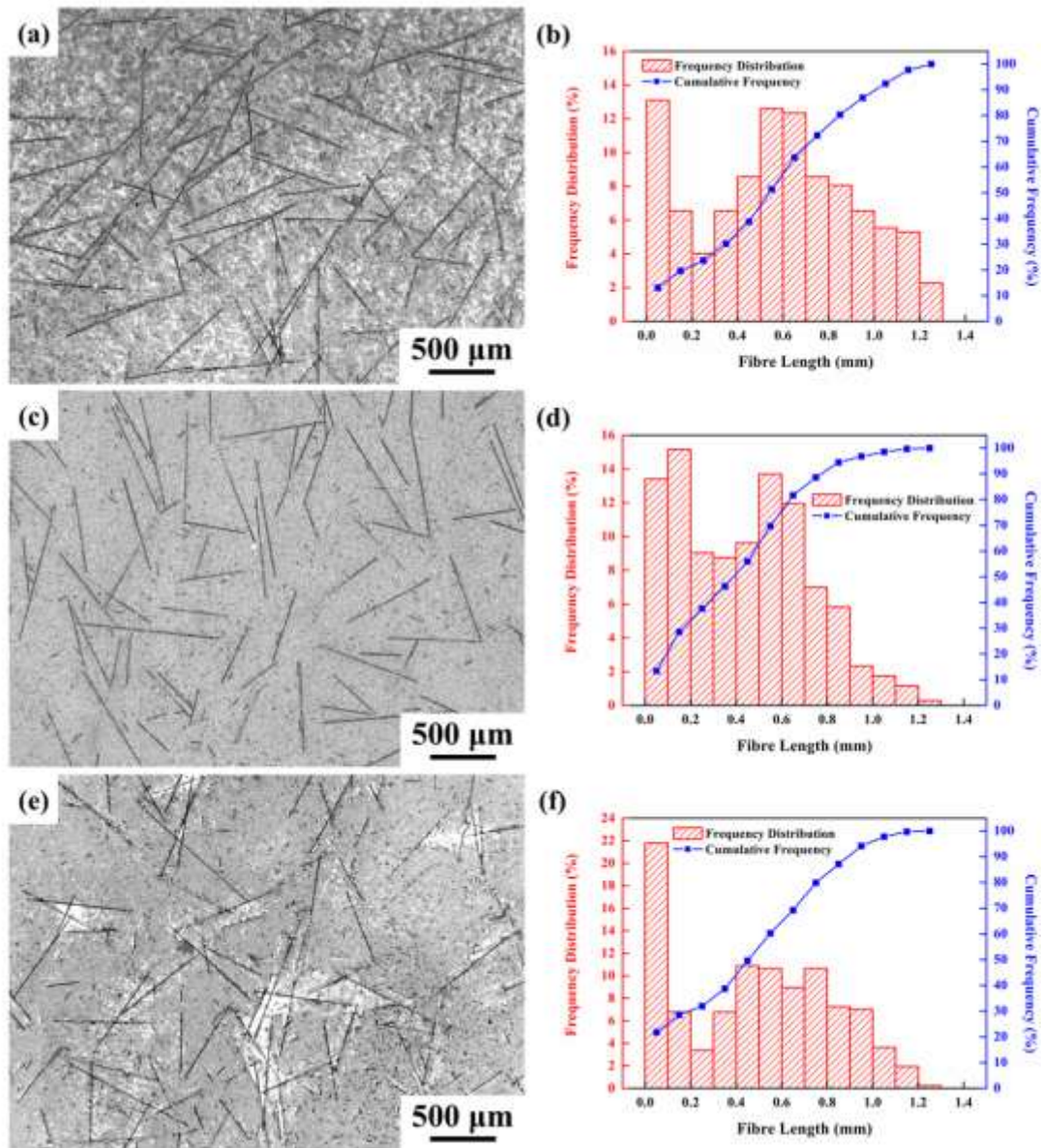


**Fig. 3.4** Typical fibre length distribution and statistical results after mechanical mixing of SiC slurry and fibre-predispersed solution. (a), (c) and (e) are the typical length distribution in the slurry whose fibre amount in final sintered samples were 5, 10 and 15 vol.% respectively. (b), (d) and (f) are the corresponding statistical results of (a), (c) and (e), respectively.

Since the fibre length observation was carried out in the slurry to make the green tapes and no obvious mechanical damage could be occurred during dissolution and

observation, the observed fibre length distribution would be as same as that in the  $C_{sf}/SiC$  green tapes. Moreover, since no significant mechanical damage would be occurred during debinding and pressureless sintering, it could be speculated that the average fibre length in sintered 5, 10 and 15 vol.%  $C_{sf}/SiC$  composites would be 0.6, 0.55 and 0.5 mm, respectively. Although the average fibre length (0.5 to 0.6 mm) after mixing was only one-sixth or -fifth of original length (3 mm), it is still much longer than in other  $C_{sf}/SiC$  composites using ball-milling. Zhang et al. [242] found that the average fibre length decreased from original 3 mm to 60  $\mu m$  in the final composites after 2 h ball-milling. Thus, the fibre length in present work is about ten times of that in Zhang's work, indicating mixing the SiC slurry with the fibre-predispersed solution is an effective method for adding fibres with limited breakage.

### 3.3 Microstructure of $C_{sf}/SiC$ multilayer composites

#### 3.3.1 Green tapes

After tape casting and drying, the green  $C_{sf}/SiC$  tapes were obtained. A good fibre dispersion before tape casing is essential to the subsequent processes. A comparison of fibre aggregation and good dispersion in green tapes is shown in Fig. 3.5. The fibre aggregations (marked by red arrows) were clear observed in Fig. 3.5a.

Roughness profiles of upper-side (in contact with air) of SiC and  $C_{sf}/SiC$  green tapes are shown in Fig. 3.6. It is obvious that the roughness on the upper-side face increased with fibre amount (Fig. 3.6). Cross section surface of stacked green tapes of 10 vol.%  $C_{sf}/SiC$  is shown in Fig. 3.7. The fibres were well distributed in the green tape, and no fibre bundle was observed.

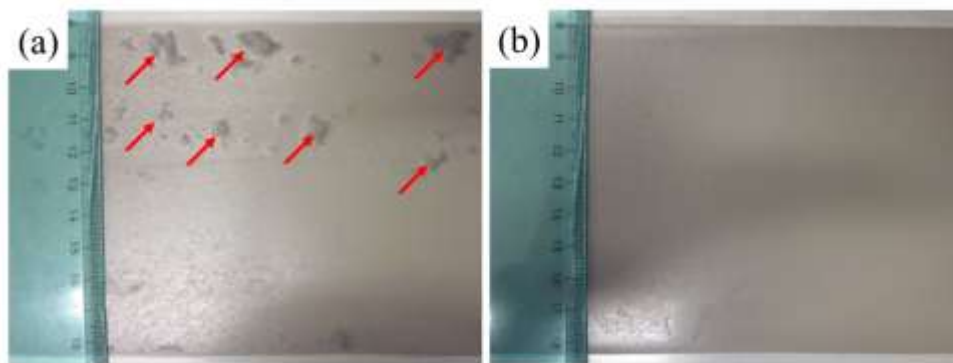


Fig. 3.5 Comparison of (a) fibre aggregation and (b) good fibre dispersion in  $C_{sf}/SiC$  green tapes.

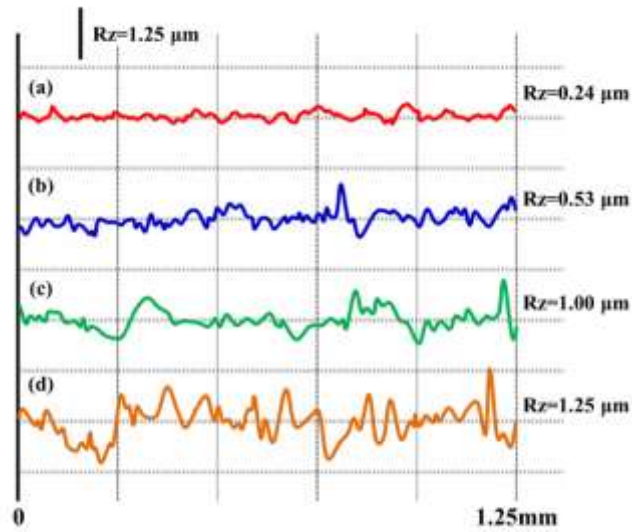


Fig. 3.6 Roughness profiles of upper-side (in contact with air) of SiC and  $C_{sf}/SiC$  green tapes (a) SiC, (b) 5 vol.%, (c) 10 vol.%, (d) 15 vol.%  $C_{sf}/SiC$  green tapes.

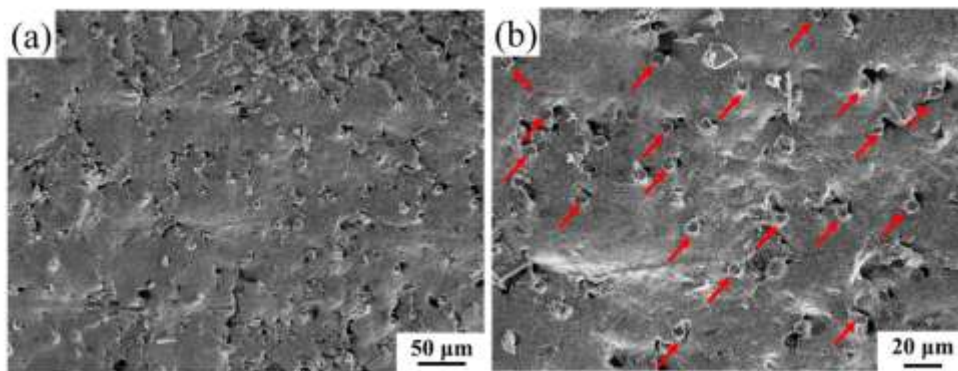


Fig. 3.7 Cross section surface of stacked green tapes of 10 vol.%  $C_{sf}/SiC$ . (a) lower magnification and (b) higher magnification.

### 3.3.2 Debinded samples

Fracture surface of  $C_{sf}/SiC$  multilayer composites (5, 10 and 15 vol.%) after debinding are shown in Fig. 3.8a, b and c, respectively. Fibre bundles were not observed, which indicates that the fibres are homogeneously distributed in the tape. Moreover, the fibres tended to align fairly well along the tape casting direction, since orientation of fibres in different directions was rarely observed.

Generally, anisotropic phases are supposed to be oriented along tape casting direction since the slurry is sheared when passing the casting blade. This phenomenon is more obvious in the slurry containing whiskers [327, 328] or short fibres [229, 330, 332].

Such an alignment will be frozen in the green tape due to high viscosity of the slurry and its pseudoplastic rheological behavior [344]. Therefore, anisotropic shrinkage behavior could be observed in the final products because of the anisotropic green tape microstructure [345]. It should be noted that even in the slurry containing platelet shaped particles, which demonstrate the most anisotropic green tape microstructure, not all particles are completely oriented in the casting direction [346]. The shrinkage behavior of SiC multilayer and  $C_{sf}/SiC$  multilayer composites will be described in detail in “4.1 Shrinkage behavior”.

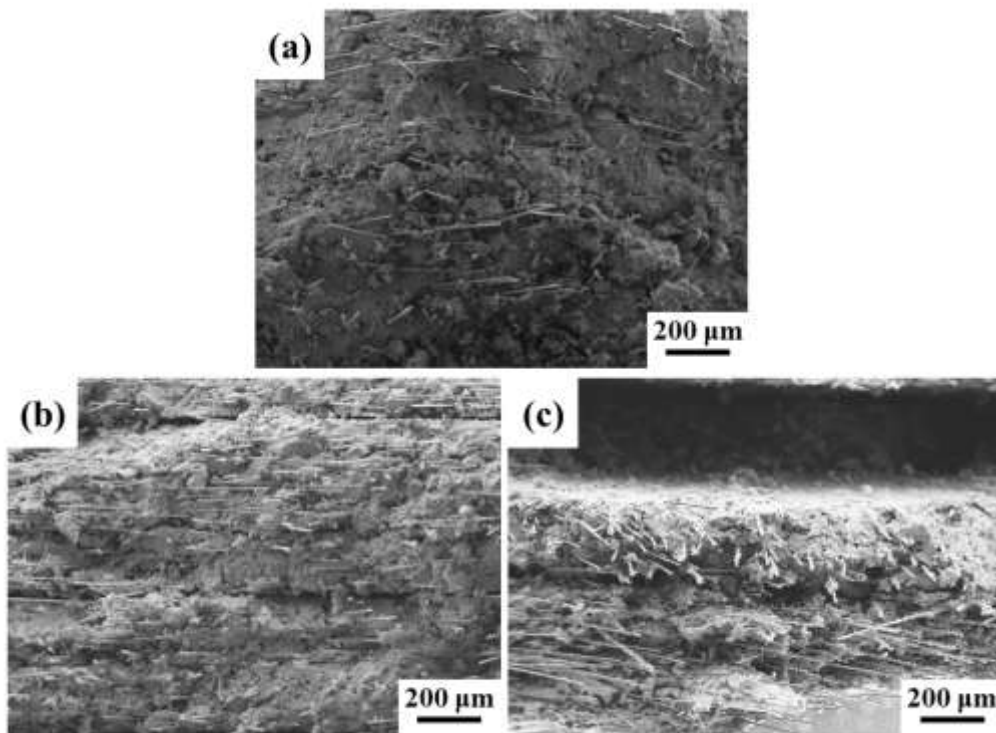
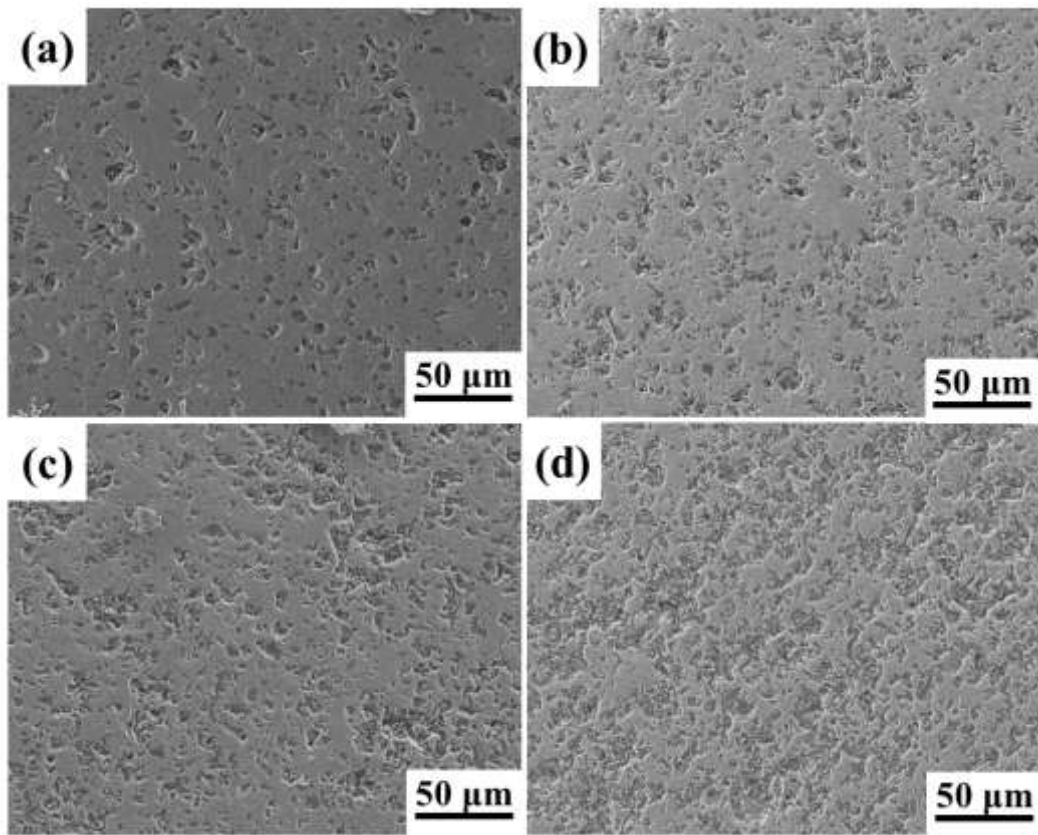


Fig. 3.8 Fracture surface of  $C_{sf}/SiC$  multilayers with different fibre amount after debinding. (a) 5 vol.%, (b) 10 vol.% and (c) 15 vol.%.

### 3.3.3 Sintered $C_{sf}/SiC$ multilayer composites

Representative morphologies of sintered SiC multilayer and  $C_{sf}/SiC$  multilayer composites are shown in Fig. 3.9. The microstructure observation was carried out in the middle part of the samples, and the polished surface was perpendicular to the tape casting direction. SiC multilayer was well sintered with few small residual pores. However, there were many pores in  $C_{sf}/SiC$  multilayer composites, while amount and size of pores increased with fibre amount. Unexpectedly, it is very hard to observe the fibre in the composite. It is well evident that the grain size of SiC became smaller

after addition of short C fibres, which is a typical phenomenon in ceramic composite after addition of reinforcement [330, 347].



**Fig. 3.9** Representative morphologies of sintered SiC multilayer and C<sub>sf</sub>/SiC multilayer composites. (a) SiC multilayer, (b) 5 vol.%, (c) 10 vol.% and (d) 15 vol% C<sub>sf</sub>/SiC multilayer composites.

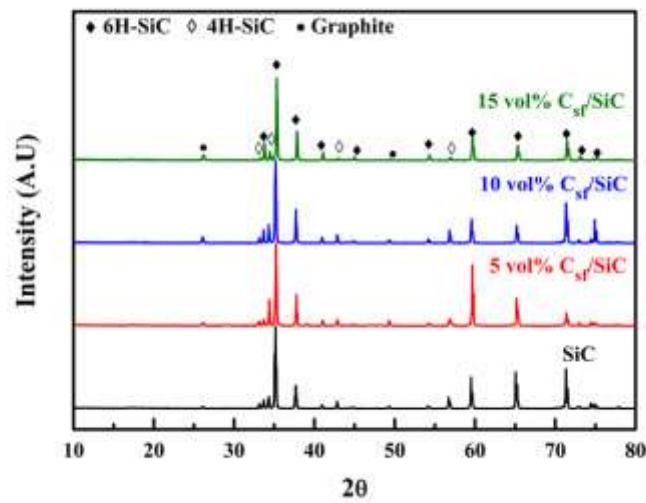


**Fig. 3.10** XRD patterns of SiC multilayer and C<sub>sf</sub>/SiC multilayer composites.

**Fig. 3.10** shows XRD patterns of SiC multilayer and C<sub>sf</sub>/SiC multilayer composites. The peak intensity of graphite increased with the fibre amount. 6H-SiC ( $\alpha$  phase) was the main phase in SiC multilayer and C<sub>sf</sub>/SiC multilayer composites. However, formation of 4H-SiC was detected by XRD after sintering (**Fig. 3.10**).

# Chapter 4. Mechanical properties of C<sub>sf</sub>/SiC multilayer composite

In this chapter, the mechanical properties and related behavior of SiC multilayer and C<sub>sf</sub>/SiC multilayer composites will be discussed. Since the mechanical properties are usually strongly affected by the relative density, which is with the total porosity, the densification behavior of SiC multilayer and C<sub>sf</sub>/SiC multilayer composites will be discussed firstly.

## 4.1 Shrinkage behavior

Density and shrinkage of SiC multilayer and C<sub>sf</sub>/SiC multilayer composites are listed in Table 4.1. The relative density of the composite containing C fibres decreased with the fibre amount. The C<sub>sf</sub>/SiC multilayer composites demonstrated significant anisotropic shrinkage behavior in X, Y and Z directions. Moreover, it is well evident that the addition of short C fibres hindered the shrinkage in the plane containing the fibres (X and Y directions) but improved the densification perpendicular to that plane (Z direction) during sintering. The higher the fibre amount, the lower the shrinkage in length.

Table 4.1 Density and shrinkage of the SiC multilayer and C<sub>sf</sub>/SiC composites

Materials	Fibre amount (vol%)	Relative density (%)	Shrinkage (%)		
			X	Y	Z
SiC multilayer	0	88.8	19.1	20.7	21.4
	5	83.1	5.1	19.0	31.7
C <sub>sf</sub> /SiC multilayer composites	10	81.3	3.9	15.1	26.4
	15	72.0	3.0	13.1	29.8

As mentioned in “3.3.2 Debinded samples”, anisotropic phases are supposed to be oriented along tape casting direction since the slurry is sheared when passing the

casting blade. This phenomenon is more obvious in the slurry containing whiskers [327, 328] or short fibres [229, 330, 332]. Such an alignment will be frozen in the green tape due to high viscosity of the slurry and its pseudoplastic rheological behavior [344]. Therefore, anisotropic shrinkage behavior could be observed in the final products because of the anisotropic green tape microstructure [345].

With the shrinkages in three directions, the shrinkage anisotropy factors ( $\Psi_{XZ}$  and  $\Psi_{YZ}$ ) [345], which are used to describe the microstructure anisotropy, could be calculated by Eq. 4.1 and 4.2, respectively.

$$\Psi_{XZ} = 100 \times \left(1 - \frac{\xi_X}{\xi_Z}\right) \quad (4.1)$$

$$\Psi_{YZ} = 100 \times \left(1 - \frac{\xi_Y}{\xi_Z}\right) \quad (4.2)$$

where  $\xi_X$ ,  $\xi_Y$  and  $\xi_Z$  are the shrinkage in X, Y and Z directions, respectively. The calculated  $\Psi_{XZ}$  and  $\Psi_{YZ}$  of SiC multilayer and  $C_{sf}/SiC$  multilayer composites are listed in Table 4.2.

**Table 4.2** Calculated  $\Psi_{XZ}$  and  $\Psi_{YZ}$  of SiC multilayer and  $C_{sf}/SiC$  multilayer composites

Materials	Fibre amount (vol%)	$\Psi_{XZ}$	$\Psi_{YZ}$
SiC multilayer	0	10.7	3.27
	5	83.9	40.1
$C_{sf}/SiC$ multilayer composites	10	85.2	42.8
	15	89.9	56.0

The calculated  $\Psi_{XZ}$  and  $\Psi_{YZ}$  of SiC multilayer were 10.7 and 3.3, respectively. These values are close to the result in ground standard alumina particles [345], which indicates the faint orientation of raw SiC particles in the green tape along tape casting

direction (X direction). However, after addition of short C fibre, the  $\Psi_{XZ}$  and  $\Psi_{YZ}$  increased sharply to more than 80 and 40, respectively. Furthermore, the values of  $\Psi_{XZ}$  and  $\Psi_{YZ}$  increased with the increased fibre amount. The high value of  $\Psi_{XZ}$  and  $\Psi_{YZ}$  indicates most of the fibres were aligned along the tape casting direction while some fibres were aligned in Y direction. Anyway, most of fibres were in the tape casting plane (X-Y plane) according to the calculation, and it is confirmed by the microstructure observation (Fig. 3.7 and Fig. 3.8).

Compared the relative density and shrinkage value in three directions, it is clear that the decreased relative density in  $C_{sf}/SiC$  multilayer composites should be attributed to the low shrinkage in X and Y directions, especially in X direction. It is easy to conclude that these fibres exerted delaying effect on shrinkage along fibre direction [330, 348]. Since most of the fibre were aligned along X direction, the shrinkage in X direction (most fibre along this direction) was greatly inhibited and the delaying effect increased with the fibre amount. Because a small amount of fibres were along other direction in the tape plane, these fibres also inhibited the shrinkage in Y direction.

In present work, B and C were used as sintering aids. The addition of B activates the sintering process by promoting the formation of a liquid phase, Si-B-C [349]. The role of free carbon is to react with the  $SiO_2$  layer on the surface of SiC particles, preventing reaction between the SiC and the  $SiO_2$  layer at high temperature [331, 349]. Carbon also inhibits grain growth of SiC [331]. Addition of short C fibre could slightly increase the amount of free C, which could be a benefit for the densification. However, the short C fibre has delaying effect on shrinkage along fibre direction, which is detrimental to the densification. Therefore, the addition of short C fibres improved the densification in Z direction and hindered the shrinkage in X and Y directions (the plane containing the fibres).

## 4.2 Mechanical properties of $C_{sf}/SiC$ multilayer composite

### 4.2.1 Stress/displacement curves

Representative bending curves of SiC multilayer and  $C_{sf}/SiC$  multilayer composites are shown in Fig. 4.1. The stress/displacement curve of SiC multilayer rose up to a maximum, and then fell abruptly, corresponding to fracture of multilayer without crack deflection. This characteristic was also observed in  $C_{sf}/SiC$  multilayer composites.

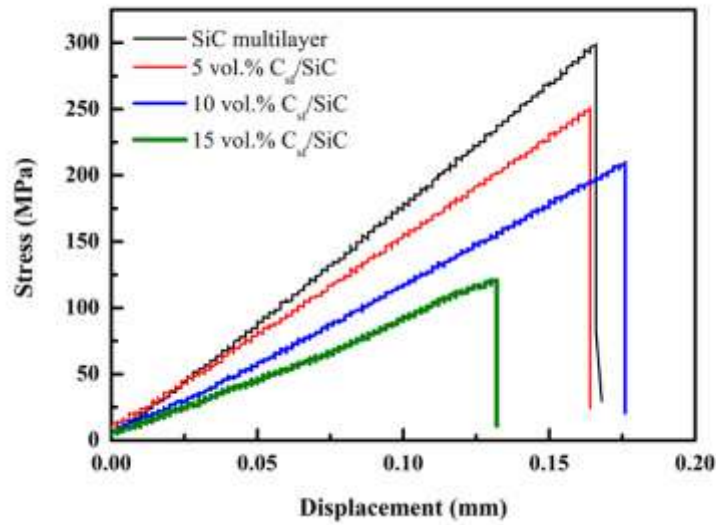


Fig. 4.1 Representative bending curve of SiC multilayer and  $C_{sf}/SiC$  multilayer composites.

However, ladder-like curve, which corresponds to failure of single layer and crack deflection, is an important characteristic for dense SiC multilayer, especially in buckles [262]. One sample of 5 vol.%  $C_{sf}/SiC$  multilayer composite presented ladder-like curve (Fig. 4.2), and crack deflection in 5 vol.%  $C_{sf}/SiC$  multilayer composite was also observed (as shown in enlarged view in Fig. 4.3). These phenomenon indicate the addition of C fibre would not change the crack deflection at weak interface.

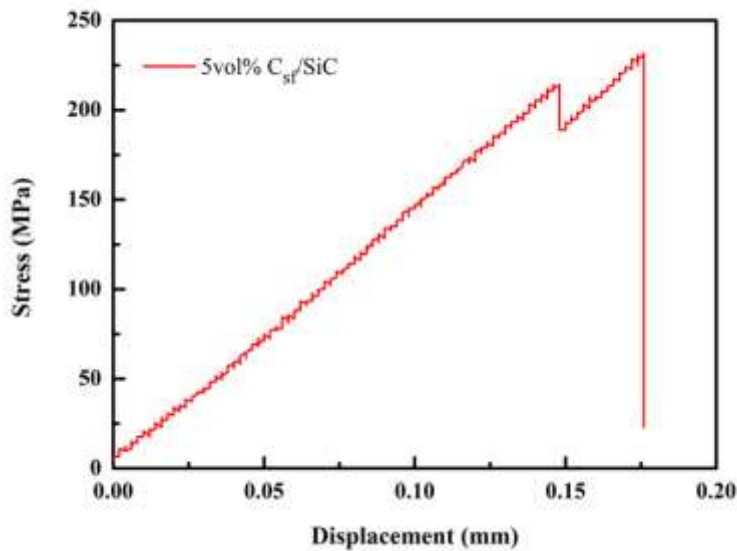


Fig. 4.2 Ladder-like bending curve in 5vol%  $C_{sf}/SiC$  multilayer composite.

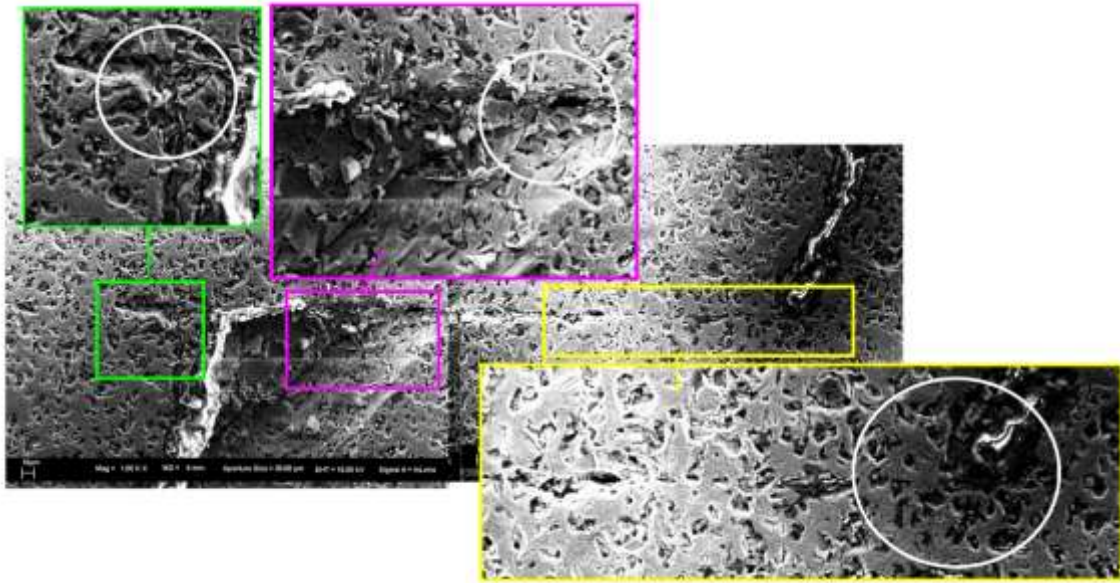


Fig. 4.3 Crack deflection in 5vol.% C<sub>sf</sub>/SiC multilayer composite.

## 4.2.2 Mechanical properties

Relationships among fibre amount, relative density and elastic modulus or bending strength of SiC multilayer and C<sub>sf</sub>/SiC multilayer composites are shown in Fig. 4.4. Since the elastic modulus of C fibre (240 GPa) is lower than that of SiC (450 GPa), elastic modulus of C<sub>sf</sub>/SiC multilayer composites should decrease with the increase of fibre amount. Moreover, addition of C fibres decreased the relative density and then increased the residual porosity, which leads to the worsening in elastic modulus. The combined effects lead the elastic modulus to decrease linearly with fibre amount.

As discussed in “3.2 Dispersion of short carbon fibres in SiC slurry”, the average fibre length (Fig. 3.4) in present system is much longer than that in Zhang et al. [242]’s work. Zhang et al. [242] reported that increase of short carbon fibre from 10 to 30 vol.% improved flexural strength from 213 to 416 MPa. Thus, the addition of short C fibre in present work should also demonstrate improvement effect on the bending strength. However, the addition of short C fibres increased the residual porosity. Bending strength of C<sub>sf</sub>/SiC multilayer composites decreased with fibre amount. This behavior implies that bending strength is affected more significantly by the residual porosity. Actually, a very strong relationship between bending strength and relative density has been reported for SiC-based composites reinforced with short SiC fibres [228, 229] or C fibres [233, 237, 241]. These results suggest that the bending strength

may be greatly limited by the amount of residual porosity. The rationale behind this hypothesis may be that pores lower the initial microcracking stress in the matrix.

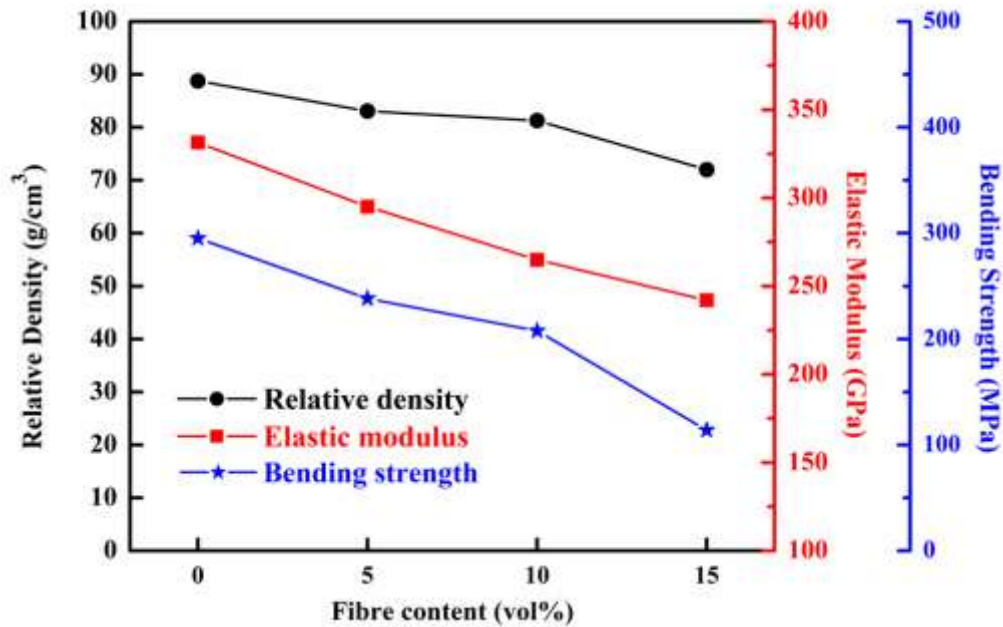


Fig. 4.4 Relationships among fibre content, relative density and elastic modulus or bending strength of SiC multilayer and C<sub>sf</sub>/SiC multilayer composites.

### 4.2.3 Fracture toughness

Relationships among fibre amount, relative density and fracture toughness ( $K_{IC}$ ) of SiC multilayer and C<sub>sf</sub>/SiC multilayer composites are shown in Fig. 4.5a. The fracture toughness of C<sub>sf</sub>/SiC multilayer composites decreased slightly with the increase of fibre amount, which should be due to the increase porosity (Fig. 4.5a).

The fracture toughness value of SiC multilayer was about 2.24 MPa·m<sup>1/2</sup>. However, it should be noted that the multilayer composites composed by alternative layers of SiC and C<sub>sf</sub>/SiC layer demonstrated improved fracture toughness than that of SiC multilayer (Fig. 4.6). The fracture toughness of SiC/(5 vol.% C<sub>sf</sub>/SiC) and SiC/(10 vol.% C<sub>sf</sub>/SiC) multilayer composites were 2.41 and 2.35 MPa·m<sup>1/2</sup>, respectively. They were 7.5% and 4.9% higher than that of SiC multilayer, respectively. The improvement of fracture toughness in the SiC/(C<sub>sf</sub>/SiC) multilayer composites should be attributed to the residual thermal stress [324, 325]. These interesting results

indicate that the fracture toughness of SiC-based thermal protection system could be improved through designing its architecture.

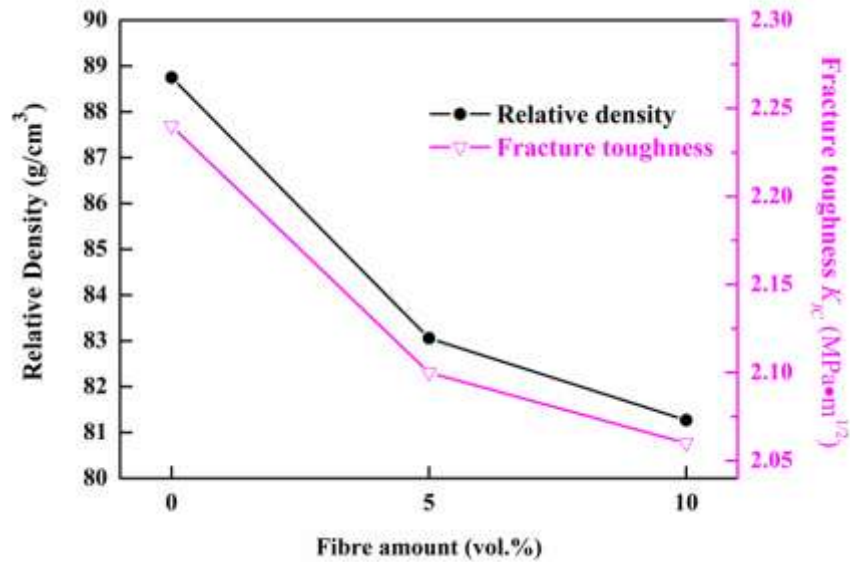


Fig. 4.5 Relationships among fibre amount, relative density and fracture toughness ( $K_{IC}$ ) of SiC multilayer and  $C_{sf}/SiC$  multilayer composites

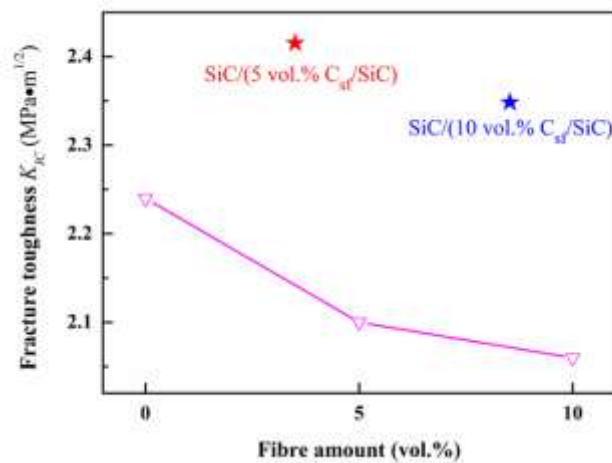


Fig. 4.6 Fracture toughness of multilayer composites composed by alternative layers of SiC and  $C_{sf}/SiC$  layer.

#### 4.2.4 Fracture surface

The fracture surface of SiC multilayer and  $C_{sf}/SiC$  multilayer composites are shown in Fig. 4.7. The fracture behaviour of SiC multilayer and  $C_{sf}/SiC$  multilayer composites

was catastrophic, and few fibre pull-out was observed (as pointed out by red arrows in Fig. 4.7c and d). In present work, the carbon fibres were not surfaced treated, and then they were in direct contact with SiC matrix. Generally, the interface between uncoated fibre and matrix is very strong, and would make the interfacial debonding or fibre pull-out more difficult [236, 237]. As mentioned above, the SiC grain size decreased with the increase of fibre amount (Fig. 3.9). Finer grain would also be beneficial to strength. However fibres can affect the strength in several other ways: the addition of short C fibres hinders the shrinkage during sintering and results in enhanced residual porosity, which is detrimental to strength; on the other hand it also produces slight increase of free C amount which could help sintering.

The addition of short carbon fibre hinders the shrinkage in plane containing fibres and leads to the increase of residual porosity, which resulted in the decrease the elastic modulus, bending strength and fracture toughness. Therefore, the sintering process of  $C_{sf}/SiC$  multilayer composites should be improved for application requiring high mechanical strength. This last result could be achieved by applying pressure during sintering, optimizing other sintering parameters or using more effective sintering aids.

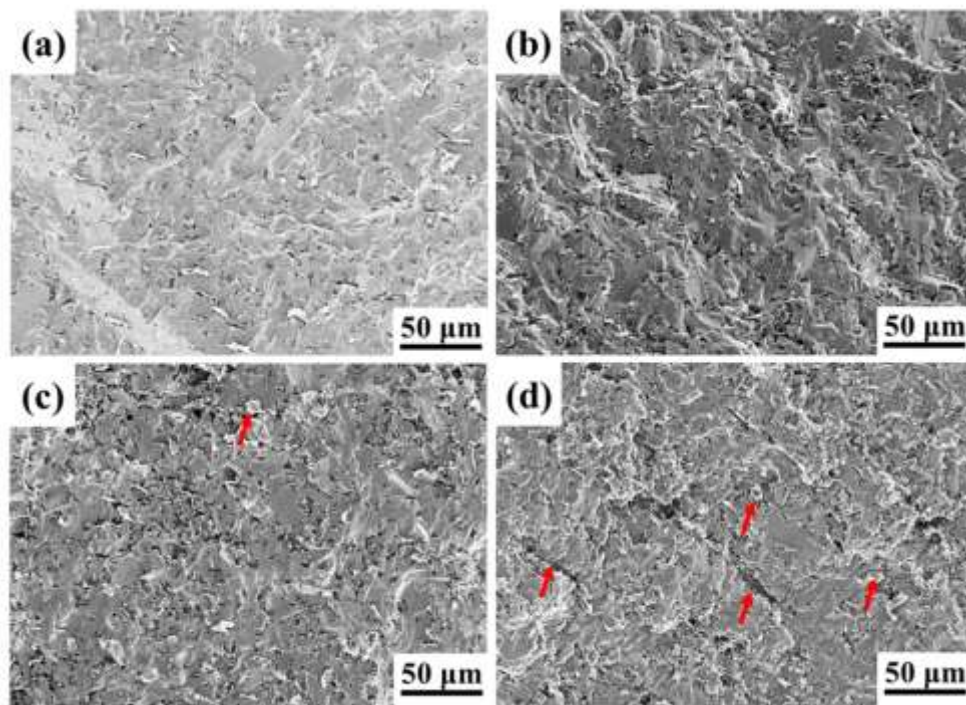


Fig. 4.7 Fracture surface of SiC multilayer and  $C_{sf}/SiC$  multilayer composites. (a) SiC multilayer, (b) 5, (c) 10 and (d) 15 vol.%  $C_{sf}/SiC$  multilayer composites.

# Chapter 5. Thermophysical properties of $C_{sf}/SiC$ multilayer composite

Besides mechanical properties, the thermophysical properties, such as oxidation resistance and thermal conductivity, are also very important for the application in thermal protection system. The mechanical behavior of  $C_{sf}/SiC$  multilayer composite has been illustrated in “Chapter 4 Mechanical properties of  $C_{sf}/SiC$  multilayer composite”. In this chapter, the oxidation properties, thermal expansion and thermal conductivities will be discussed.

## 5.1 Oxidation properties

The oxidation curves (from TGA measurements in air) of  $SiC$  multilayer and  $C_{sf}/SiC$  multilayer composites are shown in Fig. 5.1. It is well evident that the weight loss of  $C_{sf}/SiC$  multilayer composites was larger than that of  $SiC$  multilayer and was increased with the increase of fibre amount and porosity, owing to the oxidation of C fibres.

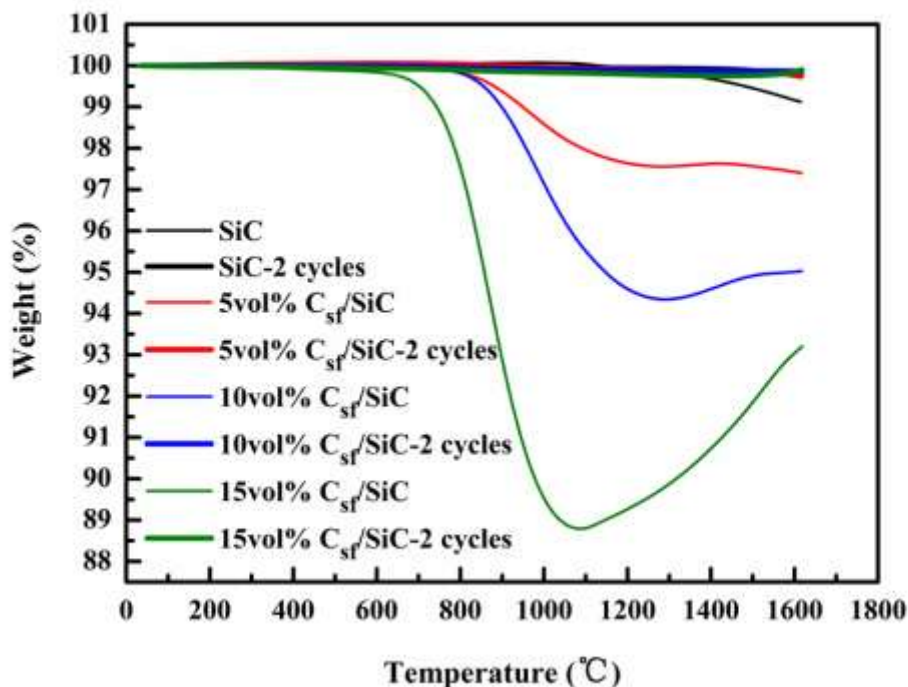


Fig. 5.1 Oxidation curves of  $SiC$  multilayer and  $C_{sf}/SiC$  multilayer composites.

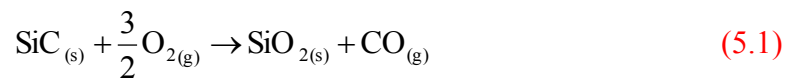
The oxidation curves of  $C_{sf}/SiC$  multilayer composites could be divided into three

zones. Up to 600 °C, the oxidation of SiC multilayer and C<sub>sf</sub>/SiC multilayer composites was negligible. However, between 600 and 1300 °C (zone 2), SiC multilayer and C<sub>sf</sub>/SiC multilayer composites underwent a progressive loss of weight (Table 5.1).

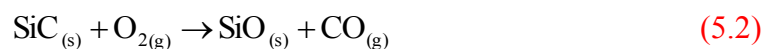
Table 5.1 Comparison of weight loss during oxidation and carbon amount in materials

Materials	C fibre content		Free carbon content (wt.%)	Maximum weight loss up to 1300 °C (wt.%)	
	in volume	in weight		First	Second
	(vol%)	(wt.%)		oxidation	Oxidation
SiC multilayer	0	0	4.5	0.2	< 0.1
C <sub>sf</sub> /SiC	5	2.8	4.4	2.4	0.1
multilayer	10	5.8	4.2	5.7	0.1
composites	15	8.9	4.1	11.2	0.2

Depending on the oxygen partial pressure and temperature, oxidation of SiC will lead to the formation of a condensed phase oxide, SiO<sub>2</sub>(s), or a volatile sub-oxide, SiO(g) [350]. At low temperature and high oxygen partial pressure, the condensed SiO<sub>2</sub> would be formed at the surface of SiC bulk. The condensed SiO<sub>2</sub> is protective and could prevent inner material from further oxidation [351]. Thus, the formation of SiO<sub>2</sub> is termed as “passive oxidation” (Eq.5.1) [350, 351]:



At high temperature and low oxygen partial pressure, the volatile SiO would be formed. Its formation could not protect the inner materials and SiC will be characterized by significant mass loss. Thus, the formation of SiO is termed as “active oxidation” (Eq.5.2) [352]:



It is worth to note that the occurrence of passive oxidation (Eq.5.1) will cause the

weight gain, and occurrence of active oxidation (Eq.5.2) will cause the weight loss. Moreover, the active oxidation would occur only at very low oxygen partial pressure [353].

Therefore, the weight loss could not be ascribed to oxidation of SiC, since the passive oxidation mechanism involves a weight gain, and the condition of oxidation test (oxygen partial pressure of 0.21) was very far from those typical of active oxidation [353, 354]. The second oxidation curves of SiC multilayer and C<sub>sf</sub>/SiC multilayer composites (resulting from a second run in TGA equipment) showed negligible weight loss between 600 and 1300 °C, which indicates that the weight loss phenomenon was due to the oxidation of residual C (carbon was added to the slurry in order to help sintering and an additional amount of carbon also forms owing to the pyrolysis of plasticizers and binders) or C fibre that get in touch with the gaseous atmosphere. Moreover, the neglective weight loss of SiC multilayer and C<sub>sf</sub>/SiC multilayer composites indicates that the passive oxidation of SiC was still occurred after addition of short fibres.

The weight ratios between SiC, carbon (added as sintering aid) and short C fibre were designed for obtaining multilayer composites with final fibre volume percent of 5, 10 and 15, respectively. From the amount of solid components weighted for the preparation of these materials and knowing the amount of free carbon coming from thermal decomposition of binder and plasticizer (Fig. 2.9), it is possible to calculate the weight percent of free carbon and carbon fibres contained in SiC multilayer and C<sub>sf</sub>/SiC multilayer composites (Table 5.1). In SiC multilayer, the carbon amount is 4.5 wt.%. In C<sub>sf</sub>/SiC multilayer composites, the total amount of carbon that can burn is given by the sum of carbon fibre and free carbon. Since the weight loss of multilayer SiC during the first run was only 0.2 wt.%, it is obvious that the passivating silica layer works well as barrier in this case. In C<sub>sf</sub>/SiC multilayer composites containing carbon fibre, the weight loss occurring during the first oxidation run was higher and increased with the increase of fibre amount and material porosity. However, in the composites with 5 and 10 vol% C fibre, the weight losses are slightly lower than C fibre amount, and much lower than total carbon percent. Therefore, the passivating silica layer also grants protection to the C<sub>sf</sub>/SiC multilayer composites. In the 15 vol.% C<sub>sf</sub>/SiC multilayer composite, the weight loss is very significant, and it is higher than C fibre amount. Conclusively the weight loss of C<sub>sf</sub>/SiC multilayer composites is related to fibre amount and porosity.

Actually, after the first run a passivating silica layer has grown on the specimen surface, thus providing protection against further oxidation. Therefore, the weight changes of SiC multilayer and C<sub>sf</sub>/SiC multilayer composites during second oxidation cycle were negligible.

Above 1300 °C of the first run, weight loss was observed in SiC multilayer due to oxidation of residual carbon. However, weight gain was found in C<sub>sf</sub>/SiC multilayer composites, which should be due to the passive oxidation of SiC [350, 351].

## 5.2 Specific heat capacity

According to Eq.2.6, it is necessary to obtain the specific heat capacity in order to calculate the thermal conductivity. The measured specific heat capacity of SiC multilayer and C<sub>sf</sub>/SiC multilayer composites from room temperature to 600 °C is plotted in Fig. 5.2. The specific heat capacity of SiC multilayer and C<sub>sf</sub>/SiC multilayer composites increased with temperature and fibre amount from room temperature to 600 °C.

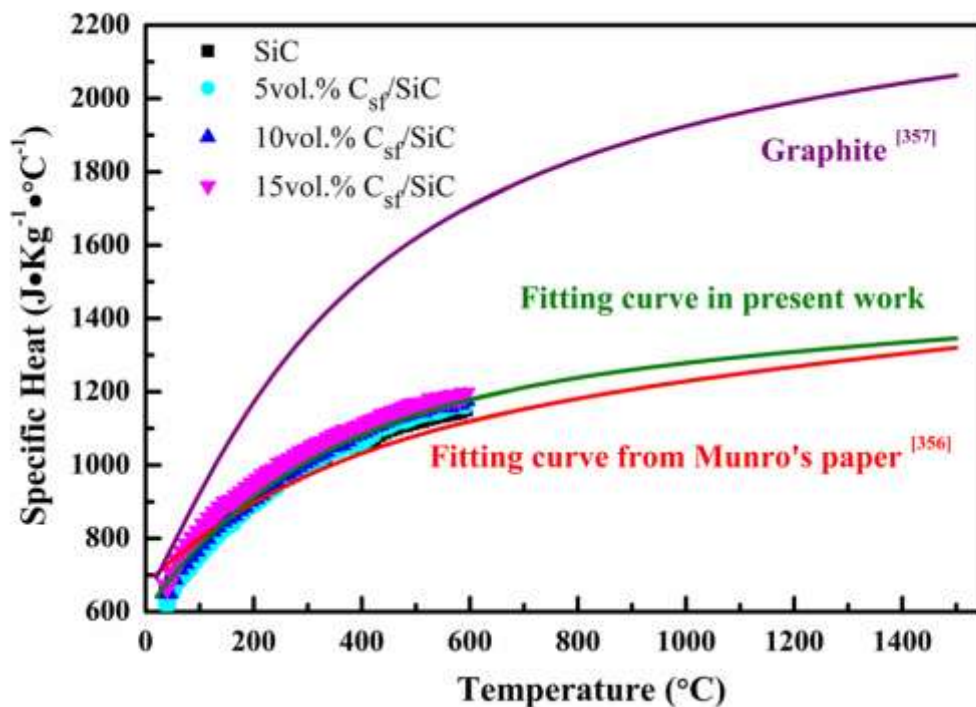


Fig. 5.2 Temperature dependence of specific heat capacity of SiC multilayer and C<sub>sf</sub>/SiC multilayer composites. The red line is the fitting curve in Munro's work [355], the olive line is the fitting result in present work, and purple line is the specific heat of graphite [356].

The measured data was fitted to estimate its specific heat capacity at high temperature (above 600 °C). The fitting result of measured data and fitting result from Munro's paper [355] are also shown in Fig. 5.2. Since there was about 4.5 wt.% graphite in the sintered SiC multilayer, the specific heat capacity of graphite is shown in Fig. 5.2 for comparison [356]. The specific heat capacity represents the absorption ability of heat, and it could be calculated from the contribution of the constituents. Since the specific heat capacity of graphite is higher than SiC, especially at high temperature, the measured  $C_p$  in present work slightly increased with the fibre amount due to the contribution of graphite (Table 5.1), and was slightly higher than Munro's fitting curves above 100 °C.

The fitting equation reported by Munro and in present work for specific heat capacity is written as Eq.5.3 [355] and 5.4, respectively. It should be noted that fitting equation used in present work was based on the Munro's equation, and only the value in his equation was slightly changed. Since the value difference among specific heat were very little, Eq.5.4 was used for thermal conductivity calculation in SiC multilayer and  $C_{sf}/SiC$  multilayer composites in present work.

$$C_p = 1110 + 0.15T - 425 \exp(-0.003T) \quad (5.3)$$

$$C_p = 1200 + 0.1T - 600 \exp(-0.0033T) \quad (5.4)$$

where  $T$  is the temperature in °C.

### 5.3 Thermal expansion behavior

The relative length changes of SiC, 5 and 10 vol.%  $C_{sf}/SiC$  multilayer composites in different directions from room temperature to 1500 °C are shown in Fig. 5.3a, b and c, respectively. The relative length change increased with variation of temperature, and no significant difference among the thermal expansion behavior of SiC and  $C_{sf}/SiC$  multilayer composites in three directions was observed. For comparison, the relative length changes of SiC, 5 and 10 vol.%  $C_{sf}/SiC$  multilayer composites in X direction are shown in Fig. 5.4. There is no significant difference among the thermal expansion behavior of SiC and  $C_{sf}/SiC$  multilayer composites below 1300 °C was found. However, between 1300 and 1500 °C, the relative length change decreased with the increase of fibre amount. This behavior should be attributed to the increase of porosity after addition of fibre since there was no obvious difference amount 5 and 10 vol.%

$C_{sf}/SiC$  multilayer composites in different directions.

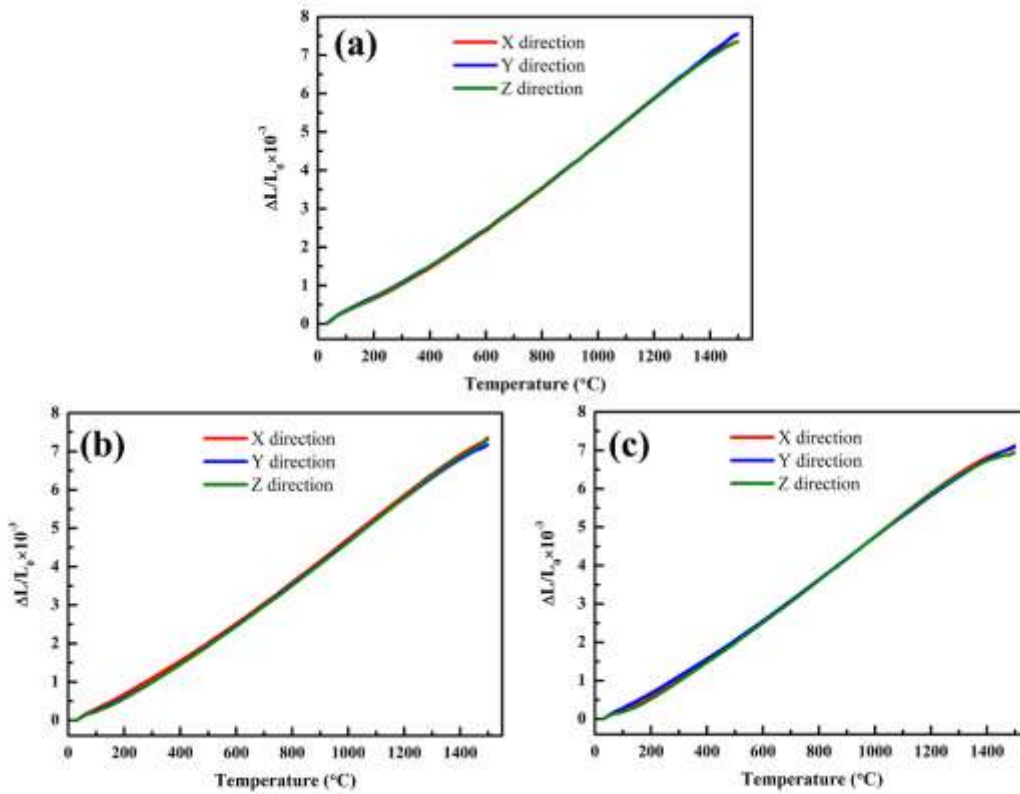


Fig. 5.3 The relative length changes of (a) SiC, (b) 5 and (c) 10 vol.%  $C_{sf}/SiC$  multilayer composites in different directions from room temperature to 1500  $^{\circ}C$ .

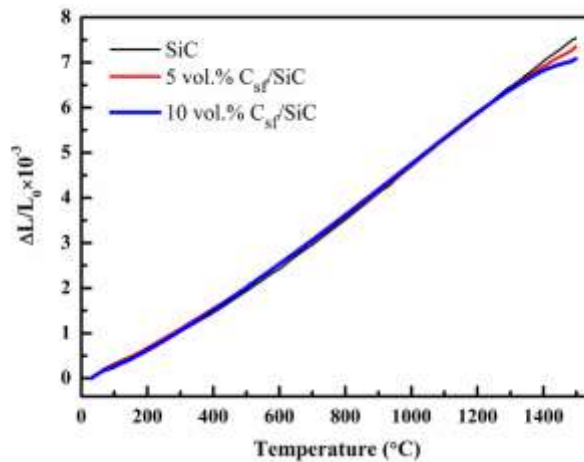


Fig. 5.4 The relative length changes of SiC and  $C_{sf}/SiC$  multilayer composites in X direction.

Although CTE of C fibre in axial direction is very low (close to zero) [357], SiC matrix also exhibits a low CTE (about  $4 \times 10^{-6} / ^{\circ}C$ ). Moreover, the fibre amount in

present work was low (5 and 10 vol.%). Thus, the thermal expansion behavior of  $C_{sf}/SiC$  multilayer composites was slightly affected by the addition of short C fibre. As a representative, only thermal expansion behavior of SiC multilayer was discussed in below.

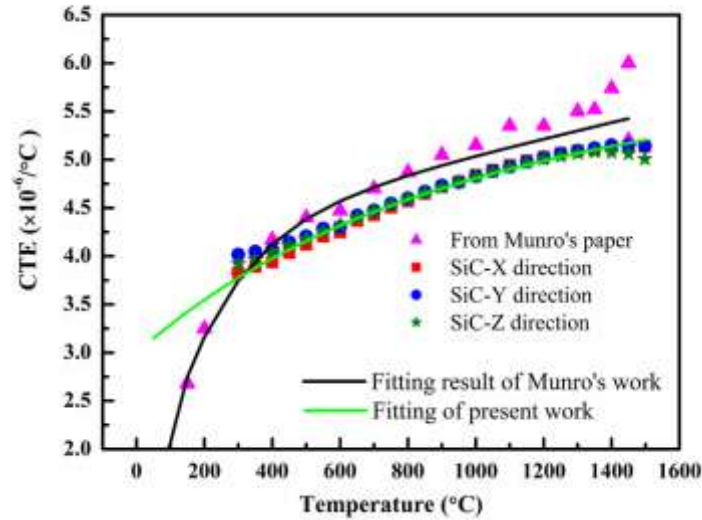


Fig. 5.5 Temperature dependence of CTE of SiC multilayer in X, Y and Z directions.

The average CTEs from 300 to 1500 °C were shown in Fig. 5.5. The CTEs of SiC multilayer in different directions were very close, and slightly increased with temperature. The CTEs of SiC multilayer increased from  $3.7 \times 10^{-6} /^{\circ}C$  at 300 °C to  $5.0 \times 10^{-6} /^{\circ}C$  at 1500 °C. The CTE data and corresponded fitting curve of a sintered  $\alpha$ -SiC from Munro's paper was also shown in Fig. 5.5 [355]. The equation given by Munro is expressed as Eq.5.5:

$$\alpha(10^{-6} /^{\circ}C) = 4.22 + 8.33 \cdot 10^{-4} T - 3.51 \cdot \exp(-0.00527T) \pm 10\% \quad (5.5)$$

After changed some parameters in Eq.5.5, the fitting result for SiC multilayer could be given as Eq.5.6:

$$\alpha(10^{-6} /^{\circ}C) = 5 + 3 \cdot 10^{-4} T - 2 \cdot \exp(-0.0014T) \quad (5.6)$$

Since no significant difference of the thermal expansion behavior of SiC multilayer and  $C_{sf}/SiC$  multilayer composites in different directions was found, their thermal expansion behavior could be considered as isotropic. Therefore, their mass density of at high temperature could be calculated according to Eq.5.7:

$$\rho(T) = \rho_0 \cdot [1 + \alpha \cdot (T - 25)]^{-3} \quad (5.7)$$

where  $\rho_0$  is the density at the room temperature (25 °C).

## 5.4 Thermal diffusivity properties

Fig. 5.6 shows the thermal diffusivities-temperature relationship of SiC multilayer, 5 and 10 vol.% C<sub>sf</sub>/SiC multilayer composites in three directions before and after oxidation treatment.

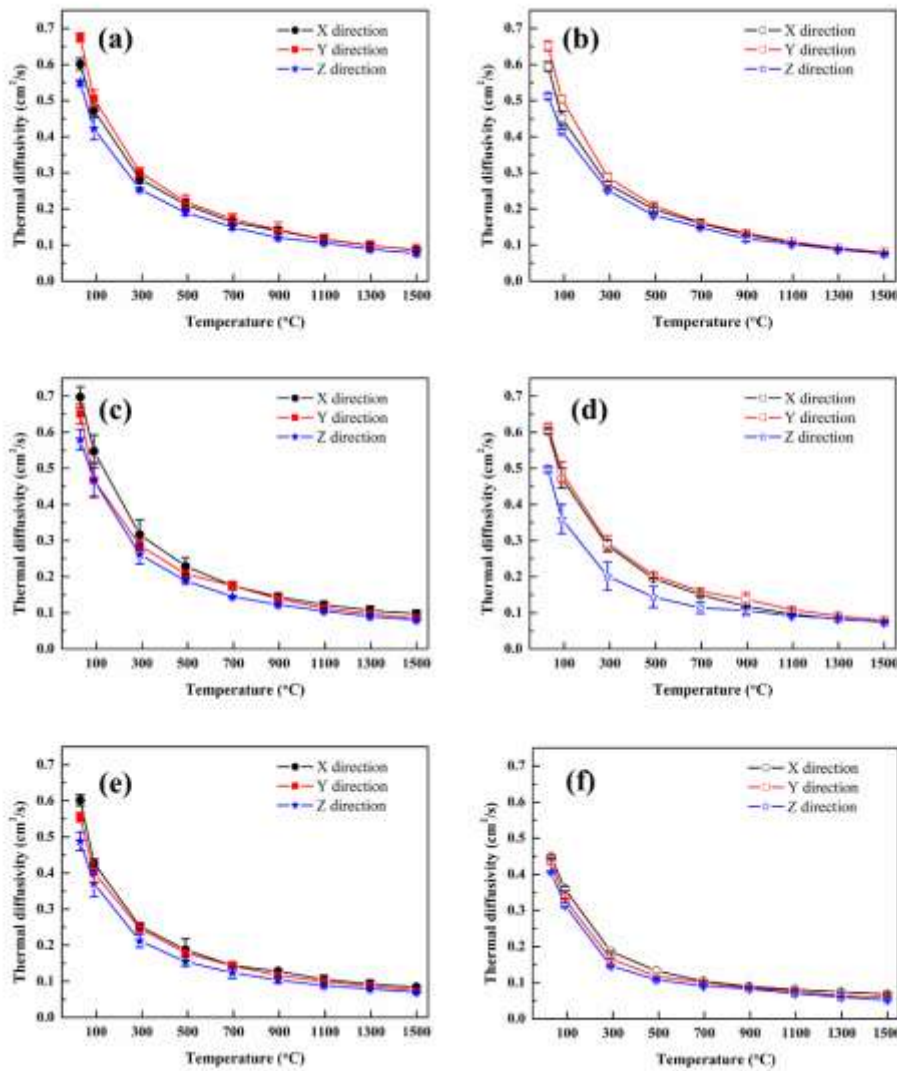


Fig. 5.6 Thermal diffusivities-temperature relationship of (a) (b) SiC multilayer, (c) (d) 5 and (e) (f) 10vol% C<sub>sf</sub>/SiC multilayer composites in three directions. (a) (c) (e) are before oxidation treatment and (b) (d) (f) are after oxidation treatment, respectively.

Regardless of testing directions, materials and oxidation treatment, their thermal diffusivities decreased with the increase of temperature in the present testing range. The thermal diffusivity in Z direction was the lowest among the three directions in all materials due to the presence of interface between layers. However, it is very interesting that the thermal diffusivity of SiC multilayer in Y direction was slightly higher than in X direction. For 5 and 10 vol.% C<sub>sf</sub>/SiC multilayer composites, thermal diffusivities were found in this order: X > Y > Z.

For SiC multilayer, the thermal diffusivities in all directions were slightly decreased after oxidation treatment. To be more clear, the thermal diffusivities of SiC multilayer and C<sub>sf</sub>/SiC multilayer composites in Z direction from 30 to 1500 °C before and after oxidation treatment are shown in Fig. 5.7a and b, respectively. The decrease of thermal diffusivities after oxidation treatment was more significant in C<sub>sf</sub>/SiC multilayer composites, especially in 10 and 15 vol.% C<sub>sf</sub>/SiC multilayer composites. This phenomenon will be discussed in more detail in “5.5 Thermal conductivity properties”.

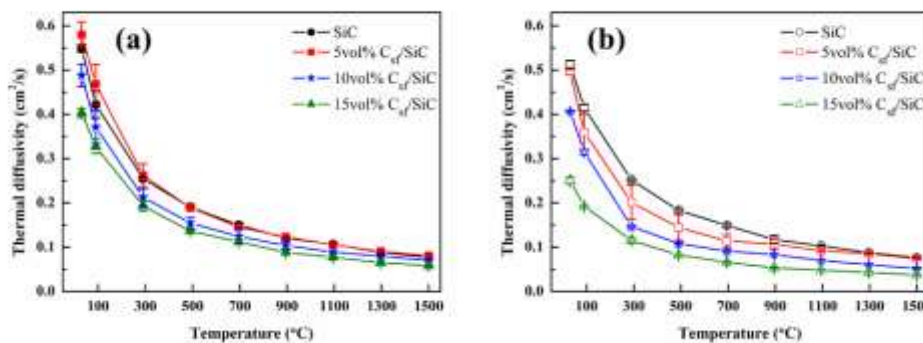


Fig. 5.7 Thermal diffusivities of SiC multilayer and C<sub>sf</sub>/SiC multilayer composites in Z direction from 30 to 1500 °C (a) before and (b) after oxidation treatment.

## 5.5 Thermal conductivity properties

Fig. 5.8 shows the thermal conductivities-temperature relationship of SiC multilayer, 5 and 10 vol.% C<sub>sf</sub>/SiC multilayer composites in three directions before and after oxidation treatment. The thermal conductivities of SiC multilayer and C<sub>sf</sub>/SiC multilayer composites in Z direction from 30 to 1500 °C before and after oxidation treatment are shown in Fig. 5.9a and b, respectively.

According to Eq.2.6, the thermal conductivity shows the similar trend as diffusivity when density and specific heat are same or close (as in the present work). Regardless of testing directions, fibre amount and oxidation treatment, the thermal conductivities decreased at elevated temperature (from 30 to 1500 °C). In order to illustrate the effect of fibre addition and oxidation treatment, only thermal conductivities at room temperature are used for comparison and discussion.

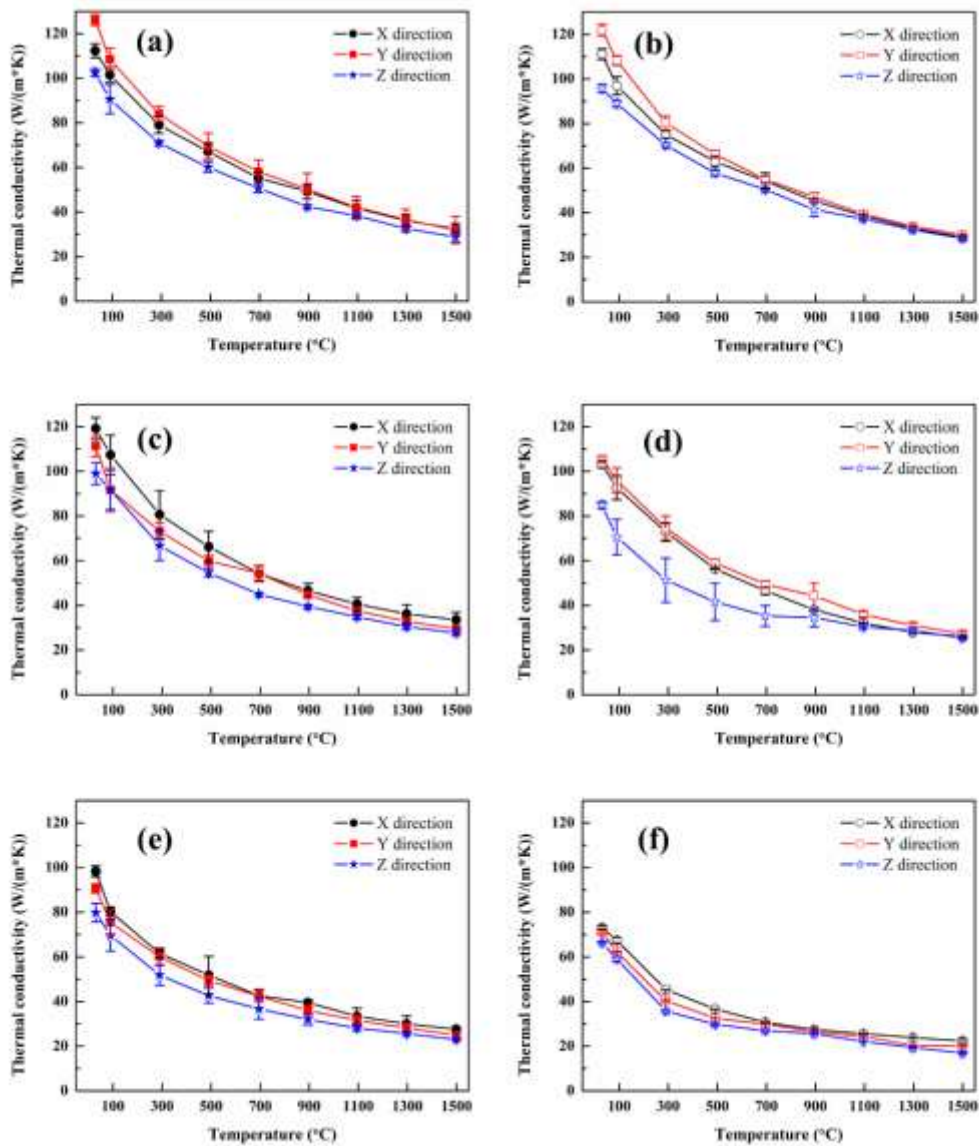


Fig. 5.8 Thermal conductivities-temperature relationship of (a) (b) SiC multilayer, (c) (d) 5 and (e) (f) 10vol% C<sub>sf</sub>/SiC multilayer composites in three directions. (a) (c) (e) are before oxidation treatment and (b) (d) (f) are after oxidation treatment, respectively.

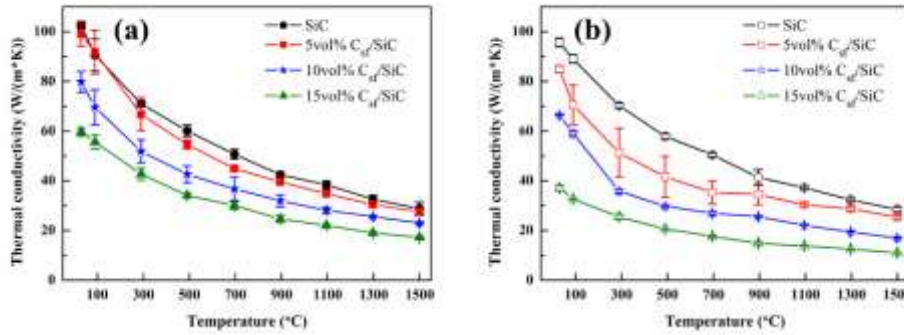


Fig. 5.9 Thermal conductivities of SiC multilayer and  $C_{st}/SiC$  multilayer composites in Z direction from 30 to 1500 °C (a) before and (b) after oxidation treatment.

### 5.5.1 SiC multilayer

Comparison of thermal conductivities comparison of SiC multilayer in X, Y and Z directions at room temperature before and after oxidation is shown in Fig. 5.10. It is obvious that the thermal conductivities in all directions slightly decreased after oxidation treatment. Moreover, it is very interesting that SiC multilayer showed highest thermal conductivity in Y direction instead of X direction.

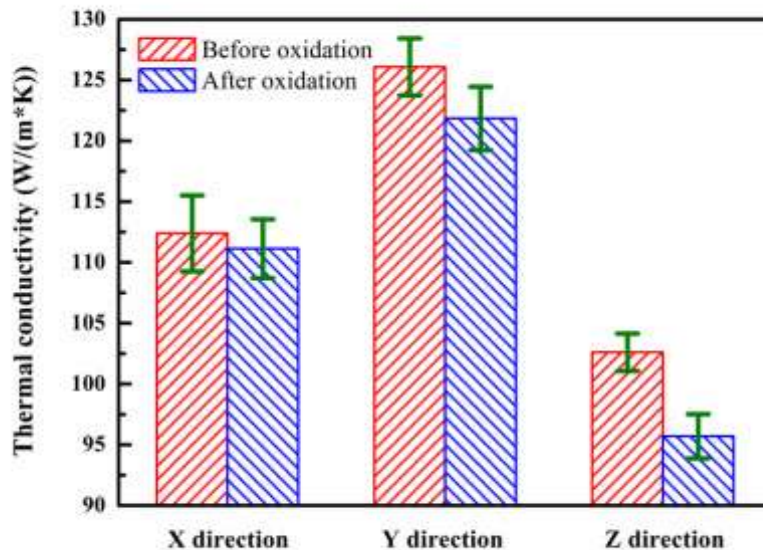


Fig. 5.10 Thermal conductivities comparison of SiC multilayer in X, Y and Z directions at room temperature before and after oxidation.

In order to understand its thermal conductivity behavior in different directions, microstructure of SiC multilayer in different direction (or different plane) was observed, as shown in Fig. 5.11.

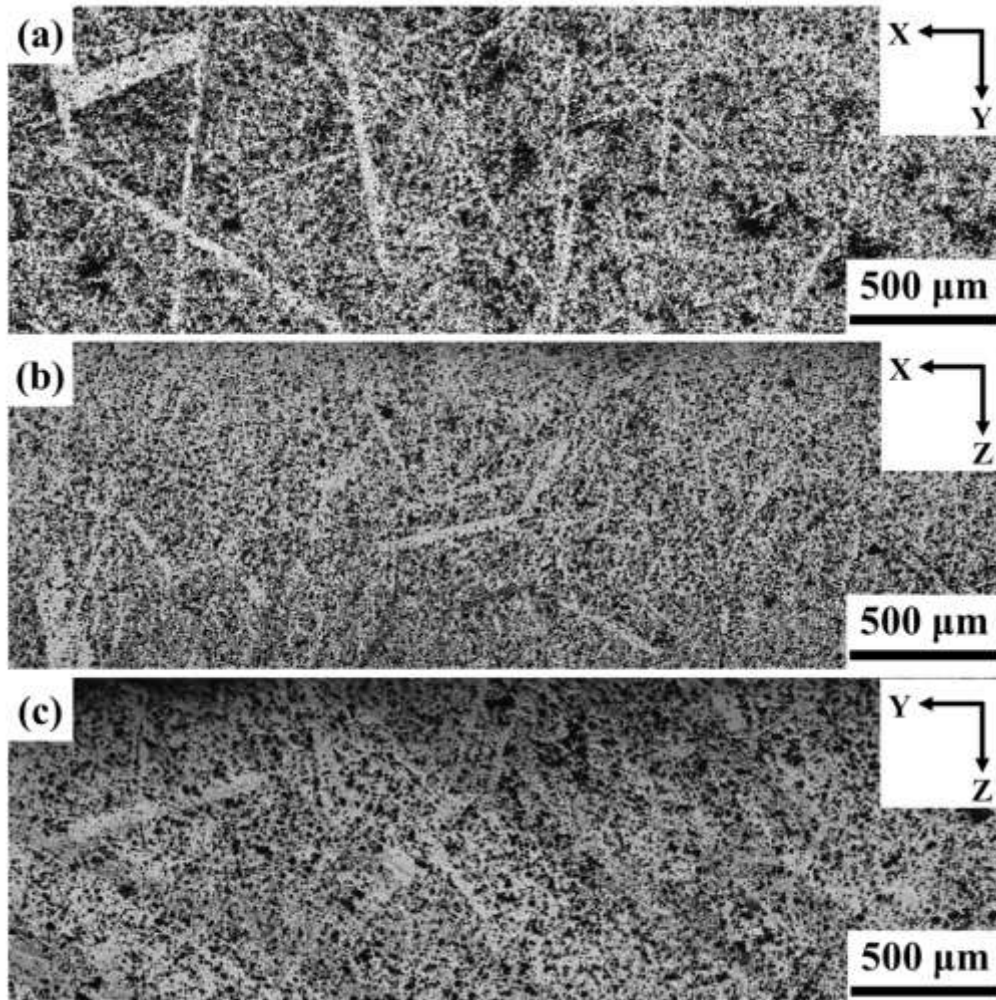


Fig. 5.11 Microstructure of SiC multilayer in (a) X-Y plane, (b) X-Z plane and (c) Y-Z plane.

The interface between SiC layers in the sintered SiC multilayer was not clear. However, the interface could be observed in the fracture surface of sintered SiC SiC multilayer buckle (Fig. 5.12) [262]. There were elongated SiC grains partially aligned in X, Y and Z directions, especially in Y direction (Fig. 5.11a). As discussed in “4.1 Shrinkage behavior”, although anisotropic phases are supposed to be oriented along tape casting direction, there was faint orientation of raw SiC particles in the green tape along tape casting direction. However, the orientation and growth of SiC grains could also be affected by the sintering process [358, 359]. Although the SiC grain growth mechanism in present system has not been well understood, the pressureless sintering

process may also contribute to the faint grain orientation difference in three directions.

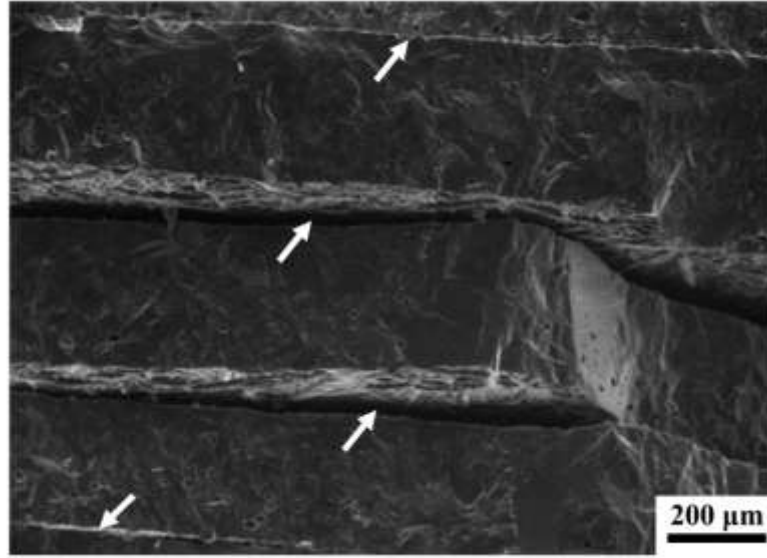


Fig. 5.12 Fracture surface of sintered SiC multilayer buckle [262].

Heat transfer in ceramic materials is usually predominantly via phonons, which travel through the material until they are scattered. Therefore, the thermal conductivity in SiC multilayer is limited by intrinsic phonon scattering, which could be affected by grain boundaries, pores, impurities and dislocations. Phonon mean free path (PMFR,  $l$ ) could be calculated by Eq.5.8:

$$l = \frac{3\kappa}{\rho \cdot v \cdot C_p} \quad (5.8)$$

$$v = \sqrt{\frac{E}{\rho}} \quad (5.9)$$

where  $v$  and  $E$  are the group velocity of the phonons and elastic modulus, respectively.

The elastic modulus and density of SiC multilayer at room temperature were 331 GPa, and 2.894 g/cm<sup>3</sup>, respectively. Thus, the calculated  $v$  was  $1.07 \times 10^4$  m/s, which is close to the Liu's calculation in hot-pressed SiC ( $1.16 \times 10^4$  m/s) [360] and theoretical value ( $1.33 \times 10^4$  m/s) [361]. The calculated PMFRs of SiC multilayer in X, Y and Z directions were 16.8, 18.9 and 15.4 nm, respectively. The PMFR of pure 6H-SiC at room temperature is 29.4 nm [360]. The impurity in the sintered SiC multilayer is a reason for the decreased of the PMFR [362]. Moreover, since the sintered SiC

multilayer was not fully dense (relative density was about 90%), the residual pores could also decrease the thermal conductivity [363, 364]. Generally, the less scatter of phonon and higher thermal conductivity would be found with the larger grain at constant condition. Therefore, the different average size and number of elongated SiC grain in different directions also contribute to the different PMFR. Usually, the thermal conductivity increased linearly with grain size [365-367]. Thus, the Y directions demonstrated the highest PMFR and thermal conductivity. Moreover, the interface between SiC layers would also detrimental to the movement of phonon and conduction of heat, which lead to lowest thermal conductivity in Z direction in SiC multilayer. After oxidation treatment, a thin layer of silica was formed surrounding the samples [260, 263]. The formed silica layer presents very low thermal conductivity (less than 2 W/(m·K)) [368], which results to the slight decrease of thermal conductivity in SiC multilayer in all directions.

### 5.5.2 C<sub>sf</sub>/SiC multilayer composites

The effect of fibre addition on the thermal conductivities of C<sub>sf</sub>/SiC multilayer composites before and after oxidation in X, Y and Z directions are shown in Fig. 5.13a, b and c, respectively.

In X direction before oxidation treatment, the thermal conductivity firstly slightly increased after addition of 5 vol.% short C fibre (from 112.4 to 119.2 W/(m·K)), and then decreased with further fibre addition (98.4 W/(m·K) in 10 vol.% C<sub>sf</sub>/SiC multilayer composite). However, in Y and Z directions, the thermal conductivities decreased with the increase of fibre amount before oxidation treatment. After oxidation treatment, the thermal conductivities decreased with the increase of fibre amount regardless of test directions.

Comparison of thermal conductivities comparison of 5 and 10 vol.% C<sub>sf</sub>/SiC multilayer composites in X, Y and Z directions at room temperature before and after oxidation is shown in Fig. 5.14. Different to SiC multilayer, the thermal conductivities of C<sub>sf</sub>/SiC multilayer composites before oxidation were in this order: X > Y > Z regardless of fibre amount. It is obvious that the thermal conductivities in all directions decreased after oxidation treatment. The order of thermal conductivities in 10 vol.% C<sub>sf</sub>/SiC multilayer composites did not change after oxidation treatment. However, after oxidation treatment, it is very interesting that the 5 vol.% C<sub>sf</sub>/SiC multilayer composites showed highest thermal conductivity in Y direction, which was

slightly higher than in X direction.

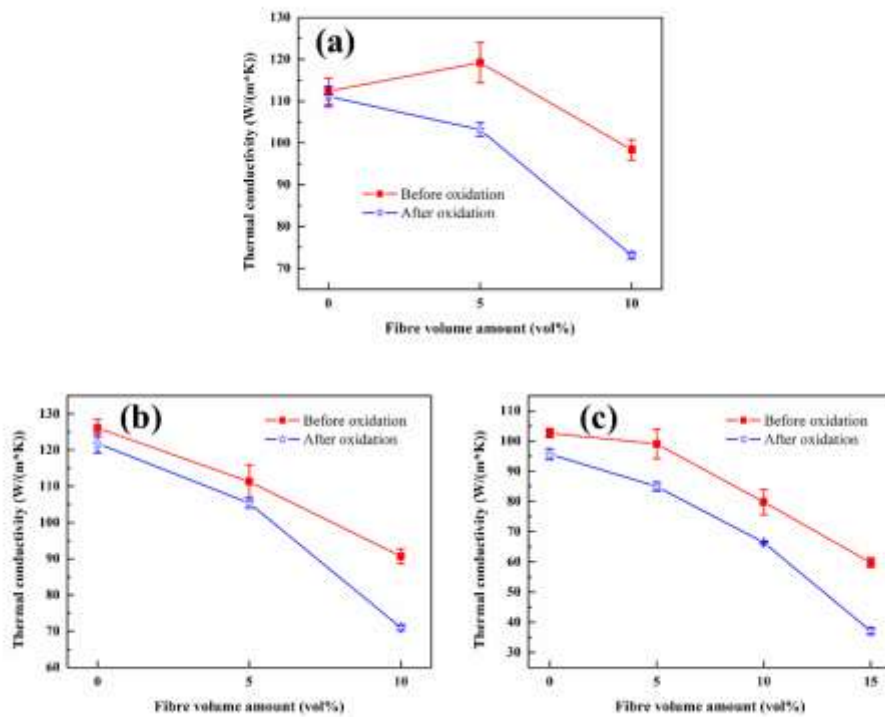


Fig. 5.13 Thermal conductivities of SiC multilayer and C<sub>sf</sub>/SiC multilayer composites before and after oxidation in (a) X, (b) Y and (c) Z directions.

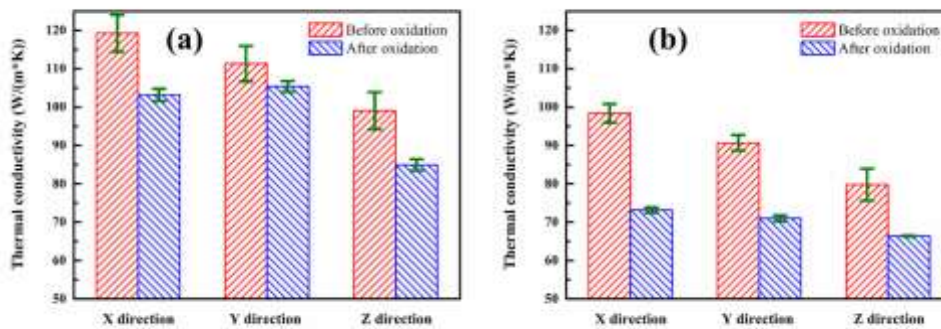


Fig. 5.14 Thermal conductivities comparison of (a) 5 and (b) 10 vol.% C<sub>sf</sub>/SiC multilayer composites in X, Y and Z directions at room temperature before and after oxidation.

The carbon fibres used in the present work were PAN-based, whose thermal conductivity is usually in the range between 20-125 W/(m·K) in their axial direction [369]. Moreover, since the sintering temperature in the present work was 2200 °C,

carbonization or graphitization are expected to occur [370, 371], which will further improve the thermal conductivity of carbon fibres [372, 373].

Addition of short C fibre would generate several opposite effects. The higher thermal conductivity of C fibre would be beneficial for the increase of thermal conductivities in plane containing fibre, especially in tape casting direction (X direction). However, on the other hand, the addition of C fibre inhibited the shrinkage of composites (also especially in X direction), which will lead to the decrease of thermal conductivities. Moreover, the grain growth of SiC was also strongly inhibited by the addition of fibres (Fig. 3.9), which results in the decreased of thermal conductivity. Therefore, the influence of fibre addition on thermal conductivity of C<sub>sf</sub>/SiC multilayer composites is the competitive result among these effects. Thus, in X direction before oxidation, the thermal conductivities firstly slightly increased after addition of 5 vol.% fibre and then further decreased in 10 vol.% C<sub>sf</sub>/SiC multilayer composites (Fig. 5.13a). In Y and Z directions, due to the increased porosity and reduced grain size, the thermal conductivities decreased with fibre amount (Fig. 5.13b and c).

Before oxidation treatment, since fibre aligned along tape casting direction, C<sub>sf</sub>/SiC multilayer composites demonstrated highest thermal conductivity in X direction regardless of fibre amount. Moreover, due to the presence of the interface between adjacent layers, Z direction showed lowest thermal conductivity. However, more fibre would be oxidized in samples for testing thermal conductivity in X direction because of the fibres' alignment. Therefore, 5 vol.% C<sub>sf</sub>/SiC multilayer composites showed even slight higher thermal conductivity in Y than in X direction after oxidation treatment.

In order to illustrate the anisotropic behavior in thermal conductivity, an anisotropic factor ( $\Phi$ ) was introduced. The anisotropic factor ( $\Phi$ ) could be calculated by Eq.5.10:

$$\phi = \frac{(\kappa_X - \kappa_Z)}{\kappa_Z} \times 100 \quad (5.10)$$

where  $\kappa_X$  and  $\kappa_Z$  are thermal conductivity in X and Z directions, respectively.

The calculated  $\Phi$  of SiC multilayer and C<sub>sf</sub>/SiC multilayer composites is shown in Fig. 5.15. From room temperature to 1500 °C, the  $\Phi$  values of SiC multilayer were mainly in the range of 8.5 and 13.2. However, the values of  $\Phi$  in C<sub>sf</sub>/SiC multilayer composites were from 15.2 to 24.1, which is almost two times of that of SiC multilayer. It indicates that the thermal conductivity properties of C<sub>sf</sub>/SiC multilayer

composites are highly anisotropic.  $C_{sf}/SiC$  multilayer composites demonstrated higher thermal conductivity in X direction and lower thermal conductivity in Z direction, which is favorable for thermal protection system.

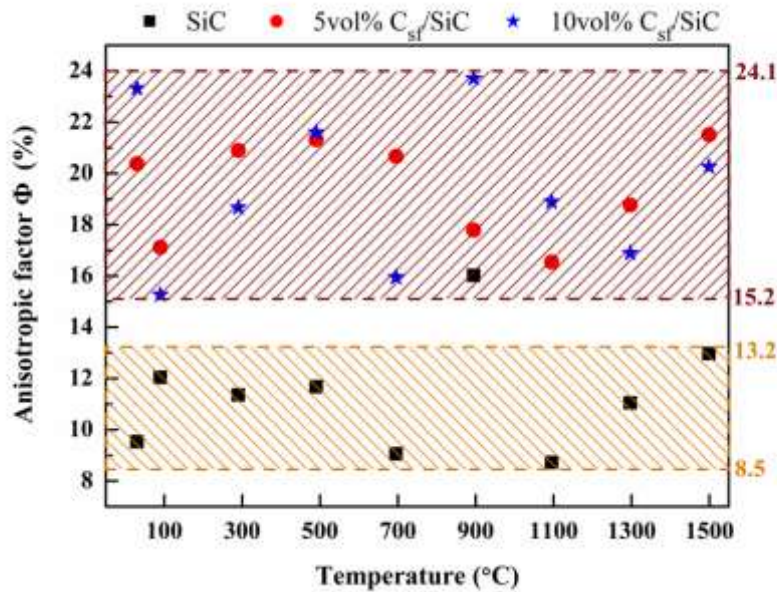


Fig. 5.15 Anisotropic factor  $\Phi$  of SiC multilayer and  $C_{sf}/SiC$  multilayer composites at different temperature.

The addition of short C fibre hinders the shrinkage in plane containing fibre, especially in X direction, which leads to the increase of residual porosity. The residual porosity seems to be the main parameter affecting the mechanical properties. Therefore, the sintering process of  $C_{sf}/SiC$  multilayer composites should be improved for application requiring high mechanical strength. This last result could be achieved by applying pressure during sintering, optimizing other sintering parameters or using more effective sintering aids. However, for thermal protection systems, which do not require high mechanical strength, the residual porosity would be beneficial providing the decrease of thermal conductivity through the thickness.  $C_{sf}/SiC$  multilayer composites display acceptable thermal conductivity in plane (X and Y directions) due to the presence of carbon fibre, and showed decreased thermal conductivity in Z direction due to increased porosity and interface between adjacent layers. Therefore, this kind of composite layers could be integrated into a thermal protection system structure designed as shown in Fig. 5.16. The outer dense SiC layers are expected to grant excellent oxidation resistance (Fig. 5.1) and fairly good heat conductivity in the plane. The  $C_{sf}/SiC$  composite layers in the middle of the multilayer architecture could

grant acceptable thermal conductivity in plane and provide decreased thermal conductivity through the TPS thickness.

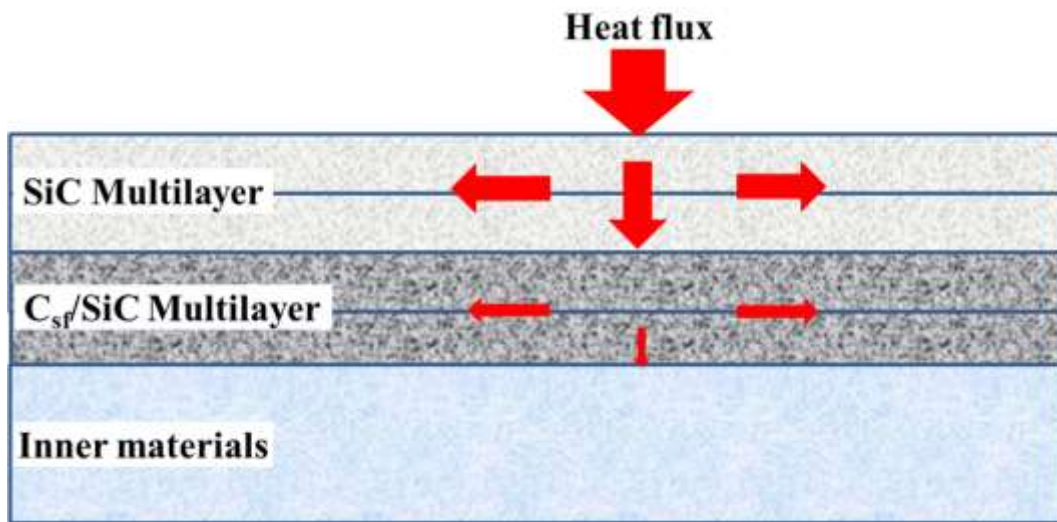


Fig. 5.16 Prospective application of C<sub>sf</sub>/SiC multilayer for thermal protection system.

## Conclusions

This thesis addressed on the fabrication, microstructure, mechanical and thermophysical properties of silicon carbide multilayer composites containing short carbon fibres ( $C_{sf}/SiC$ ) prepared by tape casting and pressureless sintering. The short C fibres were firstly dispersed in solvents with the aid of dispersant and then mixed with SiC slurry to limit fibre breakage. The relative densities, mechanical properties, oxidation behavior of  $C_{sf}/SiC$  multilayer composites were evaluated. Thermal expansion, diffusivity and conductivity behavior in three directions were tested. The effect of addition of short C fibres on shrinkage, mechanical and thermophysical behavior was discussed.

Triton X100 was found to be the best one for Toho Tenax HTC124 (with water soluble coating) among BYK-163, BYK-410, BYK-2150, BYK-9076, BYK-9077 and Triton X100 dispersants. The average fibre length in sintered 5, 10 and 15 vol.%  $C_{sf}/SiC$  composites were about 0.6, 0.55 and 0.5 mm, respectively. Although the average fibre length (0.5 to 0.6 mm) after mixing was only one-sixth or -fifth of original length (3 mm), it is still much longer than in other  $C_{sf}/SiC$  composites using ball-milling, indicating that mixing the SiC slurry with the fibre-predispersed solution is an effective method for adding fibres with limited breakage.

Fibres were homogeneously distributed in the tapes and tended to align fairly well along the tape casting direction. The relative density of the composite containing short C fibres decreased with the fibre amount. The  $C_{sf}/SiC$  multilayer composites demonstrated significant anisotropic shrinkage behavior in different directions, while the addition of short C fibres hindered the shrinkage in the plane containing the fibres (length and width directions) during sintering. Elastic modulus decreased with increased fibre amount and porosity, while bending strength and fracture toughness also presented a very strong relationship with the relative density. These behaviors imply that bending properties are affected significantly by residual porosity. Moreover, due to residual thermal stress, the fracture toughness of  $SiC/(C_{sf}/SiC)$  multilayer composites was higher than that of SiC multilayer, which indicates that the fracture toughness of SiC-based thermal protection system could be improved through designing its architecture.

The weight loss during oxidation tests was larger for  $C_{sf}/SiC$  multilayer composites than for SiC multilayer and increased with the porosity and the fibre amount. Passive

oxidation of SiC was still occurred after addition of short fibres. Specific heat of SiC multilayer and C<sub>sf</sub>/SiC multilayer composites increased with temperature, and specific heat of C<sub>sf</sub>/SiC multilayer composites slightly increased with fibre amount. However, no significant different in thermal expansion behavior of SiC, 5 and 10 vol.% C<sub>sf</sub>/SiC multilayer composites in different directions was found.

In X direction before oxidation treatment, the thermal conductivity firstly slightly increased after addition of 5 vol.% short C fibre, and then decreased with further fibre addition. However, in Y and Z directions, the thermal conductivities decreased with the increase of fibre amount before oxidation treatment. After oxidation treatment, the thermal conductivities decreased with the increase of fibre amount regardless of test directions. Since fibre aligned along tape casting direction, C<sub>sf</sub>/SiC multilayer composites demonstrated highest thermal conductivity in X direction regardless of fibre amount. Moreover, due to the presence of the interface between adjacent layers, Z direction showed lowest thermal conductivity. Because of the oxidation of C fibre (in C<sub>sf</sub>/SiC multilayer composites) and formation of silica (both in SiC multilayer and C<sub>sf</sub>/SiC multilayer composites), thermal conductivities of SiC multilayer and C<sub>sf</sub>/SiC multilayer composites decreased after oxidation treatment.

# Publications/ Conference proceedings

## ◆ Journal Publications

1. **W.S Yang**, S. Biamino, E. Padovano, L. Fuso, M. Pavese, S. Marchisio, D. Vasquez, C. Vega Bolivar, P. Fino, C. Badini. Microstructures and mechanical properties of short carbon fibre/SiC multilayer composites prepared by tape casting. *Composites Science and Technology*. 2012, 72: 675–680.
2. **W.S Yang**, L. Fuso, S. Biamino, D. Vasquez, C. Vega Bolivar, P. Fino, C. Badini. Fabrication of short carbon fibre reinforced SiC multilayer composites by tape casting. *Ceramics International*. 2012, 38(2): 1011–1018.
3. **W.S Yang**, S. Biamino, E. Padovano, M. Pavese, S. Marchisio, G. D'Amico, S. Ceresa Mio, X. Chen, P. Fino, C. Badini. Thermophysical properties of SiC multilayer prepared by tape casting and pressureless sintering. *Composite Structures*. 2013, 96: 469–475.
4. **W.S Yang**, S. Biamino, E. Padovano, M. Pavese, S. Marchisio, X. Chen, P. Fino, C. Badini. Microstructure and mechanical properties of milled fibre/SiC multilayer composites prepared by tape casting and pressureless sintering. *Materials and Design*. Submitted.
5. **W.S Yang**, S. Biamino, E. Padovano, M. Pavese, P. Fino, C. Badini. Thermophysical properties of short carbon fibre/SiC multilayer composites prepared by tape casting and pressureless sintering. *Journal of the European Ceramic Society*. Submitted.
6. **Wenshu Yang**, Claudio Badini, Laura Fuso, Sara Biamino, Matteo Pavese, Claudia Vega Bolivar, Paolo Fino. Preparation and prospective application of short carbon fiber/SiC multilayer composites by tape casting. *World Journal of Engineering*. 2011, 8(4): 331–334.
7. E. Padovano, C. Badini, S. Biamino, M. Pavese, **W.S. Yang**, P. Fino. Pressureless sintering of ZrB<sub>2</sub>-SiC composite laminates using boron and carbon as sintering aids. *Composite Structures*. Submitted.

## ◆ Conference proceedings

1. **Wenshu Yang**, Claudio Badini, Laura Fuso, Sara Biamino, Claudia Vega Bolivar,

Paolo Fino. Preparation of short carbon fiber/SiC multilayer composites by tape casting. 19<sup>th</sup> Annual International Conference on Composites or Nano Engineering. Shanghai. 2011, 7. 1291–1293.

2. **Wenshu Yang**, Elisa Padovano, Laura Fuso, Matteo Pavese, Silvia Marchisio, Dreidy Vasquez, Claudia Vega bolivar, Paolo Fino, Claudio Badini. Preparation, microstructure and properties of C<sub>sf</sub>/SiC multilayer composites by tape casting and pressureless sintering. International Conference on Mechanics of Nano, Micro and Macro Composite Structures. Turin, Italy, 2012, June 18-20.

# Reference

- [1] X. Zhang, J. Han, S. Meng. Ablation behavior of ZrB<sub>2</sub>-SiC ultra high temperature ceramics under simulated atmospheric re-entry conditions. *Composites Science and Technology*. 2008, 68: 1718–1726.
- [2] B. Behrens, M. Müller. Technologies for thermal protection systems applied on re-usable launcher. *Acta Astronautica*. 2004, 55: 529–536.
- [3] E. Venkatapathy, B. Laub, G.J. Hartman, J.O. Arnold, M.J. Wright, G.A. Allen Jr. Thermal protection system development, testing, and qualification for atmospheric probes and sample return missions: Examples for Saturn, Titan and Stardust-type sample return. *Advances in Space Research*. 2009, 44: 138–150
- [4] W. Krenkel, F. Berndt. C/C-SiC composites for space applications and advanced friction systems. *Materials Science and Engineering A*. 2005, 412: 177–181.
- [5] E.P. Carton, M. Stuivinga, H. Keizers, H.J. Verbeek, P.J. van der Put. Shock Wave Fabricated Ceramic-Metal Nozzles. *Applied composite materials*. 1999, 6: 139–165.
- [6] Y. Li, G. Qiao, Z. Jin. Machinable Al<sub>2</sub>O<sub>3</sub>/BN composite ceramics with strong mechanical properties. *Materials Research Bulletin*. 2002, 37: 1401–1409.
- [7] E. Wuchina, M. Opeka, S. Causey, K. Buesking, J. Spain, A. Cull, J. Routbort, F. Guitierrez-Mora. Designing for ultrahigh-temperature applications: The mechanical and thermal properties of HfB<sub>2</sub>, HfC<sub>x</sub>, HfN<sub>x</sub> and  $\alpha$ Hf(N). *Journal of Materials Science*. 2004, 39: 5939–5949.
- [8] A.K. Khanra, A. Khanra. Electrical discharge machining behavior of hotpress MoSi<sub>2</sub>. *Journal of Materials Science*. 2005, 40: 3027–3030.
- [9] L. He, Y. Zhou, Y. Bao, Z. Lin, J. Wang. Synthesis, physical, and mechanical properties of bulk Zr<sub>3</sub>Al<sub>3</sub>C<sub>5</sub> ceramic. *Journal of the American Ceramic Society*. 2007, 90: 1164–1170.
- [10] G.M. Song, Y.J. Wang, Y. Zhou. Elevated temperature ablation resistance and thermophysical properties of tungsten matrix composites reinforced with ZrC particles. *Journal of Materials Science*. 2001, 36: 4625–4631.
- [11] C. Friedrich, R. Gadow, T. Schirmer. Lanthanum hexaaluminate-a new material for atmospheric plasma spraying of advanced thermal barrier coatings. *Journal of Thermal Spray Technology*. 2001, 10: 592–598.
- [12] A. Navrotsky, L. Benoist, H. Lefebvre. Direct calorimetric measurement of enthalpies of phase transitions at 2000°–2400 °C in yttria and zirconia. *Journal of the American Ceramic Society*. 2005, 88: 2942–2944.
- [13] A. Rezaie, W.G. Fahrenholtz, G.E. Hilmas. Oxidation of zirconium diboride-silicon carbide at 1500 °C at a low partial pressure of oxygen. *Journal of the American Ceramic Society*. 2006, 89: 3240–3245.
- [14] S. Zhu, W.G. Fahrenholtz, G. E. Hilmas. Influence of silicon carbide particle size on the microstructure and mechanical properties of zirconium diboride-silicon carbide ceramics. *Journal of the European Ceramic Society*. 2007, 27: 2077–2083.
- [15] N. Altinkok, , A. Demir, I. Ozsert. Processing of Al<sub>2</sub>O<sub>3</sub>/SiC ceramic cake preforms and their liquid Al metal infiltration. *Composites Part A: Applied Science and Manufacturing*. 2003, 34: 577–582.

- [16] L.C. Sim, S.R. Ramanan, H. Ismail, K.N. Seetharamu, T.J. Goh. Thermal characterization of Al<sub>2</sub>O<sub>3</sub> and ZnO reinforced silicone rubber as thermal pads for heat dissipation purposes. *Thermochimica Acta*. 2005, 430: 155–165.
- [17] E.P. Song, J. Ahn, S. Lee, N.J. Kim. Microstructure and wear resistance of nanostructured Al<sub>2</sub>O<sub>3</sub>-8 wt.%TiO<sub>2</sub> coatings plasma-sprayed with nanopowders. *Surface and Coatings Technology*. 2006, 201: 1309–1315.
- [18] V. Balaji, A.N. Tiwari, R.K. Goyal. Study on high-performance poly (etheretherketone)/Si<sub>3</sub>N<sub>4</sub> nanocomposites: New electronic substrate materials. *Polymer Engineering & Science*. 2011, 51: 509–517.
- [19] D. Gu, Y. Shen, Z. Lu. Preparation of TiN-Ti<sub>5</sub>Si<sub>3</sub> in-situ composites by selective laser melting. *Materials Letters*. 2009, 63: 1577–1579.
- [20] Y. Zhou, K. Hirao, K. Watari, Y. Yamauchi, S. Kanzaki. Thermal conductivity of silicon carbide densified with rare-earth oxide additives. *Journal of the European Ceramic Society*. 2004, 24: 265–270.
- [21] N.F. Fahim. Thermal conductivity of plasma-sprayed W/SiC composite for high-temperature energy applications. *Surface and Coatings Technology*. 2008, 202: 1696–1703.
- [22] M. Gasch, D. Ellerby, E. Irby, S. Beckman, M. Gusman, S. Johnson. Processing, properties and arc jet oxidation of hafnium diboride/silicon carbide ultra high temperature ceramics. *Journal of Materials Science*. 2004, 39: 5925–5937.
- [23] Y.Q. Liu, G. Shao, P. Tsakiropoulos. On the oxidation behaviour of MoSi<sub>2</sub>. *Intermetallics*. 2001, 9: 125–136.
- [24] L. Zhao, D. Jia, X. Duan, Z. Yang, Y. Zhou. Oxidation of ZrC-30 vol.% SiC composite in air from low to ultrahigh temperature. *Journal of the European Ceramic Society*. 2012, 32: 947–954.
- [25] K.S. Ravichandran. Thermal residual stresses in a functionally graded material system. *Materials Science and Engineering A*. 1995, 201: 269–276.
- [26] B. Wang, Y. Mai, X. Zhang. Thermal shock resistance of functionally graded materials. *Acta Materialia*. 2004, 52: 4961–4972.
- [27] D.S. Fox. Oxidation behavior of chemically-vapor-deposited silicon carbide and silicon nitride from 1200° to 1600 °C. *Journal of the American Ceramic Society*. 1998, 81: 945–950.
- [28] N.S. Müller, V. Kilikoglou, P.M. Day, G. Vekinis. The influence of temper shape on the mechanical properties of archaeological ceramics. *Journal of the European Ceramic Society*. 2010, 30: 2457–2465.
- [29] J. Qian, Z. Jin. Preparation and characterization of porous, biomorphic SiC ceramic with hybrid pore structure. *Journal of the European Ceramic Society*. 2006, 26: 1311–1316.
- [30] V. Lysenko, P.H. Roussel, B. Remaki, G. Delhomme, A. Dittmar, D. Barbier, V. Strikha, C. Martelet. Study of nano-porous silicon with low thermal conductivity as thermal insulating material. *Journal of Porous Materials*. 2000, 7: 177–182.
- [31] M.M. Hossain, K. Shivakumar. Compression fatigue performance of a fire resistant syntactic foam. *Composite Structures*. 2011, 94: 290–298.
- [32] F.C. Buciuman, B. Kraushaar-Czarnetzki. Preparation and characterization of ceramic foam supported nanocrystalline zeolite catalysts. *Catalysis Today*. 2001, 69: 337–342.
- [33] U.F. Vogt, L. Györfy, A. Herzog, T. Graule, G. Plesch. Macroporous silicon

- carbide foams for porous burner applications and catalyst supports. *Journal of Physics and Chemistry of Solids*. 2007, 68: 1234–1238.
- [34] V.S.R. Murthy, K. Srikanth, C.B. Raju. Abrasive wear behaviour of SiC whisker-reinforced silicate matrix composites. *Wear*. 1998, 223:79–92.
- [35] J.P. Parmigiani, M.D. Thouless. The roles of toughness and cohesive strength on crack deflection at interfaces. *Journal of the Mechanics and Physics of Solids*. 2006, 54: 266–287.
- [36] Y. Zhao, H. Fu, A. Peng, Y. Ma, D. Xiao, J. Yao. Low-dimensional nanomaterials based on small organic molecules: preparation and optoelectronic properties. *Advanced Materials*. 2008, 20: 2859–2876.
- [37] H. Kaya. The application of ceramic-matrix composites to the automotive ceramic gas turbine. *Composites Science and Technology*. 1999, 59: 861–872.
- [38] G.C. Wei, P.F. Becher. Improvements in mechanical properties in SiC by the addition of TiC Particles. *Journal of the American Ceramic Society*. 1984, 67: 571–574.
- [39] H. Endo, M. Ueki, H. Kubo. Microstructure and mechanical properties of hot-pressed SiC-TiC composites. *Journal of Materials Science*. 1991, 26: 3769–3774.
- [40] H. Endo, M. Ueki, H. Kubo. Hot pressing of SiC-TiC composites. *Journal of Materials Science*. 1990, 25: 2503–2506.
- [41] K. Chae, K. Niihara, D. Kim. Effect of Cr<sub>3</sub>C<sub>2</sub> Addition on the sintering of SiC-TiC composite. *Journal of the American Ceramic Society*. 1996, 79: 3305–3308.
- [42] K. Cho, Y. Kim, H. Choi, J. Lee. In situ-toughened silicon carbide-titanium carbide composites. *Journal of the American Ceramic Society*. 1996, 79: 1711–1713.
- [43] K. Cho, H. Choi, J. Lee, Y. Kim. Microstructure and fracture toughness of in-situ toughened SiC-TiC composites. *Journal of Materials Science Letters*. 1998, 17: 1081–1084.
- [44] H. An, Y. Kim, J. Lee. Effect of initial  $\alpha$ -phase content of SiC on microstructure and mechanical properties of SiC-TiC composites. *Journal of the European Ceramic Society*. 2001, 21: 93–98.
- [45] T. Lin, J. Chang, M. Hon. The growth and characteristics of CVD SiC-TiC in-situ composites. *Ceramics International*. 1998, 24: 256–272.
- [46] Y. Kim, S. Lee, Y. Lee. Pressureless sintering of SiC-TiC composites with improved fracture toughness. *Journal of Materials Science*. 2000, 35: 5569–5574.
- [47] Y. Luo, S. Li, W. Pan, L. Li. Fabrication and mechanical evaluation of SiC-TiC nanocomposites by SPS. *Materials Letters*. 2004, 58: 150–153.
- [48] M.A. Janney. Mechanical properties and oxidation behavior of a hot-pressed SiC-15-vol.-%-TiB<sub>2</sub> composite. *American Ceramic Society Bulletin*. 1987, 66: 322-324.
- [49] K. Cho, H. Choi, J. Lee. Effects of additive amount on microstructure and fracture toughness of SiC-TiB<sub>2</sub> composites. *Ceramics International*. 1998, 24: 299–305.
- [50] K. Cho, H. Choi, J. Lee, Y. Kim. In situ enhancement of toughness of SiC-TiB<sub>2</sub> composites. *Journal of Materials Science*. 1998, 33: 211–214.
- [51] J.J Kim, S.K. Park. Solid-particle erosion of hot-pressed silicon carbide and SiC-TiB<sub>2</sub> composite. *Journal of Materials Science Letters*. 1997, 16: 821–823.

- [52] J.J. Kim, S.K. Park. Solid particle erosion of SiC and SiC-TiB<sub>2</sub> composite hot-pressed with Y<sub>2</sub>O<sub>3</sub>. *Wear*. 1998, 222: 114–119.
- [53] D. Kuo, W.M. Kriven. Mechanical behavior and microstructure of SiC and SiC/TiB<sub>2</sub> ceramics. *Journal of the European Ceramic Society*. 1998, 18: 51–57.
- [54] Y. Miyamoto, Y.C. Hyun, Y. Takano, O. Yamada, M. Koizumi. High pressure combustion sintering of TiB<sub>2</sub>-TiC and TiB<sub>2</sub>-SiC ceramic composites. *Journal of the Japan Society of Powder and Powder Metallurgy*. 1988, 35: 651–654.
- [55] T. Tani, S. Wada. SiC matrix composites reinforced with internally synthesized TiB<sub>2</sub>. *Journal of Materials Science*. 1990, 25: 157–160.
- [56] Y. Ohya, M.J. Hoffmann, G. Petzow. Sintering of in-situ synthesized SiC-TiB<sub>2</sub> composites with improved fracture toughness. *Journal of the American Ceramic Society*. 1992, 75: 2479–2483.
- [57] Y. Ohya, M.J. Hoffmann, G. Petzow. Mechanical properties of hot-pressed SiC-TiB<sub>2</sub>/TiC composites synthesized in situ. *Journal of Materials Science Letters*. 1993, 12: 149–152.
- [58] G.J. Zhang, Z.Z. Jin, X.M. Yue. Reaction synthesis of TiB<sub>2</sub>-SiC composites from TiH<sub>2</sub>-Si-B<sub>4</sub>C. *Materials Letters*. 1995, 25: 97–100.
- [59] G.J. Zhang, X.M. Yue, Z.Z. Jin, J.Y. Dai. In-situ synthesized TiB<sub>2</sub> toughened SiC. *Journal of the European Ceramic Society*. 1996, 16: 409–412.
- [60] T. Tani, S. Wada. Pressureless-sintered and HIPed SiC-TiB<sub>2</sub> composites from SiC-TiO<sub>2</sub>-B<sub>4</sub>C-C powder compacts. *Journal of Materials Science*. 1991, 26: 3491–3496.
- [61] D. Bucevac, S. Boskovic, B. Matovic, V. Krstic. Toughening of SiC matrix with in-situ created TiB<sub>2</sub> particles. *Ceramics International*. 2010, 36: 2181–2188.
- [62] Y.W. Kim, M. Mitomo, H. Emoto, J.G. Lee. Effect of initial  $\alpha$ -phase content on microstructure and mechanical properties of sintered silicon carbide. *Journal of the American Ceramic Society*. 1998, 81: 3136–3140.
- [63] D. Cho, Y.W. Kim, W. Kim. Strength and fracture toughness of in situ-toughened silicon carbide. *Journal of Materials Science*. 1997, 32: 4777–4782.
- [64] G.D. Zhan, M. Mitomo, Y.W. Kim. Microstructural control for strengthening of silicon carbide ceramics. *Journal of the American Ceramic Society*. 1999, 82: 2924–2926.
- [65] J.Y. Kim, H.G. An, Y.W. Kim, M. Mitomo. R-curve behaviour and microstructure of liquid-phase sintered  $\alpha$ -SiC. *Journal of Materials Science*. 2000, 35: 3693–3697.
- [66] N.P. Padture. In situ-toughened silicon carbide. *Journal of the American Ceramic Society*. 1994, 77: 519–523.
- [67] N.P. Padture, B.R. Lawn. Toughness properties of a silicon carbide with an in situ induced heterogeneous grain structure. *Journal of the American Ceramic Society*. 1994, 77: 2518–2522.
- [68] J.Y. Kim, Y.W. Kim, J.G. Lee, K.S. Cho. Effect of annealing on mechanical properties of self-reinforced alpha-silicon carbide. *Journal of Materials Science*. 1999, 34: 2325–2330.
- [69] Y.W. Kim, M. Mitomo, H. Hirotsuru. Grain growth and fracture toughness of fine-grained silicon carbide ceramics. *Journal of the American Ceramic Society*. 1995, 78: 3145–3148.
- [70] S.K. Lee, D.K. Kim, C.H. Kim. Flaw-tolerance and R-curve behavior of

- liquid-phase-sintered silicon carbides with different microstructures. *Journal of the American Ceramic Society*. 1995, 78: 65–70.
- [71] S.G. Lee, W.H. Shim, J.Y. Kim, Y.W. Kim, W.T. Kwon. Effect of sintering-additive composition on fracture toughness of liquid-phase-sintered SiC ceramics. *Journal of Materials Science Letters*. 2001, 20: 143–146.
- [72] Y.W. Kim, M. Mitomo, G.D. Zhan. Microstructure control of liquid-phase sintered  $\beta$ -SiC by seeding. *Journal of Materials Science Letters*. 2001, 20: 2217–2220.
- [73] D. Sciti, S. Guicciardi, A. Bellosi. Effect of annealing treatments on microstructure and mechanical properties of liquid-phase-sintered silicon carbide. *Journal of the European Ceramic Society*. 2001. 21: 621–632.
- [74] Z.Z. Chen, E.W. Shi, Y.Q. Zheng, W.J. Li, B. Xiao, J.Y. Zhuang. Growth of hex-pod-like  $\text{Cu}_2\text{O}$  whisker under hydrothermal conditions. *Journal of Crystal Growth*. 2003, 249: 294–300.
- [75] A.E. Giannakopoulos, K. Breder. Synergism of toughening mechanisms in whisker-reinforced ceramic-matrix composites. *Journal of the American Ceramic Society*. 1991, 74: 194–202.
- [76] J.J. Petrovic, J.V. Milewski, D.L. Rohr, F. D. Gac. Tensile mechanical properties of SiC whiskers. *Journal of Materials Science*. 1985, 20: 1167–1177.
- [77] J.H. She, D.L. Jiang, S.H. Tan, Ji.K. Guo. Hot isostatic pressing of particle- and whisker-reinforced silicon carbide matrix composites. *Key Engineering Materials*. 1995, 45: 108–110.
- [78] S.H. Kim, Y.W. Kim, M. Mitomo. Microstructure and fracture toughness of liquid-phase-sintered  $\beta$ -SiC containing  $\beta$ -SiC whiskers as seeds. *Journal of Materials Science*. 2003, 38:1117–1121.
- [79] L. Zhang, H. Yang, X. Guo, J. Shen, X. Zhu. Preparation and properties of silicon carbide ceramics enhanced by TiN nanoparticles and SiC whiskers. *Scripta Materialia*. 2011, 65: 186–189.
- [80] Y. Hua, L. Zhang, L. Cheng, J. Wang. Silicon carbide whisker reinforced silicon carbide composites by chemical vapor infiltration. *Materials Science and Engineering A*. 2006, 428: 346–350.
- [81] Y. Hua, L. Zhang, L. Cheng, Z. Li, J. Du. Microstructure and mechanical properties of  $\text{SiC}_p/\text{SiC}$  and  $\text{SiC}_w/\text{SiC}$  composites by CVI. *Journal of Materials Science*. 2010, 45:392–398.
- [82] Y. Hua, L. Zhang, L. Cheng, Z. Li, J. Du. Microstructure and high temperature strength of  $\text{SiC}_w/\text{SiC}$  composites by chemical vapor infiltration. *Materials Science and Engineering A*. 2010, 527: 5592-5595.
- [83] H. Wu, M. Gao, D. Zhu, S. Zhang, Y. Pan, H. Pan, Y. Liu, F.J. Oliveira, J.M. Vieira. SiC whisker reinforced multi-carbides composites prepared from  $\text{B}_4\text{C}$  and pyrolyzed rice husks via reactive infiltration. *Ceramics International*. 2012. 38: 3519–3527.
- [84] M.S. Dresselhaus, G. Dresselhaus, R. Saito. Physics of carbon nanotubes. *Carbon*. 1995, 33: 883–891.
- [85] J. Cho, A.R. Boccaccini. M.S.P. Shaffer. Ceramic matrix composites containing carbon nanotubes. *Journal of Materials Science*. 2009, 44: 1934–1951.
- [86] A. Peigney. Composite materials: Tougher ceramics with nanotubes. *Nature Materials*. 2003, 2: 15–16.
- [87] F. Inam, H. Yan, M. Reece, T. Peijs. Dimethylformamide: an effective dispersant

- for making ceramic-carbon nanotube composites. *Nanotechnology*. 2008, 19: 4484–4488.
- [88] J. Sun, L. Gao, M. Iwasa, T. Nakayama, K. Niihara. Failure investigation of carbon nanotube/3Y-TZP nanocomposites. *Ceramics International*. 2005, 31: 1131–1134.
- [89] Z. Xia, L. Riester, W.A. Curtin, H. Li, B.W. Sheldon, J. Liang, B. Chang, J.M. Xu. Direct observation of toughening mechanisms in carbon nanotube ceramic matrix composites. *Acta Materialia*. 2004, 52: 931–944.
- [90] R.Z. Ma, J. Wu, B.Q. Wei, J. Liang, D.H. Wu. Processing and properties of carbon nanotubes–nano-SiC ceramic. *Journal of Materials Science*. 1998, 33: 5243–5246.
- [91] G.D. Zhan, J.D. Kuntz, J. Wan, A.K. Mukherjee. Single-wall carbon nanotubes as attractive toughening agents in alumina-based nanocomposites. *Nature Materials*. 2003, 2: 38–42.
- [92] R. Kamalakaran, F. Lupo, N. Grobert, T. Scheu, N.Y. Jin-Phillipp, M. Rühle. Microstructural characterization of C-SiC-carbon nanotube composite flakes. *Carbon*. 2004, 42: 1–4.
- [93] E.T. Thostenson, P.G. Karandikar, T.W. Chou. Fabrication and characterization of reaction bonded silicon carbide/carbon nanotube composites. *Journal of Physics D: Applied Physics*. 2005, 38: 3962–3965.
- [94] Y. Wang, Z. Iqbal, S. Mitra. Rapid, low temperature microwave synthesis of novel carbon nanotube–silicon carbide composite. *Carbon*. 2006, 44: 2804–2808.
- [95] Y. Li, L. Fernandez-Recio, P. Gerstel, V. Srot, P.A. van Aken, G. Kaiser, M. Burghard, J. Bill. Chemical modification of single-walled carbon nanotubes for the reinforcement of precursor-derived ceramics. *Chemistry of Materials*. 2008, 20: 5593–5599.
- [96] H.Z Wang, X.D Li, J. Ma, G.Y Li, T.J Hu. Fabrication of multi-walled carbon nanotube-reinforced carbon fiber/silicon carbide composites by polymer infiltration and pyrolysis process. *Composites Science and Technology*. 2012, 72: 461–466.
- [97] D. Jiang, J. Zhang, Z. Lv. Multi-wall carbon nanotubes (MWCNTs)–SiC composites by laminated technology. *Journal of the European Ceramic Society*. 2012, 32: 1419–1425.
- [98] K. Hirota, Y. Takaura, M. Kato, Y. Miyamoto. Fabrication of carbon nanofiber(CNF)-dispersed Al<sub>2</sub>O<sub>3</sub> composites by pulsed electric-current pressure sintering and their mechanical and electrical properties. *Journal of Materials Science*. 2007, 42: 4792–4800.
- [99] K. Hirota, H. Hara, M. Kato. Mechanical properties of simultaneously synthesized and consolidated carbon nanofiber (CNF)-dispersed SiC composites by pulsed electric-current pressure sintering. *Materials Science and Engineering A*. 2007, 458: 216–225.
- [100] K. Shimoda, T. Hinoki, A. Kohyama. Effect of carbon nanofibers (CNFs) content on thermal and mechanical properties of CNFs/SiC nanocomposites. *Composites Science and Technology*. 2010, 70: 387–392.
- [101] J. Kita, H. Suemasu, I.J. Davies, S. Koda, K. Itatani. Fabrication of silicon carbide composites with carbon nanofiber addition and their fracture toughness. *Journal of Materials Science*. 2010, 45: 6052–6058.

- [102] T. Taguchi, Y. Hasegawa, S. Shamoto. Effect of carbon nanofiber dispersion on the properties of PIP-SiC/SiC composites. *Journal of Nuclear Materials*. 2011, 417: 348–352.
- [103] A. Borrell, R. Torrecillas, V.G. Rocha, A. Fernández, V. Bonache, M.D. Salvador. Effect of CNFs content on the tribological behaviour of spark plasma sintering ceramic–CNFs composites. *Wear*. 2012, 274–275: 94–99.
- [104] W. Yang, H. Araki, A. Kohyama, S. Thaveethavorn, H. Suzuki, T. Noda. Fabrication in-situ SiC nanowires/SiC matrix composite by chemical vapour infiltration process. *Materials Letters*. 2004, 58: 3145–3148.
- [105] W. Yang, H. Araki, A. Kohyama, S. Thaveethavorn, H. Suzuki, T. Noda. Process and mechanical properties of in situ silicon carbide-nanowire-reinforced chemical vapor infiltrated silicon. *Journal of the American Ceramic Society*. 2004, 87: 1720–1725.
- [106] W. Yang, H. Araki, A. Kohyama, Y. Katoh, Q. Hu, H. Suzuki, T. Noda. Tyranno-SA/SiC composite with SiC nanowires in the matrix by CVI process. *Journal of Nuclear Materials*. 2004, 329–333: 539–543.
- [107] W. Yang, H. Araki, C. Tang, S. Thaveethavorn, A. Kohyama, H. Suzuki, T. Noda. Single-crystal SiC nanowires with a thin carbon coating for stronger and tougher ceramic composites. *Advanced Materials*. 2005, 17: 1519–1523.
- [108] C.S. Zheng, Q.Z. Yan, M. Xia, C.C. Ge. In situ preparation of SiC/Si<sub>3</sub>N<sub>4</sub>-NW composite powders by combustion synthesis. *Ceramics International*. 2012, 38: 487–493.
- [109] M. Singh, T.P. Shpargel, G.N. Morscher, R. Asthana. Active metal brazing and characterization of brazed joints in titanium to carbon–carbon composites. *Materials Science and Engineering A*. 2005, 412: 123–128.
- [110] J. Yang, F. Chan. Detection of bolt loosening in C-C composite thermal protection panels: I. Diagnostic principle. *Smart Materials and Structures*. 15: 581–590.
- [111] G. Rohini, K.R. Rao. Carbon-carbon composites- an overview. *Defense Science Journal*. 1993, 43: 369–383.
- [112] H.A. Aglan. The effect of intermediate graphitization on the mechanical and fracture behavior of 2-D C/C composites. *Carbon*. 1993, 31: 1121–1129.
- [113] S. Kumar, A. Kumar, A. Shukla, A.K. Gupta, R. Devi. Capillary infiltration studies of liquids into 3D-stitched C-C preforms: Part A: Internal pore characterization by solvent infiltration, mercury porosimetry, and permeability studies. *Journal of the European Ceramic Society*. 2009, 29: 2643–2650.
- [114] O. Siron, G. Chollon, H. Tsuda, H. Yamauchi, K. Maeda, K. Kosak. Microstructural and mechanical properties of filler-added coal-tar pitch-based C/C composites: the damage and fracture process in correlation with AE waveform parameters. *Carbon*. 2000, 38: 1369–1389.
- [115] R. Luo. Friction performance of C/C composites prepared using rapid directional diffused chemical vapor infiltration processes. *Carbon*. 2002, 40: 1279–1285.
- [116] P. Delhaès, M. Trinquécoste, J.-F. Lines, A. Cosculluela, J.-M. Goyhénèche, M. Couzi. Chemical vapor infiltration of C/C composites: Fast densification processes and matrix characterizations. *Carbon*. 2005, 43: 681–691.
- [117] P.D. Matzinos, J.W. Patrick, A. Walker. The efficiency and mechanism of densification of 2-D C/C composites by coal-tar pitch impregnation. *Carbon*.

- 2000, 38: 1123–1128.
- [118] R. Luo, C. Yang, J. Cheng. Effect of preform architecture on the mechanical properties of 2D C/C composites prepared using rapid directional diffused CVI processes. *Carbon*. 2002, 40: 2221–2228.
- [119] J.D. Chen, C.P. Ju. Friction and wear of PAN/pitch-, PAN/CVI- and pitch/resin/CVI- based carbon/carbon composites. *Wear*. 1994, 174: 129–135.
- [120] I.J. Davies, R.D. Rawlings. Mechanical properties in compression of CVI-densified porous carbon/carbon composite. *Composites Science and Technology*. 1999, 59: 97–104.
- [121] K. Lee, H. Cheng, J. Chen. Effect of densification cycles on continuous friction behavior of carbon–carbon composites. *Wear*. 2006, 260: 99–108.
- [122] B. Wielage, A.G. Odeshi, H. Mucha, H. Lang, R. Buschbeck. A cost effective route for the densification of carbon–carbon composites. *Journal of Materials Processing Technology*. 2003, 132: 313–322.
- [123] R. Luo, T. Liu, J. Li, H. Zhang, Z. Chen, G. Tian. Thermophysical properties of carbon/carbon composites and physical mechanism of thermal expansion and thermal conductivity. *Carbon*. 2004, 42: 2887–2895.
- [124] D.D. Jayaseelan, R.G. de Sá, P. Brown, W.E. Lee. Reactive infiltration processing (RIP) of ultra high temperature ceramics (UHTC) into porous C/C composite tubes. *Journal of the European Ceramic Society*. 2011, 31: 361–368.
- [125] T. Sogabe, O. Okada, K. Kuroda, M. Inagaki. Improvement in properties and air oxidation resistance of carbon materials by boron oxide impregnation. *Carbon*. 1997, 35: 67–72.
- [126] E.L. Corral, L.S. Walker. Improved ablation resistance of C-C composites using zirconium diboride and boron carbide. *Journal of the European Ceramic Society*. 2010, 30: 2357–2364.
- [127] H. Fang, J. Jeon, J. Zhu, Z. Yin. Inhibition of liquid Si infiltration into carbon–carbon composites by the addition of Al to the Si slurry pre-coating: mechanism analysis. *Carbon*. 2002, 40: 2559–2565.
- [128] L.M. Manocha, S. Manocha, K.B. Patel, P. Glogar. Oxidation behaviour of Carbon/Carbon composites impregnated with silica and silicon oxycarbide. *Carbon*. 2000, 38: 1481–1491.
- [129] S.R. Dhakate, V. Raman, T.L. Dhami, O.P. Bahl. Synthesis of methyltriethoxysilane (MTEOS) derived SiC incorporated carbon-carbon composites. *Journal of Materials Science Letters*. 2001, 20: 811–813.
- [130] S. Park, M. Seo. The effects of MoSi<sub>2</sub> on the oxidation behavior of carbon/carbon composites. *Carbon*. 2001, 39: 1229–1235.
- [131] X. Shen, K. Li, H. Li, H. Du, W. Cao, F. Lan. Microstructure and ablation properties of zirconium carbide doped carbon/carbon composites. *Carbon*. 2010, 48: 344–351.
- [132] S. Li, K. Li, H. Li, Y. Li, Q. Yuan. Effect of HfC on the ablative and mechanical properties of C/C composites. *Materials Science and Engineering A*. 2009, 517: 61–67.
- [133] H. He, K. Zhou, X. Xiong, B. Huang. Investigation on decomposition mechanism of tantalum ethylate precursor during formation of TaC on C/C composite material. *Materials Letters*. 2006, 60: 3409–3412.
- [134] Z. Chen, W. Wu, Z. Chen, X. Cong, J. Qiu. Microstructural characterization on ZrC doped carbon/carbon composites. *Ceramics International*. 2012, 38: 761–

767.

- [135] H. Fritze, J. Jojic, T. Witke, C. Rüscher, S. Weber, S. Scherrer, R. Weiß, B. Schultrich, G. Borchardt. Mullite based oxidation protection for SiC-C/C composites in air at temperatures up to 1900 K. *Journal of the European Ceramic Society*. 1998, 18: 2351–2364.
- [136] J. Huang, X. Zeng, H. Li, X. Xiong, Y. Fu. Influence of the preparation temperature on the phase, microstructure and anti-oxidation property of a SiC coating for C/C composites. *Carbon*. 2004, 42: 1517–1521.
- [137] W. Kowbel, J.C. Withers, P.O. Ransone. CVD and CVR Silicon-based functionally gradient coatings on C-C composites. *Carbon*. 1995, 33: 415–426.
- [138] H.T. Tsou, W. Kowbel. Design of multilayer plasma-assisted CVD coatings for the oxidation protection of composite materials. *Surface and Coatings Technology*. 1996, 79: 139–150.
- [139] H.T. Tsou, W. Kowbel. A hybrid PACVD B<sub>4</sub>C/CVD Si<sub>3</sub>N<sub>4</sub> coating for oxidation protection of composites. *Carbon*. 1995, 33: 1289–1292.
- [140] J.N. Stuecker, D.A. Hirschfeld, D.S. Martin. Oxidation protection of carbon-carbon composites by sol-gel ceramic coatings. *Journal of Materials Science*. 1999, 34: 5443–5447.
- [141] M. Aparicio, A. Durán. Yttrium silicate coatings for oxidation protection of carbon-silicon carbide composites. *Journal of the American Ceramic Society*. 2000, 83: 1351–1355.
- [142] K. Li, D. Hou, H. Li, Q. Fu, G. Jiao. Si–W–Mo coating for SiC coated carbon/carbon composites against oxidation. *Surface and Coatings Technology*. 2007, 201: 9598–9602.
- [143] T. Feng, H. Li, Q. Fu, X. Yang, H. Wu. The oxidation behavior and mechanical properties of MoSi<sub>2</sub>-CrSi<sub>2</sub>-SiC-Si coated carbon/carbon composites in high-temperature oxidizing atmosphere. *Corrosion Science*. 2011, 53: 4102–4108.
- [144] Y. Chu, Q. Fu, H. Li, K. Li. Thermal fatigue behavior of C/C composites modified by SiC-MoSi<sub>2</sub>-CrSi<sub>2</sub> coating. *Journal of Alloys and Compounds*. 2011, 509: 8111–8115.
- [145] F. Smeacetto, M. Ferraris, M. Salvo. Multilayer coating with self-sealing properties for carbon-carbon composites. *Carbon*. 2003, 41: 2105–2111.
- [146] Y. Zhang, H. Li, X. Yao, K. Li, S. Zhang. C/SiC/Si-Mo-B/glass multilayer oxidation protective coating for carbon/carbon composites. *Surface and Coatings Technology*. 2011, 206: 492–496.
- [147] J. Huang, X. Zeng, H. Li, X. Xiong, G. Sun. ZrO<sub>2</sub>-SiO<sub>2</sub> gradient multilayer oxidation protective coating for SiC coated carbon/carbon composites. *Surface and Coatings Technology*. 2005, 190: 255–259.
- [148] Y. Zhang, H. Li, Q. Fu, X. Yao, K. Li, G. Jiao. An oxidation protective Si-Mo-Cr coating for C/SiC coated carbon/carbon composites. *Carbon*. 2008, 46: 179–182.
- [149] S.R. Choi, R.W. Kowalik, D.J. Alexander, N.P. Bansal. Elevated-temperature stress rupture in interlaminar shear of a Hi-Nic SiC/SiC ceramic matrix composite. *Composites Science and Technology*. 2009, 69: 890–897.
- [150] Y. Katoh, K. Ozawa, T. Hinoki, Y. Choi, L.L. Snead, A. Hasegawa. Mechanical properties of advanced SiC fiber composites irradiated at very high temperatures. *Journal of Nuclear Materials*. 2011, 417: 416–420.
- [151] A.R. Bunsell, A. Piant. A review of the development of three generations of

- small diameter silicon carbide fibres. *Journal of Materials Science*. 2006, 41: 823–839.
- [152] T. Shimoo, Y. Morisada, K. Okamura. Oxidation behavior of Si-M-C-O fibers under wide range of oxygen partial pressures. *Journal of Materials Science*. 2002, 37: 4361–4368.
- [153] J.A. DiCarlo, H.M. Yun, J.B. Hurst. Fracture mechanisms for SiC fibers and SiC/SiC composites under stress-rupture conditions at high temperatures. *Applied Mathematics and Computation*. 2004, 152: 473–481.
- [154] T. Taguchi, T. Nozawa, N. Igawa, Y. Katoh, S. Jitsukawa, A. Kohyama, T. Hinoki, L.L. Snead. Fabrication of advanced SiC fiber/F-CVI SiC matrix composites with SiC/C multi-layer interphase. *Journal of Nuclear Materials*. 2004, 329–333: 572–576.
- [155] A. Kohyama, M. Kotani, Y. Katoh, T. Nakayasu, M. Sato, T. Yamamura, K. Okamura. High-performance SiC/SiC composites by improved PIP processing with new precursor polymers. *Journal of Nuclear Materials*. 2000, 283–287: 565–569.
- [156] Y. Gowayed, G. Ojard, R. Miller, U. Santhosh, J. Ahmad, R. John. Correlation of elastic properties of melt infiltrated SiC/SiC composites to in situ properties of constituent phases. *Composites Science and Technology*. 2010, 70: 435–441.
- [157] T. Yano, K. Budiyo, K. Yoshida, T. Iseki. Fabrication of silicon carbide fiber-reinforced silicon carbide composite by hot-pressing. *Fusion Engineering and Design*. 1998, 41: 157–163.
- [158] Y. Katoh, M. Kotani, H. Kishimoto, W. Yang, A. Kohyama. Properties and radiation effects in high-temperature pyrolyzed PIP-SiC/SiC. *Journal of Nuclear Materials*. 2001, 289: 42–47.
- [159] J.B.J. Hegeman, J.G. van der Laan, M. van Kranenburg, M. Jong, D. d’Hulst, P. ten Pierick. Mechanical and thermal properties of SiC<sub>f</sub>/SiC composites irradiated with neutrons at high temperatures. *Fusion Engineering and Design*. 2005, 75–79: 789–793.
- [160] A. Sayano, C. Sutoh, S. Suyama, Y. Itoh, S. Nakagawa. Development of a reaction-sintered silicon carbide matrix composite. *Journal of Nuclear Materials*. 1999, 271–272: 467–471.
- [161] S.P. Lee, J.S. Park, Y. Katoh, A. Kohyama, D.H. Kim, J.K. Lee, H.K. Yoon. Process, microstructure and flexural properties of reaction sintered Tyranno SA/SiC composites. *Journal of Nuclear Materials*. 2002, 307–311: 1191–1195.
- [162] A. Ortona, A. Donato, G. Filacchioni, U. De Angelis, A. La Barbera, C.A. Nannetti, B. Riccardi, J. Yeatman. SiC-SiC<sub>f</sub> CMC manufacturing by hybrid CVI-PIP techniques: process optimization. *Fusion Engineering and Design*. 2000, 51–52: 159–163.
- [163] C.A. Nannetti, B. Riccardi, A. Ortona, A. La Barbera, E. Scafè, G. Vekinis. Development of 2D and 3D Hi-Nicalon fibres/SiC matrix composites manufactured by a combined CVI-PIP route. *Journal of Nuclear Materials*. 2002, 307–311: 1196–1199.
- [164] M. Kotani, A. Kohyama, Y. Katoh. Development of SiC/SiC composites by PIP in combination with RS. *Journal of Nuclear Materials*. 2001, 289: 37–41.
- [165] S.P. Lee, Y. Katoh, J.S. Park, S. Dong, A. Kohyama, S. Suyama, H.K. Yoon. Microstructural and mechanical characteristics of SiC/SiC composites with modified-RS process. *Journal of Nuclear Materials*. 2001, 289: 30–36.

- [166] C.A. Nannetti, A. Ortona, D.A. de Pinto, B. Riccardi. Manufacturing SiC-fiber-reinforced SiC matrix composites by improved CVI/slurry infiltration/polymer impregnation and pyrolysis. *Journal of the American Ceramic Society*. 2004, 87: 1205–1209.
- [167] Y. Zhu, S.Zhu, Z. Huang, S. Dong, D. Jiang. Properties and microstructure of KD-I/SiC composites by combined process of CVI/RB/PIP. *Materials Science and Engineering A*. 2008, 477: 198–203.
- [168] Y. Katoh, S.M. Dong, A. Kohyama. Thermo-mechanical properties and microstructure of silicon carbide composites fabricated by nano-infiltrated transient eutectoid process. *Fusion Engineering and Design*. 2002, 61–62: 723–731.
- [169] Y. Katoh, A. Kohyama, T. Nozawa, M. Sato. SiC/SiC composites through transient eutectic-phase route for fusion applications. *Journal of Nuclear Materials*. 2004, 329–333: 587–591.
- [170] J.S. Park, A. Kohyama, T. Hinoki, K. Shimoda, Y.H. Park. Efforts on large scale production of NITE-SiC/SiC composites. *Journal of Nuclear Materials*. 2007, 367–370: 719–724.
- [171] K. Shimoda, J.S. Park, T. Hinoki, A. Kohyama. Influence of pyrolytic carbon interface thickness on microstructure and mechanical properties of SiC/SiC composites by NITE process. *Composites Science and Technology*. 2008, 68: 98–105.
- [172] K. Shimoda, T. Hinoki, H. Kishimoto, A. Kohyama. Enhanced high-temperature performances of SiC/SiC composites by high densification and crystalline structure. *Composites Science and Technology*. 2011, 71: 326–332.
- [173] S. Novak, K. Mejak, G. Dražić. The preparation of LPS SiC-fibre-reinforced SiC ceramics using electrophoretic deposition. *Journal of Materials Science*. 2006, 41: 8093–8100.
- [174] S. Novak, K. Rade, K. König, A.R. Boccaccini. Electrophoretic deposition in the production of SiC/SiC composites for fusion reactor applications. *Journal of the European Ceramic Society*. 2008, 28: 2801–2807.
- [175] A. Iveković, G. Dražić, S. Novak. Densification of a SiC-matrix by electrophoretic deposition and polymer infiltration and pyrolysis process. *Journal of the European Ceramic Society*. 2011, 31: 833–840
- [176] K. Shimoda, T. Hinoki, Y. Katoh, A. Kohyama. Development of the tailored SiC/SiC composites by the combined fabrication process of ICVI and NITE methods. *Journal of Nuclear Materials*. 2009, 384: 103–108.
- [177] E. López-Honorato, P.J. Meadows, R.A. Shatwell, P. Xiao. Characterization of the anisotropy of pyrolytic carbon by Raman spectroscopy. *Carbon*. 2010, 48: 881–890.
- [178] C. Labrugère, A. Guette, R. Naslain. Effect of ageing treatments at high temperatures on the microstructure and mechanical behaviour of 2D nicalon/C/SiC composites. 1: Ageing under vacuum or argon. *Journal of the European Ceramic Society*. 1997, 17: 623–640.
- [179] T. Hinoki, W. Yang, T. Nozawa, T. Shibayama, Y. Katoh, A. Kohyama. Improvement of mechanical properties of SiC/SiC composites by various surface treatments of fibers. *Journal of Nuclear Materials*. 2001, 289: 23–29.
- [180] W. Yang, A. Kohyama, Y. Katoh, H. Araki, J. Yu, T. Noda. Effect of carbon and silicon carbide/carbon interlayers on the mechanical behavior of Tyranno-SA-

- fiber-reinforced silicon carbide-matrix composites. *Journal of the American Ceramic Society*. 2003, 86: 851–856.
- [181] S. Jacques, A. Guette, F. Langlais, R. Naslain, S. Goujard. Preparation and characterization of 2D SiC/SiC composites with composition-graded C(B) interphase. *Journal of the European Ceramic Society*. 1997, 17: 1083–1092.
- [182] F. Rebillat, J. Lamon, A. Guette. The concept of a strong interface applied to SiC/SiC composites with a BN interphase. *Acta Materialia*. 2000, 48: 4609–4618.
- [183] S. Le Gallet, F. Rebillat, A. Guette, X. Bourrat, F. Doux. Influence of a multilayered matrix on the lifetime of SiC/BN/SiC minicomposites. *Journal of Materials Science*. 2004, 39: 2089–2097.
- [184] S. Jacques, M.P. Berthet, B. Bonnetot. SiC/SiC composites prepared with a BN interphase processed by LP-CVD from molecular precursor. *Materials Science Forum*. 2005, 494: 443–450.
- [185] Z. Wang, L. Gao, Y. Ding, B. Wu, H. Zhou, P. He, S. Dong. Microstructure observation and analysis of 3D carbon fiber reinforced SiC-based composites fabricated through filler enhanced polymer infiltration and pyrolysis. *Ceramics International*. 2012, 38: 535–540.
- [186] C. Droillard, J. Lamon. Fracture toughness of 2D-woven SiC/SiC CVI-composites with multilayered interphases. *Journal of the American Ceramic Society*. 1996, 79: 849–858.
- [187] H. Mei. Measurement and calculation of thermal residual stress in fiber reinforced ceramic matrix composites. *Composites Science and Technology*. 2008, 68: 3285–3292.
- [188] W. Yang, A. Kohyama, T. Noda, Y. Katoh, T. Hinoki, H. Araki, J. Yu. Interfacial characterization of CVI-SiC/SiC composites. *Journal of Nuclear Materials*. 2002, 307–311: 1088–1092.
- [189] S. Bertrand, R. Pailler, J. Lamon. Influence of Strong Fiber/Coating Interfaces on the Mechanical Behavior and Lifetime of Hi-Nicalon/(PyC/SiC)<sub>n</sub>/SiC Minicomposites. *Journal of the American Ceramic Society*. 2001, 84: 787–794.
- [190] W. Yang, H. Araki, A. Kohyama, H. Suzuki, T. Noda. Effects of SiC sub-layer on mechanical properties of Tyranno-SA/SiC composites with multiple interlayers. *Ceramics International*. 2005, 31: 525–531.
- [191] S. Bertrand, O. Boisron, R. Pailler, J. Lamon, R.R. Naslain. (PyC/SiC)<sub>n</sub> and (BN/SiC)<sub>n</sub> nanoscale-multilayered interphases by pressure pulsed-CVI. *Key Engineering Materials*. 1998, 164–165: 357–360.
- [192] O. Rapaud, S. Jacques, H. Di-Murro, H. Vincent, M.P. Berthet, J. Bouix. SiC/SiC minicomposites with (PyC/TiC)<sub>n</sub> interphases processed by pressure-pulsed reactive CVI. *Journal of Materials Science*. 2004, 39: 173–180.
- [193] Z. Wang, S. Dong, P. He, L. Gao, H. Zhou, J. Yang, D.g Jiang. Fabrication of carbon fiber reinforced ceramic matrix composites with improved oxidation resistance using boron as active filler. *Journal of the European Ceramic Society*. 2010, 30: 787–792.
- [194] K. Naito, Y. Tanaka, J.M. Yang, Y. Kagawa. Tensile properties of ultrahigh strength PAN-based, ultrahigh modulus pitch-based and high ductility pitch-based carbon fibers. *Carbon*. 2008, 46: 189–195.
- [195] J. Nie, Y. Xu, L. Zhang, L. Cheng, J. Ma. Microstructure and tensile behavior of multiply needled C/SiC composite fabricated by chemical vapor infiltration.

- Journal of Materials Processing Technology. 2009, 209: 572–576.
- [196] Z. Wang, L. Gao, Y. Ding, B. Wu, H. Zhou, P. He. Microstructure observation and analysis of 3D carbon fiber reinforced SiC-based composites fabricated through filler enhanced polymer infiltration and pyrolysis. *Ceramics International*. 2012, 38: 535–540.
- [197] K. Suresh, K. Sweety, K. Anil, S. Anupam, A.K. Gupta, G.R. Devi. Mechanical properties of LSI based 3D-stitched-C-SiC composites prepared by coal-tar pitch as carbon precursor. *Scripta Materialia*. 2008, 58: 826–829.
- [198] Y. Cai, Y. Xu, B. Li, S. Fan, L. Zhang, L. Cheng, L. Yu. Low-cost preparation and frictional behaviour of a three-dimensional needled carbon/silicon carbide composite. *Journal of the European Ceramic Society*. 2009, 29: 497–503.
- [199] S. Chen, H. Hu, Y. Zhang, X. He, M. Mei. Rapid densification of C/SiC composites by joint processes of CLVD and PIP. *Materials Letters*. 2011, 65: 3137–3139.
- [200] M. Yan, W. Song, Z.H. Chen. In situ growth of a carbon interphase between carbon fibres and a polycarbosilane-derived silicon carbide matrix. *Carbon*. 2011, 49: 2869–2872.
- [201] Z. Wang, S.M. Dong, Y.S. Ding, X.Y. Zhang, H.J. Zhou, J.S. Yang, B. Lu. Mechanical properties and microstructures of C<sub>f</sub>/SiC-ZrC composites using T700SC carbon fibers as reinforcements. *Ceramics International*. 2011, 37: 695–700.
- [202] Q. Zhou, S. Dong, Y. Ding, Z. Wang, Z. Huang, D. Jiang. Three-dimensional carbon fiber-reinforced silicon carbide matrix composites by vapor silicon infiltration. *Ceramics International*. 2009, 35: 2161–2169.
- [203] Y. Liu, L. Zhang, L. Cheng, X. Luan, W. Yang, W. Zhang, Y. Xu, Q. Zeng. Preparation and oxidation resistance of 2D C/SiC composites modified by partial boron carbide self-sealing matrix. *Materials Science and Engineering A*. 2008, 498: 430–436.
- [204] H. Hu, , Q. Wang, Z. Chen, C. Zhang, Y. Zhang, J. Wang. Preparation and characterization of C/SiC–ZrB<sub>2</sub> composites by precursor infiltration and pyrolysis process. *Ceramics International*. 2010, 36: 1011–1016.
- [205] C. Tong, L. Cheng, X. Yin, L. Zhang, Y. Xu. Oxidation behavior of 2D C/SiC composite modified by SiB<sub>4</sub> particles in inter-bundle pores. *Composites Science and Technology*. 2008, 68: 602–607.
- [206] F. Shi, X. Yin, X. Fan, L. Cheng, L. Zhang. A new route to fabricate SiB<sub>4</sub> modified C/SiC composites. *Journal of the European Ceramic Society*. 2010, 30: 1955–1962.
- [207] J.P. Viricelle, P. Goursat, D. Bahloul-Hourlier. Oxidation behaviour of a multi-layered ceramic-matrix composite (SiC)<sub>f</sub>/C/(SiBC)<sub>m</sub>. *Composites Science and Technology*. 2001, 61: 607–614.
- [208] L. Quemard, F. Rebillat, A. Guette, H. Tawil, C. Louchet-Pouillier. Self-healing mechanisms of a SiC fiber reinforced multi-layered ceramic matrix composite in high pressure steam environments. *Journal of the European Ceramic Society*. 2007, 27: 2085–2094.
- [209] Y. Liu, L. Cheng, L. Zhang, W. Yang, S. Zhou, W. Zhang. Fracture behavior and mechanism of 2D C/SiC–BC<sub>x</sub> composite at room temperature. *Materials Science and Engineering A*. 2011, 528: 1436–1441.
- [210] C. Zhang, S. Qiao, K. Yan, Y. Liu, Q. Wu, D. Han, M. Li. Mechanical properties

- of a carbon fiber reinforced self-healing multilayered matrix composite at elevated temperatures. *Materials Science and Engineering A*. 2011, 528: 3073–3078.
- [211] J.D. Webster, M.E. Westwood, F.H. Hayes, R.J. Day, R. Taylor, A. Duran, M. Aparicio, K. Rebstock, W.D. Vogel. Oxidation protection coatings for C/SiC based on yttrium silicate. *Journal of the European Ceramic Society*. 1998, 18: 2345–2350.
- [212] L. Cheng, Y. Xu, L. Zhang, X. Luan. Oxidation and defect control of CVD SiC coating on three-dimensional C/SiC composites. *Carbon*. 2002, 40: 2229–2234.
- [213] Y. Xu, L. Cheng, L. Zhang, H. Ying, W. Zhou. Oxidation behavior and mechanical properties of C/SiC composites with Si-MoSi<sub>2</sub> oxidation protection coating. *Journal of Materials Science*. 1999, 34: 6009–6014.
- [214] T. Damjanović, Chr. Argiris, G. Borchardt, H. Leipner, R. Herbig, G. Tomandl, R. Weiss. Oxidation protection of C/C-SiC composites by an electrophoretically deposited mullite precursor. *Journal of the European Ceramic Society*. 2005, 25: 577–587.
- [215] M. Pavese, P. Fino, C. Badini, A. Ortona, G. Marino. HfB<sub>2</sub>/SiC as a protective coating for 2D C<sub>f</sub>/SiC composites: Effect of high temperature oxidation on mechanical properties. *Surface and Coatings Technology*. 2008, 202: 2059–2067.
- [216] J. Liu, L. Zhang, Q. Liu, L. Cheng, Y. Wang. Polymer-derived SiOC-barium-strontium aluminosilicate coatings as an environmental barrier for C/SiC composites. *Journal of the American Ceramic Society*. 2010, 93: 4148–4152.
- [217] J. Liu, L. Zhang, J. Yang, L. Cheng, Y. Wang. Fabrication of SiCN-Sc<sub>2</sub>Si<sub>2</sub>O<sub>7</sub> coatings on C/SiC composites at low temperatures. *Journal of the European Ceramic Society*. 2012, 32: 705–710.
- [218] Y. Liu, L. Cheng, L. Zhang, S. Wu, D. Li, Y. Xu. Oxidation protection of multilayer CVD SiC/B/SiC coatings for 3D C/SiC composite. *Materials Science and Engineering A*. 2007, 466: 172–177.
- [219] S. Wu, L. Cheng, W. Yang, Y. Liu, L. Zhang, Y. Xu. Oxidation protective multilayer CVD SiC coatings modified by a graphitic B-C interlayer for 3D C/SiC composite. *Applied Composite Materials*. 2006, 13: 397–406.
- [220] Y. Xiang, W. Li, S. Wang, Z.H. Chen. Ablative property of ZrC-SiC multilayer coating for PIP-C/SiC composites under oxy-acetylene torch. *Ceramics International*. 2012, 38: 2893–2897.
- [221] X.H. Zheng, Y.G. Du, J.Y. Xiao, W.J. Zhang, L.C. Zhang. Double layer oxidation resistant coating for carbon fiber reinforced silicon carbide matrix composites. *Applied Surface Science*. 2009, 255: 4250–4254.
- [222] Y. Xiang, W. Li, S. Wang, Z. Chen. Oxidation behavior of oxidation protective coatings for PIP-C/SiC composites at 1500 °C. *Ceramics International*. 2012, 38: 9–13.
- [223] F. Yang, X. Zhang, J. Han, S. Du. Characterization of hot-pressed short carbon fiber reinforced ZrB<sub>2</sub>-SiC ultra-high temperature ceramic composites. *Journal of Alloys and Compounds*. 2009, 472: 395–399.
- [224] J. Meinhardt, T. Woyke, F. Raether, A. Kienzle. Measurement and simulation of the oxidation of carbon fibers and C/SiC ceramic. *Journal Advances in Science and Technology*. 2006, 45: 1489–1494.
- [225] K. Itatani, K. Hattori, D. Harima, M. Aizawa, I. Okada, I.J. Davies, H. Suemasu,

- A. Nozue. Mechanical and thermal properties of silicon-carbide composites fabricated with short Tyranno® Si-Zr-C-O fibre. *Journal of Materials Science*. 2001, 36: 3679–3686.
- [226] M. Sato, K. Itatani, T. Tanaka, I.J. Davies, S. Koda. Effect of chopped Si-Al-C fiber addition on the mechanical properties of silicon carbide composite. *Journal of Materials Science*. 2006, 41:7466–7473.
- [227] K. Itatani, T. Tanaka, I.J. Davies. Thermal properties of silicon carbide composites fabricated with chopped Tyranno® Si-Al-C fibres. *Journal of the European Ceramic Society*. 2006, 26: 703–710.
- [228] J.S. Lee, K. Yoshida, T. Yano. Influence of fiber volume fraction on the mechanical and thermal properties of unidirectionally aligned short-fiber-reinforced SiC composites. *Journal of the Ceramic Society of Japan*. 2002, 110: 985–989.
- [229] J.S. Lee, M. Imai, T. Yano. Fabrication and mechanical properties of oriented SiC short-fiber-reinforced SiC composite by tape casting. *Materials Science and Engineering A*. 2003, 339: 90–95.
- [230] J.S. Lee, T. Yano. Fabrication of short-fiber-reinforced SiC composites by polycarbosilane infiltration. *Journal of the European Ceramic Society*. 2004, 24: 25–31.
- [231] C.P. Ju, C.K. Wang, H.Y. Cheng, J.H. Chern Lin. Process and wear behavior of monolithic SiC and short carbon fiber-SiC matrix composite. *Journal of Materials Science*. 2000, 35: 4477–4484.
- [232] R. Li, Q. Shen, L. Zhang. Fabrication of short-C<sub>f</sub>/SiC functionally graded materials. *Materials Science Forum*. 2003, 423–425: 253–256.
- [233] Y. Zhou, H. Hyuga, K. Hirao, Y. Yamauchi. Processing and tribological properties of SiC/carbon short fibre composites. *Journal of the Ceramic Society of Japan*. 2006, 114: 323–328.
- [234] H. Tang, X. Zeng, X. Xiong, L. Li, J. Zou. Mechanical and tribological properties of short-fiber-reinforced SiC composites. *Tribology International*. 2009, 42: 823–827.
- [235] X. He, Y. Zhou, D. Jia, Y. Guo. Effect of sintering additives on microstructures and mechanical properties of short-carbon-fiber-reinforced SiC composites prepared by precursor pyrolysis–hot pressing. *Ceramics International*. 2006, 32: 929–934.
- [236] X. He, Y. Guo, Y. Zhou, D. Jia. Microstructures of short-carbon-fiber-reinforced SiC composites prepared by hot-pressing. *Materials Characterization*. 2008, 59: 1771–1775.
- [237] X. He, Y. Guo, Z. Yu, Y. Zhou, D. Jia. Study on microstructures and mechanical properties of short-carbon-fiber-reinforced SiC composites prepared by hot-pressing. *Materials Science and Engineering A*. 2009, 527: 334–338.
- [238] Y. Zhang, Y. Zhang, J. Han, L. Hu. The effect of sintering additive on fracture behavior of carbon-whisker-reinforced silicon carbide composites. *Materials Science and Engineering A*. 2008, 480: 62–67.
- [239] Y.L. Zhang, Y.M. Zhang, J.C. Han, Y.Y. Han, W. Yao. Fabrication of toughened Cf/SiC whisker composites and their mechanical properties. *Materials Letters*. 2008, 62: 2810–2813.
- [240] Y. Zhang, Y. Zhang, J. Han, Y. Zhou, L. Hu, W. Yao, W. Qu. The effect of annealing temperature on micro-structure and mechanical properties of C/SiC

- composites. *Materials Science and Engineering A*. 2008, 497: 383–387.
- [241] Y. Ding, S. Dong, Z. Huang, D. Jiang. Fabrication of short C fiber-reinforced SiC composites by spark plasma sintering. *Ceramics International*. 2007, 33: 101–105.
- [242] Y. Zhang, S. Li, J. Han, Y. Zhou. Fabrication and characterization of random chopped fiber reinforced reaction bonded silicon carbide composite. *Ceramics International*. 2012, 38: 1261–1266.
- [243] F. Raether, J. Meinhardt, A. Kienzle. Oxidation behaviour of carbon short fibre reinforced C/SiC composites. *Journal of the European Ceramic Society*. 2007, 27: 1217–1221.
- [244] <http://www.uibk.ac.at/geologie/staff/travertine/fig7.jpg>.
- [245] R.O. Ritchie. The conflicts between strength and toughness. *Nature Materials*. 2011, 10: 817–822.
- [246] C. Wang, Y. Huang, Q. Zan, H. Guo, S. Cai. Biomimetic structure design—a possible approach to change the brittleness of ceramics in nature. *Materials Science and Engineering C*. 2000, 11: 9–12.
- [247] W.J. Clegg, K. Kendall, N. Mcn. Alford, T. W. Button, J. D. Birchall. A simple way to make tough ceramics. *Nature*. 1990, 347: 455–457.
- [248] W.J. Clegg. The fabrication and failure of laminar ceramic composites. *Acta Metallurgica et Materialia*. 1992, 40: 3085–3093.
- [249] A.J. Phillipps, W.J. Clegg, T.W. Clyne. Fracture behaviour of ceramic laminates in bending-I. Modelling of crack propagation. *Acta Metallurgica et Materialia*. 1993, 41: 805–817.
- [250] A.J. Phillipps, W.J. Clegg, T.W. Clyne. Fracture behaviour of ceramic laminates in bending-II. Comparison of model predictions with experimental data. *Acta Metallurgica et Materialia*. 1993, 41: 819–827.
- [251] A.J. Phillipps, W.J. Clegg, T.W. Clyne. The correlation of interfacial and macroscopic toughness in SiC laminates. *Composites*. 1993, 24: 166–176.
- [252] A.J. Phillipps, W.J. Clegg, T.W. Clyne. The failure of layered ceramics in bending and tension. *Composites*. 1994, 25: 524–533.
- [253] W. Lee, S.J. Howard, W.J. Clegg. Growth of interface defects and its effect on crack deflection and toughening criteria. *Acta Materialia*. 1996, 44: 3905–3922.
- [254] K.S. Blanks, A. Kristoffersson, E. Carlström, W.J. Clegg. Crack deflection in ceramic laminates using porous interlayers. *Journal of the European Ceramic Society*. 1998, 18: 1945–1951.
- [255] J.B. Davis, A. Kristoffersson, E. Carlström, W. J. Clegg. Fabrication and crack deflection in ceramic laminates with porous interlayers. *Journal of the American Ceramic Society*. 2000, 83: 2369–2374.
- [256] C. Reynaud, F. Thévenot, T. Chartier, J.L. Besson. Mechanical properties and mechanical behaviour of SiC dense-porous laminates. *Journal of the European Ceramic Society*. 2005, 25: 589–597.
- [257] S. Tariolle, C. Reynaud, F. Thévenot, T. Chartier, J.L. Besson. Preparation, microstructure and mechanical properties of SiC-SiC and B<sub>4</sub>C-B<sub>4</sub>C laminates. *Journal of Solid State Chemistry*. 2004, 177: 487–492.
- [258] D. Leguillon, S. Tariolle, E. Martin, T. Chartier, J.L. Besson. Prediction of crack deflection in porous/dense ceramic laminates. *Journal of the European Ceramic Society*. 2006, 26: 343–349.
- [259] J. Ma, H.Z. Wang, L.Q. Weng, G.E.B. Tan. Effect of porous interlayers on crack

- deflection in ceramic laminates. *Journal of the European Ceramic Society*. 2004, 24: 825–831.
- [260] C. Badini, P. Fino, A. Ortona, C. Amelio. High temperature oxidation of multilayered SiC processed by tape casting and sintering. *Journal of the European Ceramic Society*. 2002, 2: 2071–2079.
- [261] S. Biamino, A. Antonini, C. Eisenmenger-Sittner, L. Fuso, M. Pavese, P. Fino, E. Bauer, C. Badini. Multilayer SiC for thermal protection system of space vehicles with decreased thermal conductivity through the thickness. *Journal of the European Ceramic Society*. 2010, 30: 1833–1840.
- [262] M. Pavese, P. Fino, A. Ortona, C. Badini. Potential of SiC multilayer ceramics for high temperature applications in oxidising environment. *Ceramics International*. 2008, 34: 197–203.
- [263] S. Biamino, V. Liedtke, C. Badini, G. Euchberger, I. Huertas Olivares, M. Pavese, P. Fino. Multilayer SiC for thermal protection system of space vehicles: Manufacturing and testing under simulated re-entry conditions. *Journal of the European Ceramic Society*. 2008, 28: 2791–2800.
- [264] Z. Lv, T. Zhang, D. Jiang, J. Zhang, Q. Lin. Aqueous tape casting process for SiC. *Ceramics International*. 2009, 35: 1889–1895.
- [265] R. Krishnamurthy, B.W. Sheldon. Experimental observations of high fracture resistance in silicon carbide/alumina laminated composites. *Journal of the American Ceramic Society*. 2001, 84: 2451–2453.
- [266] R. Krishnamurthy, J. Rankin, B.W. Sheldon. Effect of oxidation on crack deflection in SiC/Al<sub>2</sub>O<sub>3</sub> laminated ceramic composites. *Journal of the American Ceramic Society*. 2005, 88: 1362–1365.
- [267] D. Li, G. Qiao, Z. Jin. R-curve behavior of laminated SiC/BN ceramics. *Ceramics International*. 2004, 30: 213–217.
- [268] F. De Genua, V.M. Sglavo. High strength engineered alumina-silicon carbide laminated composites by spark plasma sintering. *Procedia Engineering*. 2011, 10: 2621–2626.
- [269] J. She, T. Inoue, K. Ueno. Multilayer Al<sub>2</sub>O<sub>3</sub>/SiC ceramics with improved mechanical behavior. *Journal of the European Ceramic Society*. 2000, 20: 1771–1775.
- [270] J.X. Zhang, Z.R. Huang, D.L. Jiang, S. H. Tan, Z. Shen, M. Nygren. Preparation of titanium nitride/alumina laminate composites. *Journal of the American Ceramic Society*. 2002, 85: 1133–1138.
- [271] Y. Zeng, D. Jiang. Fabrication and properties of laminated Al<sub>2</sub>O<sub>3</sub>/TiC composites. *Ceramics International*. 2001, 27: 597–602.
- [272] Q. Zan, C. Wang, Y. Huang, S. Zhao, C. Li. The interface-layer and interface in the Al<sub>2</sub>O<sub>3</sub>/Ti<sub>3</sub>SiC<sub>2</sub> multilayer composites prepared by in situ synthesis. *Materials Letters*. 2003, 57: 3826–3832.
- [273] Q.F. Zan, C.A. Wang, L.M. Dong, Y. Huang. High-Temperature Mechanical Properties of Al<sub>2</sub>O<sub>3</sub>/Ti<sub>3</sub>SiC<sub>2</sub> Multilayer Ceramics. *Key Engineering Materials*. 2007, 280–283: 1877–1880.
- [274] P. Boch, T. Chartier, M. Huttepain. Tape casting of Al<sub>2</sub>O<sub>3</sub>/ZrO<sub>2</sub> laminated composites, *Journal of the American Ceramic Society*. 1986, 69: C-191–C-192.
- [275] R. Bermejo, J. Pascual, T. Lube, R. Danzer. Optimal strength and toughness of Al<sub>2</sub>O<sub>3</sub>-ZrO<sub>2</sub> laminates designed with external or internal compressive layers. *Journal of the European Ceramic Society*. 2008, 28: 1575–1583.

- [276] J. Zhang, F. Ye, D. Jiangc, M. Iwasa. Preparation of bulk Si<sub>3</sub>N<sub>4</sub> from tape casting and lamination. *Ceramics International*. 2006, 32: 277–282.
- [277] Z. Yu, Z. Krstic, V.D. Krstic. Laminated Si<sub>3</sub>N<sub>4</sub>/SiC composites with self-sealed structure. *Key Engineering Materials*. 2007, 280–283: 1873–1876.
- [278] Z. Krstic, V.D. Krstic. Crack propagation and residual stress in laminated Si<sub>3</sub>N<sub>4</sub>/BN composite structures. *Journal of the European Ceramic Society*. 2011, 31: 1841–1847.
- [279] C. Li, C. Wang, Y. Huang, Q. Zan, S. Zhao. Effects of sintering aids on the microstructure and mechanical properties of laminated Si<sub>3</sub>N<sub>4</sub>/BN ceramics. *Materials Letters*. 2003, 57: 3473–3478.
- [280] Y.M. Luo, W. Pan, S. Li, J. Chen, R.G. Wang, J.Q. Li. Mechanical properties and microstructure of a Si<sub>3</sub>N<sub>4</sub>/Ti<sub>3</sub>SiC<sub>2</sub> multilayer composite. *Ceramics International*. 2002, 28: 223–226.
- [281] J-P. Hirvonen, P. Torri, R. Lappalainen, J. Likonena, H. Kung, J.R. Jervis, M. Nastasi. Oxidation of MoSi<sub>2</sub>/SiC nanolayered composite. *Journal of Materials Research*. 1998, 13: 965–973.
- [282] P. Parente, Y. Ortega, B. Savoini, M.A. Monge, A. Tucci, L. Esposito, A.J. Sánchez-Herencia. Microstructural characterization of alumina–zirconia layered ceramics using positron annihilation spectroscopy. *Acta Materialia*. 2010, 58: 3014–3021.
- [283] V.M. Sglavo, M. Bertoldi. Design and production of ceramic laminates with high mechanical resistance and reliability. *Acta Materialia*. 2006, 54: 4929–4937.
- [284] S.X. Zhang, Z.Y. Ong, T. Li, Q.F. Li, S.F. Pook. Ceramic composite components with gradient porosity by powder injection moulding. *Materials & Design*. 2010, 31: 2897–2903.
- [285] J. Requena, R. Moreno, J.S. Moya. Alumina and alumina/zirconia multilayer composites obtained by slip casting. *Journal of the American Ceramic Society*. 1989, 72: 1511–1513.
- [286] L. Zhang, V.D. Krstic. High toughness silicon carbide/graphite laminar composite by slip casting. *Theoretical and Applied Fracture Mechanics*. 1995, 24: 13–19.
- [287] Z.B. Yu, V.D. Krstic. Fabrication and characterization of laminated SiC ceramics with self-sealed ring structure. *Journal of Materials Science*. 2003, 38: 4735–4738.
- [288] O.O. Omatete, M.A. Janney, R.A. Strehlow. Gelcasting—a new ceramic forming process. *American Ceramic Society Bulletin*. 1991, 70: 1641–1649.
- [289] Y. Jia, Y. Kanno, Z.P. Xie. Fabrication of alumina green body through gelcasting process using alginate. *Materials Letters*. 2003, 57: 2530–2534.
- [290] M.A. Janney, O.O. Omatete, C.A. Walls, St.D. Nunn, R.J. Ogle, G. Westmoreland. Development of low-toxicity gelcasting systems. *Journal of the American Ceramic Society*. 1998, 81: 581–591.
- [291] J.K. Montgomery, K.T. Faber. Processing of stepped-density alumina via gelcasting and reaction bonding techniques. *Scripta materialia*. 2000, 42: 283–287.
- [292] J.K. Montgomery, K.T. Faber. Processing and surface flaw tolerance of alumina bilayers. *Journal of the American Ceramic Society*. 2005, 42: 287–292.
- [293] D.M. Baskin, M.H. Zimmerman, K.T. Faber, E.R. Fuller. Forming single-phase

- laminates via the gelcasting technique. *Journal of the American Ceramic Society*. 1997, 80: 2929–2932.
- [294] D.B. Hovis, K.T. Faber, E.A. Kenik. Texture and microstructural development in gelcast barium hexaferrite. *Journal of Materials Science*. 2008, 43: 1836–1843.
- [295] J.K. Montgomery, P.L. Drzal, K.R. Shull, K.T. Faber. Thermoreversible gelcasting: a novel ceramic processing technique. *Journal of the American Ceramic Society*. 2002, 85: 1164–1168.
- [296] J.K. Montgomery, A.S. Botha, P.L. Drzal, K.R. Shull, K.T. Faber. A thermo-reversible gelcasting technique for ceramic laminates. *Scripta Materialia*. 2003, 48: 785–789.
- [297] K. Araki, J.W. Halloran. New freeze-casting technique for ceramics with sublimable vehicles. *Journal of the American Ceramic Society*. 2004, 87: 1859–1863.
- [298] S.W. Sofie, F. Dogan. Freeze casting of aqueous alumina slurries with glycerol. *Journal of the American Ceramic Society*. 2001, 84: 1459–1464.
- [299] E. Munch, M.E. Launey, D.H. Alsem, E. Saiz, A.P. Tomsia, R.O. Ritchie. Tough, bio-inspired hybrid materials. *Science*. 2008, 322: 1516–1520.
- [300] K. Araki, J.W. Halloran. Porous ceramic bodies with interconnected pore channels by a novel freeze casting technique. *Journal of the American Ceramic Society*. 2005, 88: 1108–1114.
- [301] Y.H. Koh, I.K. Jun, J.J. Sun, H.E. Kim. In situ fabrication of a dense/porous bi-layered ceramic composite using freeze casting of a ceramic-camphene slurry. *Journal of the American Ceramic Society*. 2006, 89: 763–766.
- [302] Y. Zhang, L. Hu, J. Han. Preparation of a dense/porous bilayered ceramic by applying an electric field during freeze casting. *Journal of the American Ceramic Society*. 2009, 92: 1874–1876.
- [303] J.C. Chang, B.V. Velamakanni, F.F. Lange, D.S. Pearson. Centrifugal consolidation of  $\text{Al}_2\text{O}_3$  and  $\text{Al}_2\text{O}_3/\text{ZrO}_2$  composite slurries vs interparticle potentials: particle packing and mass segregation. *Journal of the American Ceramic Society*. 1991, 74: 2201–2204.
- [304] D.B. Marshall, J.J. Ratto, F.F. Lange. Enhanced fracture toughness in layered microcomposites of  $\text{Ce-ZrO}_2$  and  $\text{Al}_2\text{O}_3$ . *Journal of the American Ceramic Society*. 1991, 74: 2979–2987.
- [305] E. Lucchini, O. Sbaizero. Alumina/zirconia multilayer composites obtained by centrifugal consolidation. *Journal of the European Ceramic Society*. 1995, 15: 975–981.
- [306] I. Corni, M.P. Ryan, A.R. Boccaccini. Electrophoretic deposition: From traditional ceramics to nanotechnology. *Journal of the European Ceramic Society*. 2008, 28: 1353–1367.
- [307] P. Sarkar, X. Haung, P.S. Nicholson. Structural ceramic microlaminates by electrophoretic deposition. *Journal of the American Ceramic Society*. 1992, 75: 2907–2909.
- [308] P.S. Nicholson, P. Sarkar, X. Haung. Electrophoretic deposition and its use to synthesize  $\text{ZrO}_2/\text{Al}_2\text{O}_3$  micro-laminate ceramic/ceramic composites. *Journal of Materials Science*. 1993, 28: 6274–6278.
- [309] B. Hatton, P.S. Nicholson. Design and fracture of layered  $\text{Al}_2\text{O}_3/\text{TZ3Y}$  composites produced by electrophoretic deposition. *Journal of the American*

- Ceramic Society. 2001, 84: 571–576.
- [310] B. Ferrari, A.J. Sánchez-Herencia, R. Moreno. Aqueous electrophoretic deposition of Al<sub>2</sub>O<sub>3</sub>/ZrO<sub>2</sub> layered ceramics. *Materials Letters*. 1998, 35: 370–374.
- [311] R. Fischer, E. Fischer, G. De Portu, E. Roncari. Preparation of ceramic micro-laminate by electrophoresis in aqueous system. *Journal of Materials Science Letters*. 1995, 14: 25–27.
- [312] P. Hvizdoš, D. Jonsson, M. Anglada, G. Anné, O. V. der Biest. Mechanical properties and thermal shock behaviour of an alumina/zirconia functionally graded material prepared by electrophoretic deposition. *Journal of the European Ceramic Society*. 2007, 27: 1365–1371.
- [313] L. Vandeperre, O.V. der Biest, W.J. Clegg. Silicon carbide laminates with carbon interlayers by electrophoretic deposition. *Key Engineering Materials*. 1996, 127–131, 567–574.
- [314] L. Vandeperre, O.V. Der Biest, F. Bouyer, A. Foissy. SiC-graphite laminates shaped by EPD. *American Ceramic Society Bulletin*. 1998, 77: 53–58.
- [315] Ch. You, D.L. Jiang, S.H. Tan. SiC/TiC laminated structure shaped by electrophoretic deposition. *Ceramics International*. 2004, 30: 813–815.
- [316] C. You, D Jiang, S. Tan. Deposition of silicon carbide/titanium carbide laminar ceramics by electrophoresis and densification by spark plasma sintering. *Journal of the American Ceramic Society*. 2004, 87: 759–761.
- [317] L.F.G. Setz, I. Santacruz, M.T. Colomer, S.R.H. Mello-Castanho, R. Moreno. Tape casting of strontium and cobalt doped lanthanum chromite suspensions. *Journal of the European Ceramic Society*. 2010, 30: 2897–2903.
- [318] <http://www.paperandfilm.com/tapecasting.aspx>
- [319] J.X Zhang, D.L Jiang, Sh.Y Qin, Zh.R Huang. Fracture behavior of laminated SiC composites. *Ceramics International*. 2004, 30: 697–703.
- [320] S. Biamino, A. Antonini, M. Pavese, P. Fino, C. Badini. MoSi<sub>2</sub> laminate processed by tape casting: Microstructure and mechanical properties' investigation. *Intermetallics*. 2008, 16: 758–768.
- [321] W.L. Liu, J. Tan, C.B. Tang, C.C. Ge. Fabrication and mechanical properties of B<sub>4</sub>C/BN laminated ceramics. *Key Engineering Materials*. 2008, 1855: 368–372.
- [322] S. Bueno, C. Baudin. Design and processing of a ceramic laminate with high toughness and strong interfaces. *Composites Part A: Applied Science and Manufacturing*. 2009, 40: 137–143.
- [323] H. Tomaszewski, H. Węglarz, A. Wajler, M. Boniecki, D. Kalinski. Multilayer ceramic composites with high failure resistance. *Journal of the European Ceramic Society*. 2007, 27: 1373–1377.
- [324] P. Zhou, P. Hu, X. Zhang, W. Han. Laminated ZrB<sub>2</sub>-SiC ceramic with improved strength and toughness. *Scripta Materialia*. 2011, 64: 276-279.
- [325] X. Zhang, P. Zhou, P. Hu, W. Han. Toughening of laminated ZrB<sub>2</sub>-SiC ceramics with residual surface compression. *Journal of the European Ceramic Society*. 2011, 31: 2415–2423.
- [326] H. Wang, B Fan, L. Feng, D. Chen, H. Lu, H. Xu, C.A. Wang, R. Zhang. The fabrication and mechanical properties of SiC/ZrB<sub>2</sub> laminated ceramic composite prepared by spark plasma sintering. *Ceramics International*. 2012, 38: 5015–5022.
- [327] M. Wu, G.L. Messing. Fabrication of oriented SiC-whisker-reinforced mullite

- matrix composites by tape casting. *Journal of the American Ceramic Society*. 1994, 77: 2586–2592.
- [328] D.S. Lim, D.S. Park, B.D. Han, T. S. Kan. Tribological behavior of alumina reinforced with unidirectionally oriented SiC whiskers. *Wear*. 1999, 225–229: 868–873.
- [329] D.S. Lim, D.S. Park, B.D. Han, T.S. Kan, H. Jang. Temperature effects on the tribological behavior of alumina reinforced with unidirectionally oriented SiC whiskers. *Wear*. 2001, 251: 1452–1458.
- [330] L. Fuso, D. Manfredi, S. Biamino, M. Pavese, P. Fino, C. Badini. SiC-based multilayered composites containing short carbon fibres obtained by tape casting. *Composites Science and Technology*. 2009, 69: 1772–1776.
- [331] L. Stobierski, A. Gubernat, Sintering of silicon carbide I. Effect of carbon, *Ceramics International*. 2003, 29: 287–292.
- [332] C.M. Vega Bolivar, A. Antonini, S. Biamino, M. Pavese, P. Fino, C. Badini, Oxidation resistance of multilayer SiC for space vehicle thermal protection systems. *Advanced Engineering Materials*. 2010, 12: 617–622.
- [333] B.D. Zhao, P.Y. Wan, J.Q. Liu, J.G. Wang, T. Wang. Investigation of thermal instability of benzoyl peroxide in the presence of carbazole and its derivatives. *Thermochimica Acta*. 2012, 543: 232–238.
- [334] M.J. O'Neill. Measurement of specific heat functions by differential scanning calorimetry. *Analytical Chemistry*. 1966, 38: 1331–1336.
- [335] T. Wei, Z. Fan, G. Luo, S. Wang, L. Song. Dispersibility and stability improvement of graphite nanoplatelets in organic solvent by assistance of dispersant and resin. *Materials Research Bulletin*. 2009, 44: 977–983.
- [336] J.H. Moon, Y.G. Shul, H.S. Han, S.Y. Hong, Y.S. Choi, H.T. Kim. A study on UV-curable adhesives for optical pick-up: I. Photo-initiator effects. *International Journal of Adhesion and Adhesives*. 2005, 25: 301–312.
- [337] M.R. Loos, J. Yang, D.L. Feke, I. Manas-Zloczower. Effect of block-copolymer dispersants on properties of carbon nanotube/epoxy systems. *Composites Science and Technology*. 2012, 72: 482–488.
- [338] Y.H. Liao, O. Marietta-Tondin, Z. Liang, C. Zhang, B. Wang. Investigation of the dispersion process of SWNTs/SC-15 epoxy resin nanocomposites. *Materials Science and Engineering A*. 2004, 385: 175–181.
- [339] M. Shim, N. Wong, S. Kam, R.J. Chen, Y. Li, H. Dai. Functionalization of carbon nanotubes for biocompatibility and biomolecular recognition. *Nano Letters*. 2002, 2: 285–288.
- [340] Y. Geng, M.Y. Liu, J. Li, X.M. Shi, J.K. Kim. Effects of surfactant treatment on mechanical and electrical properties of CNT/epoxy nanocomposites. *Composites Part A: Applied Science and Manufacturing*. 2008, 39: 1876–1883.
- [341] J.F. Liu, W.A. Ducker. Self-assembled supramolecular structures of charged polymers at the graphite/liquid interface. *Langmuir*. 2000, 16: 3467–3473.
- [342] R. Rastogi, R. Kaushal, S.K. Tripathi, A.L. Sharma, I. Kaur, L.M. Bharadwaj. Comparative study of carbon nanotube dispersion using surfactants. *Journal of Colloid and Interface Science*. 2008, 328: 421–428.
- [343] M.F. Islam, E. Rojas, D.M. Bergey, A.T. Johnson, A.G. Yodh. High weight fraction surfactant solubilization of single-wall carbon nanotubes in water. *Nano Letters*. 2003, 3: 269–273.
- [344] G. Besendörfer, A. Roosen. Particle shape and size effects on anisotropic

- shrinkage in tape-cast ceramic layers. *Journal of the American Ceramic Society*. 2008, 91: 2514–2520.
- [345] A. Dellert, A. Heunisch, A. Roosen. The origin of anisotropic shrinkage in tape-cast green tapes. *International Journal of Applied Ceramic Technology*. 2011, 8: 1312–1319.
- [346] A. Heunisch, A. Dellert, A. Roosen. Effect of powder, binder and process parameters on anisotropic shrinkage in tape cast ceramic products. *Journal of the European Ceramic Society*. 2010, 30: 3397–3406.
- [347] H.Z. Wang, L. Gao, J.K. Guo. The effect of nanoscale SiC particles on the microstructure of Al<sub>2</sub>O<sub>3</sub> ceramics. *Ceramics International*. 2000, 26: 391–396.
- [348] W.S. Yang, L. Fuso, S. Biamino, D. Vasquez, C. Vega Bolivar, P. Fino, C. Badini. Fabrication of short carbon fibre reinforced SiC multilayer composites by tape casting. *Ceramics International*. 2012, 38: 1011–1018.
- [349] L. Stobierski, A. Gubernat. Sintering of silicon carbide II. Effect of boron. *Ceramics International*. 2003, 29: 355–361.
- [350] N.S. Jacobson, D. L. Myers. Active oxidation of SiC. *Oxidation of Metals*. 2011, 75: 1–25.
- [351] T. Narushima, T. Goto, T. Hirai. High-temperature passive oxidation of chemically vapor deposited silicon carbide. *Journal of the American Ceramic Society*. 1989, 72: 1386–1390.
- [352] L. Charpentier, M. Balat-Pichelin, F. Audubert. High temperature oxidation of SiC under helium with low-pressure oxygen—Part 1: Sintered  $\alpha$ -SiC. *Journal of the European Ceramic Society*. 2010, 30: 2653–2660.
- [353] J. Wang, L. Zhang, Q. Zeng, G.L. Vignoles, A. Guette. Theoretical investigation for the active-to-passive transition in the oxidation of silicon carbide. *Journal of the American Ceramic Society*. 2008, 91: 1665–1673.
- [354] L. Charpentier, A. Maître, M. Balat-Pichelin, S. Foucaud, F. Audubert. Influence of alumina on the passive oxidation at low oxygen pressure of hot-pressed  $\alpha$ -SiC. *Scripta Materialia*. 2009, 60: 481–484.
- [355] R.G. Munro. Material properties of a sintered-SiC. *Journal of Physical and Chemical Reference Data*. 1997, 26: 1195–203.
- [356] A.T.D. Butland, R.J. Maddison. The specific heat of graphite: An evaluation of measurements. *Journal of Nuclear Materials*. 1973, 49: 45–56.
- [357] S.H. Lee, M. Weinmann. C fiber/SiC filler/Si–B–C–N matrix composites with extremely high thermal stability. *Acta Materialia*. 2009, 57: 4374–4381.
- [358] T.S. Suzuki, T. Uchikoshi, Y. Sakka. Effect of sintering conditions on microstructure orientation in  $\alpha$ -SiC prepared by slip casting in a strong magnetic field. *Journal of the European Ceramic Society*. 2010, 30: 2813–2817.
- [359] J. Li, Y. Ye. Densification and grain growth of Al<sub>2</sub>O<sub>3</sub> nanoceramics during pressureless sintering. *Journal of the American Ceramic Society*. 2006, 89: 139–143.
- [360] D.M. Liu, B.W. Lin. Thermal conductivity in hot-pressed silicon carbide. *Ceramics International*. 1996, 22: 407–414.
- [361] N.M. Stanton, A.J. Kent, D. Lehmann. Phonon transport in 6H–silicon carbide. *Semiconductor Science and Technology*. 2003, 18: L4–L7.
- [362] T. Kinoshita, S. Munekawa. Effect of grain boundary segregation on thermal conductivity of hot-pressed silicon carbide. *Acta Metallurgica*. 1997, 45: 2001–2012.

- [363] J.H. Eom, Y.W. Kim, I.H. Song, H.D. Kim. Processing and properties of polysiloxane-derived porous silicon carbide ceramics using hollow microspheres as templates. *Journal of the European Ceramic Society*. 2008, 28: 1029–1035.
- [364] K.E. Pappacena, K.T. Faber, H. Wang, W.D. Porter. Thermal conductivity of porous silicon carbide derived from wood precursors. *Journal of the American Ceramic Society*. 2007, 90: 2855–2862.
- [365] K. Watari, K. Hirao, M. Toriyama, K. Ishizaki. Effect of grain size on the thermal conductivity of  $\text{Si}_3\text{N}_4$ . *Journal of the American Ceramic Society*. 1999, 82: 777–779.
- [366] M. Kitayama, K. Hirao, M. Toriyama, S. Kanzaki. Thermal conductivity of  $\beta\text{-Si}_3\text{N}_4$ : I, Effects of various microstructural factors. *Journal of the American Ceramic Society*. 1999, 82: 3105–3112.
- [367] B.K. Jang, Y. Sakka. Influence of microstructure on the thermophysical properties of sintered SiC ceramics. *Journal of Alloys and Compounds*. 2008, 463: 493–497.
- [368] S. Jang, S. Kang. Influence of MgO/CaO ratio on the properties of MgO–CaO– $\text{Al}_2\text{O}_3$ – $\text{SiO}_2$  glass–ceramics for LED packages. *Ceramics International*. 2012, 38S: S543–S546.
- [369] X. Huang. Fabrication and properties of carbon fibers. *Materials*. 2009, 2: 2369–2403.
- [370] S. Wang, Z.H. Chen, W.J. Ma, Q.S. Ma. Influence of heat treatment on physical–chemical properties of PAN-based carbon fiber. *Ceramics International*. 2009, 32: 291–295.
- [371] F. Yang, X. Zhang, J. Han, S. Du. Characterization of hot-pressed short carbon fiber reinforced  $\text{ZrB}_2$ –SiC ultra-high temperature ceramic composites. *Journal of Alloys and Compounds*. 2009, 472: 395–399.
- [372] G. Yuan, X. Li, Z. Dong, A. Westwood, Z. Cui, Y. Cong, H. Du, F. Kang. Graphite blocks with preferred orientation and high thermal conductivity. *Carbon*. 2012, 50: 175–182.
- [373] G.P. Wu, D.H. Li, Y. Yang, C.X. Lu, S.C. Zhang, X.T. Li, Z.H. Feng, Z.H. Li. Carbon layer structures and thermal conductivity of graphitized carbon fibers. *Journal of Materials Science*. 2012; 47: 2882–2890.